The Evolution of Photorespiration in Photosynthetic Eukaryotes

Inaugural-Dissertation

zur Erlangung des Doktorgrades

der Mathematisch-Naturwissenschaftlichen Fakultät

der Heinrich-Heine-Universität Düsseldorf

vorgelegt von

Nadine Christine Rademacher (geb. Hocken)

aus Düsseldorf

Düsseldorf, März 2016

aus dem Institut für Biochemie der Pflanzen
Heinrich-Heine-Universität Düsseldorf

Gedruckt mit Genehmigung der Mathematisch-Naturwissenschaftlichen Fakultät der Heinrich-Heine-Universität Düsseldorf

Referent: Prof. Dr. A. P. M. Weber

Korreferent: PD Dr. V. G. Maurino

Tag der mündlichen Prüfung: 13.05.2016

EIDESSTATTLICHE ERKLÄRUNG

Ich versichere an Eides Statt, dass diese Dissertation von mir selbständig und ohne unzulässige fremde Hilfe unter Beachtung der „Grundsätze zur Sicherung guter wissenschaftlicher Praxis an der Heinrich-Heine-Universität Düsseldorf“ erstellt worden ist.

Die Dissertation habe ich in der vorgelegten oder in ähnlicher Form noch bei keiner anderen Institution eingereicht.

Ich habe bisher keine erfolglosen Promotionsversuche unternommen.

Düsseldorf, der 29.03.2016

Nadine Rademacher

CONTENT

ABBREVIATIONS

(L)-2-HAOX	(L)-2- Hydroxyacid-oxidase
°C	Degree Celsius
2-OG	2-Oxoglutarate
2-PG	2-Phopsphoglycolate
2xMA	2x modified Allen's medium
3-PGA	3-Phosphoglycerate
A. thaliana	*Arabidopsis thaliana*
AMT	Ammonium transport family
ATP	Adenosine triphosphate
bp	Base pair
C. merolae	*Cyanidioschyzon merolae*
C. reinhardtii	*Chlamydomonas reinhardtii*
CA	Carbon anhydrase
CAM	Crassulacean acid metabolism
CAT	Catalase
CCB	Calvin-Benson-Bassham cycle
CCM	Carbon concentrating mechanism
CCP	Chloroplast envelope protein
cDNA	Complementary DNA/copy DNA
CFP	Cyan fluorescent protein
CH_4	Methane
ci	Inorganic carbon
CIA5	CO_2 transcription regulator
CO_2	Carbon dioxide
DNA	Deoxyribonucleic acid
DFG	Deutsche Forschungsgemeinschaft
DiT	Dicarboxylate translocator
DTT	Dithiothreitol
fd	Ferredoxin
FNR	Flavoprotein ferredoxin-NADP reductase

G3P	Glyceraldehyde-3-phosphate
GC/MS	Gas chromatography-mass spectrometry
GDC	Glycine decarboxylase
gDNA	Genomic DNA
GGT	Glutamate-glyoxylate aminotransferase
GlcD	Glycolate dehydrogenase
GLYK	Glycerate-3-kinase
GOGAT	Ferredoxin-dependent glutamate synthase
GOX	Glycolate oxidase
GS	Glutamine synthase
GSH	Glutathione
Gya	Giga years ago
h	Hour
H_2O_2	Hydrogen peroxide
HC	High carbon (5% CO_2)
HCO_3^-	Bicarbonate
HCR	High-carbon-requiring
HLA3	High-light induced gene3
HPR1	Peroxisomal hydroxypyruvate reductase
HPR2	Cytosolic hydroxypyruvate reductase
Km	Michaelis-Menten constant
LC	Low carbon (0.04% CO_2)
LHC	Light harvesting complex
LOX	Lactate oxidase
LSM	Laser scanning microscope
Mbp	Mega base pairs
ml	Milliliter
Mya	Mega years ago
N. benthamiana	*Nicotiana benthamiana*
N_2	Nitrogen
$NADP^+$	Nicotinamide adenine dinucleotide phosphate
NADPH	Nicotinamide adenine dinucleotide phosphate, reduced form
NaHCO3	Sodium hydrogen bicarbonate

NH_3	Ammonia
O_2	Oxygen
OAS	O-acetylserine
OD	Optical density
PCA	Principle component analysis
PCR	Polymerase chain reaction
PE	Paired end
PGP	2-PG phosphatase
PLGG1	Plastidic glycolate glycerate transporter
PPP	Pentose phosphate pathway
PQH_2	Plastohydroquinone
PSI	Photosystem I
PSII	Photosystem II
PTS	Peroxisomal targeting sequence
qRT PCR	Quantitative real-time PCR
rcf	Relative centrifugal force
RLP	RubisCO-like protein
RNA	Ribonucleic acid
RPKM	Reads per kilobase per million mapped reads
rpm	Revolutions per minute
RubisCO	Ribulose-1,5-bisphosphate carboxylase/oxygenase
RUBP	Ribulose-1,5-bisphosphate
SAH	S-adenosylhomocyteine
SAM	S-adenosylmethionine
SGT	Serine-glyoxylate aminotransferase
SHMT	Serine hydroxymethlytransferase
SKL	Peroxisome targeting sequence
SULTR3;1	Sulfate transporter
TCA	Citric acid cycle
UBQ	Ubiquitin
UHLPC	Ultra High Performance Liquid Chromatography
v	Volume
v/v	Volume per volume

Vmax	Maximal velocity
vs.	Versus
WT	Wild-type
YFP	Yellow fluorescent protein
γ-EC	γ-glutamylcystein
µg	Microgramm
µm	Micrometer
µmol	Micromol

PREFACE

The present PhD thesis consists of a summary of the thesis in English and German language, an introduction to the topic “photosynthesis and photorespiration in eukaryotes” and a comment to the aim of the thesis. The introduction has a special focus on the extremophile red algae *Cyanidioschyzon merolae.* Subsequent three independent manuscripts are attached to the thesis.

The first manuscript is a review with the title: “Plastidial metabolite transporters integrate photorespiration with carbon, nitrogen, and sulfur metabolism” published in 2015 in Cell Calcium (Eisenhut and Hocken *et al.,* 2015). The review gives an insight into the importance of known and so far unidentified plastidial transport proteins involved in photorespiratory metabolism and the closely connected nitrogen and sulfur cycles. Furthermore, the evolutionary origin of the established plastidial transporters is discussed.

The second manuscript “Photorespiratory glycolate oxidase is essential for the red algae *Cyanidioschyzon merolae* under ambient CO_2 conditions”, accepted for publication in the Journal of Experimental Botany in February 2016, illustrates the significance of photorespiration in red algae (Rademacher *et al*., 2016). This publication focuses on the relevance of the enzyme glycolate oxidase in the extremophile red alga *Cyanidioschyzon merolae* under photorespiratory conditions.

The third manuscript is written as a draft for a future publication. It deals with the effects of changes in carbon dioxide concentrations on gene expression in the red alga *Cyanidioschyzon merolae*, with a special interest on carbonic anhydrases.

REFERENCES:

Eisenhut M, Hocken N, Weber APM. 2015. Plastidial metabolite transporters integrate photorespiration with carbon, nitrogen, and sulfur metabolism. Cell Calcium **58**, 98–104.

Rademacher N, Kern R, Fujiwara T, Miyagishima SY, Hagemann M, Eisenhut M, Weber APM. 2016. Photorespiratory glycolate oxidase is essential for the red algae *Cyanidioschyzon merolae* under ambient CO_2 conditions. Journal of Experimental Botany**, in press**

SUMMARY

Photosynthesis evolved in cyanobacteria-like prokaryotes about 2.2 to 2.8 billion years ago in a nearly oxygen free atmosphere (reviewed in Hohmann-Marriott and Blankenship, 2011). The initial enzyme ribulose-1,5-bisphosphate carboxylase/ oxygenase (RubisCO) catalyses the carboxylation reaction of the acceptor molecule ribulose-1,5-bisphosphate (RuBP), using atmospheric carbon dioxide for the production of sugars via the Calvin-Benson-Bassham (CCB) cycle. Next to the carboxylation reaction, RubisCO also performs an oxygenation reaction of RuBP, producing 2-phosphoglycolate (2-PG) amongst others, which is toxic for the organism. The subsequent photorespiratory cycle is used for the detoxification of 2-PG and the recycling of the acceptor molecule RuBP. Due to increasing oxygen (O_2) concentrations in the atmosphere, photorespiration became an indispensable pathway in all oxygen photosynthesis performing organisms (Hagemann *et al.*, 2013). Today all key enzymes involved in photorespiration are well characterized, while many transport processes connecting the involved compartments (chloroplast, peroxisome, mitochondrion and cytosol) are still unknown (reviewed in Bauwe *et al.*, 2010). An overview of photorespiration, with special focus on transport processes and the connection to nitrogen und sulfur metabolism is given in the first review: Eisenhut M, Hocken N, Weber APM. 2015. Plastidial metabolite transporters integrate photorespiration with carbon, nitrogen, and sulfur metabolism. Cell Calcium 58, 98–104.

The photorespiratory cycle evolved in cyanobacteria and was adopted by the ancient lines of photosynthetic eukaryotes, like Glaucophytes, Rhodophytes and Chlorophytes (Eisenhut *et al.*, 2008). The study of photorespiration in these eukaryotic algae will help to understand better the evolution of this pathway. The model organism *Cyanidioschyzon merolae* (*C. merolae*) is a well characterized extremophile red algae (Rhodophyta), which is frequently used for studies especially of the evolution of photosynthesis due to its ancient structure. In order to study the function and importance of photorespiration in *C. merolae*, the evolutionary important enzyme glycolate oxidase (GOX) was chosen, catalyzing the glycolate to glyoxylate conversion in the peroxisome. GOX knock-out mutants were generated

and the analysis under different CO_2 conditions revealed a dependency of *C. merolae* on a functional photorespiratory cycle under ambient CO_2 conditions. The results of this study are presented in manuscript II: Rademacher N, Kern R, Fujiwara T, Mettler-Altmann T, Miyagishima SY, Hagemann M, Eisenhut M, Weber APM (2016) Photorespiratory glycolate oxidase is essential for survival of the red alga *Cyanidioschyzon merolae* under ambient CO_2 conditions. Journal of Experimental Botany, in press.

Finally the analysis of transcriptional changes in *C. merolae* under changing CO_2 concentrations, revealed a high increase in transcript abundances of photorespiratory genes under ambient air conditions, but only minor changes in most other pathways, including the energy metabolism. Attempts to identify components of a possible carbon concentrating mechanism in *C. merolae*, based on BlastP analysis, localization studies and genes co-expression analysis, revealed two cytosolic α-carbonic anhydrases and a possible bicarbonate transporter, induced under limiting CO_2 conditions. Detailed results are described in manuscript III: Rademacher N, Wrobel T, Rossoni A, Eisenhut M, Kurz S, Bräutigam A, Weber APM: Transcriptional response of the extremophile red algae *Cyanidioschyzon merolae* to changes in CO_2 concentrations.

REFERENCES:

Bauwe H, Hagemann M, Fernie AR. 2010. Photorespiration: players, partners and origin. Trends in Plant Science **15**, 330–336.

Eisenhut M, Ruth W, Haimovich M, Bauwe H, Kaplan A, Hagemann M. 2008. The photorespiratory glycolate metabolism is essential for cyanobacteria and might have been conveyed endosymbiontically to plants. PNAS **105**, 17199–17204.

Eisenhut M, Hocken N, Weber APM. 2015. Plastidial metabolite transporters integrate photorespiration with carbon, nitrogen, and sulfur metabolism. Cell Calcium 58, 98–104

Hagemann M, Fernie AR, Espie GS, Kern R, Eisenhut M, Reumann S, Bauwe H, Weber APM. 2013. Evolution of the biochemistry of the photorespiratory C2 cycle. Plant Biology **15**, 639–647.

Hohmann-Marriott MF, Blankenship RE. 2011. Evolution of photosynthesis. Annu Rev Plant Biol **62**, 515–548.

Rademacher N, Kern R, Fujiwara T, Mettler-Altmann T, Miyagishima SY, Hagemann M, Eisenhut M, Weber APM (2016) Photorespiratory glycolate oxidase is essential for survival of the red alga *Cyanidioschyzon merolae* under ambient CO_2 conditions. Journal of Experimental Botany, in press.

ZUSAMMENFASSUNG

Vor ca. 2,2 bis 2,8 Milliarden Jahren entwickelte sich in einer nahezu Sauerstoff freien Atmosphäre die Photosynthese in Cyanobakterien ähnlichen Prokaryoten (Hohmann-Marriott and Blankenship, 2011). Dabei katalysiert das Enzym Ribulose-1,5-bisphosphat Carboxylase/ Oxygenase (RubisCO) die Carboxylierungsreaktion des Akzeptormoleküls Ribulose-1,5-bisphosphat (RuBP), wobei aus atmosphärischem Kohlenstoffdioxid mittels des Calvin-Benson-Bassham Stoffwechselweges Zucker gewonnen wird. Neben der Carboxylierungsreaktion, führt das RubisCO Enzym auch eine Oxygenierungsreaktion von RuBP durch, bei welcher unter anderem das Zwischenprodukt 2-Phosphoglykolat (2-PG) erzeugt wird, welches toxisch für den Organismus ist. Der anschließende photorespiratorische Stoffwechselweg dient zur Detoxifizierung von 2-PG und der Rückgewinnung des Akzeptormoleküls RuBP. Auf Grund steigender Sauerstoffkonzentrationen in der Atmosphäre wurde die Photorespiration ein unabdingbarer Stoffwechselweg in allen Organismen, die Sauerstoff erzeugende Photosynthese betreiben (Hagemann *et al.*, 2013). Heute sind alle Hauptenzyme der Photorespiration bekannt und gut charakterisiert, wobei viele Transportprozesse zwischen den einzelnen Kompartimenten (Chloroplast, Peroxisom, Mitochondrium und Zytosol) noch unbekannt sind (Bauwe *et al.*, 2010).

Das erste Review gibt einen Überblick über die Photorespiration mit einem speziellen Fokus auf die Transportprozesse und die Verbindung zu Stickstoff- und Schwefel-Metabolismus: Eisenhut M, Hocken N, Weber APM. 2015. Plastidial metabolite transporters integrate photorespiration with carbon, nitrogen, and sulfur metabolism. Cell Calcium 58, 98–104.

Der photorespiratorische Zyklus entwickelte sich in den Cyanobakterien und wurde durch die ursprünglichen Linien photosynthetischer Eukaryoten, wie Glaukophyten, Rhodophyten und Chlorophyten, übernommen (Eisenhut *et al.*, 2008). Die Untersuchung der Photorespiration in diesen eukaryotischen Algen ist ein Ansatz, die Evolution dieses Stoffwechselweges besser zu verstehen. Der Modelorganismus *Cyanidioschyzon merolae* (*C. merolae*) ist eine gut charakterisierte, extremophile Rotalge (Rhodophyt), die häufig speziell für Studien zur Analyse der Evolution von

Photosynthese auf Grund ihrer ursprünglichen Eigenschaften genutzt wird. Zur Analyse von Funktion und Bedeutung der Photorespiration in *C. merolae* wurde das evolutiv wichtige Glykolatoxidase (GOX) Enzym gewählt, welches Glykolat zu Glyoxylate im Peroxisom umwandelt. Erzeugte GOX knock-out Mutanten wurden unter verschiedenen CO_2 Bedingungen analysiert und ergaben eine starke Abhängigkeit seitens *C. merolae* von einer funktionierenden Photorespiration unter ambienten CO_2 Bedingungen. Die Ergebnisse hierzu sind in Manuskript II dargestellt: Rademacher N, Kern R, Fujiwara T, Mettler-Altmann T, Miyagishima SY, Hagemann M, Eisenhut M, Weber APM (2016) Photorespiratory glycolate oxidase is essential for survival of the red alga Cyanidioschyzon merolae under ambient CO_2 conditions. Journal of Experimental Botany, in press.

Zusätzlich durchgeführte Analysen zur Identifikation von transkriptionellen Änderungen auf Grund von sich ändernden CO_2 Bedingungen ergaben einen starken Anstieg in der Transkription unter ambienten CO_2 Bedingungen von Genen die an der Photorespiration beteiligt sind. Während meist nur kleine Änderungen im Transkript von Genen gezeigt werden konnten, die in anderen Stoffwechselwegen, wie zum Beispiel dem Energiemetabolismus, involviert sind. Um mögliche Bestandteile eines Kohlenstoff-Konzentrierungs-Mechanismus zu identifizieren, wurden BlastP Analysen und Lokalisierungsstudien durchgeführt, sowie Gene untersucht, die mit photorespiratorischen Genen ko-reguliert sind. Die Analysen ergaben zwei zytosolische α-Carboanhydrasen und einen möglichen Bicarbonat Transporter, welcher unter limitierenden CO_2 Bedingungen verstärkt gebildet wird. Die detaillierten Ergebnisse hierzu sind in Manuskript III beschrieben: Rademacher N, Wrobel T, Rossoni A, Eisenhut M, Kurz S, Bräutigam A, Weber APM: Transcriptional response of the extremophile red algae *Cyanidioschyzon merolae* to changes in CO_2 concentrations.

LITERATUR:

Bauwe H, Hagemann M, Fernie AR. 2010. Photorespiration: players, partners and origin. Trends in Plant Science **15**, 330–336.

Eisenhut M, Ruth W, Haimovich M, Bauwe H, Kaplan A, Hagemann M. 2008. The photorespiratory glycolate metabolism is essential for cyanobacteria and might have been conveyed endosymbiontically to plants. PNAS **105**, 17199–17204.

Eisenhut M, Hocken N, Weber APM. 2015. Plastidial metabolite transporters integrate photorespiration with carbon, nitrogen, and sulfur metabolism. Cell Calcium 58, 98–104

Hagemann M, Fernie AR, Espie GS, Kern R, Eisenhut M, Reumann S, Bauwe H, Weber APM. 2013. Evolution of the biochemistry of the photorespiratory C2 cycle. Plant Biology **15**, 639–647.

Hohmann-Marriott MF, Blankenship RE. 2011. Evolution of photosynthesis. Annu Rev Plant Biol **62**, 515–548.

Rademacher N, Kern R, Fujiwara T, Mettler-Altmann T, Miyagishima SY, Hagemann M, Eisenhut M, Weber APM (2016) Photorespiratory glycolate oxidase is essential for survival of the red alga *Cyanidioschyzon merolae* under ambient CO_2 conditions. Journal of Experimental Botany, in press.

INTRODUCTION

Organisms performing oxygenic photosynthesis, like cyanobacteria, eukaryotic algae and plants, belong to the main biomass producers on earth. They are able to convert inorganic carbon dioxide into organic carbon compounds and oxygen by the usage of light energy, water and mineral nutrients. Thereby, photoautotrophic organisms represent the main source of carbohydrates and their existence is responsible for today's atmospheric oxygen concentration.

1 Functionality of photosynthesis

Photosynthesis describes the process in which light energy is used to incorporate inorganic carbon into organic carbon molecules, like carbohydrates, while water is decomposed and oxygen is created (Hohmann-Marriott and Blankenship, 2011). This process takes place in green organelles, called chloroplasts, which only exist in photosynthetic eukaryotes. Chloroplasts have two envelope membranes, the inner and outer membrane, as well as third membrane system inside the chloroplast that forms the thylakoids (Taiz and Zeiger, 2007). All components of the photosynthetic apparatus are embedded into the thylakoid membranes.

Photosynthesis proceeds in two main reactions. The first one is the light reaction, also called thylakoid reaction, since the photosynthetic apparatus is used to produce high-energy compounds like ATP and NADPH by the generation of a proton gradient over the thylakoid membrane and an electron transfer chain over several complexes (Eberhard *et al.*, 2008). The second one is the carbon fixation reaction, known as Calvin-Benson-Bassham-cycle (CBB), which takes place in the liquid surrounding of the thylakoid membranes, the stroma (Taiz and Zeiger, 2007).

The light reaction is initiated by the capture of light energy by light harvesting antenna proteins that transfer the energy to reaction centers. The Photosystem II uses the transferred light energy to oxidize water and the subsequent release of protons into the thylakoid lumen, the space within the thylakoid membranes. Resulting electrons are transported by the cytochrome b6f complex to the Photosystem I, utilizing an oxidation/ reduction cycle including Plastohydroquinone (PQH_2). The

transferred electrons are used in the Photosystem I to reduce $NADP^+$ to NADPH including ferredoxin (fd) and the flavoprotein ferredoxin-NADP reductase (FNR). The fourth complex, the ATP synthase, exploits the produced proton gradient to generate ATP.

In the subsequent Calvin-Benson-Bassham cycle, the generated ATP and NADPH are consumed for the production of carbohydrates from carbon dioxide CO_2 (Taiz and Zeiger, 2007). The CBB cycle is located in the chloroplast and can be divided in three main reaction parts: Carboxylation, Reduction and Regeneration (Taiz and Zeiger, 2007).

In the carboxylation part the enzyme Ribulose-1,5-bisphosphate Carboxylase/ Oxygenase, short RubisCO, catalyses the carboxylation reaction of the acceptor molecule ribulose-1,5-bisphosphate (RuBP) by the usage of one molecule atmospheric CO_2 to produce two molecules 3- Phosphoglycerate (3-PGA). In subsequent reactions, 3-PGA is reduced by the consumption of ATP and NADPH to Glyceraldehyde-3-phosphate (G3P), a carbohydrate, used for the initial production of sugars and finally starch. The last step of the CCB cycle includes the regeneration of the acceptor molecule RuBP. In total three molecules of CO_2 are needed to produce one molecule of G3P while six molecules NADPH and nine molecules ATP are consumed.

2 Evolution of photosynthetic eukaryotes and increase of atmospheric oxygen

2.1 Increase of atmospheric oxygen

The ancient atmosphere of the earth consisted of methane (CH_4), carbon dioxide (CO_2) and nitrogen (N_2) and all organisms were constrained to perform an anaerobic biochemistry. The evolution of oxygen creating organisms resulted in the accumulation of atmospheric oxygen (O_2) and changed the whole planet and life on it (reviewed in Hohmann-Marriott and Blankenship, 2011).

Increase in atmospheric O_2 up to our today's concentration of 20 % occurred in two main steps. O_2 appeared 2.4 to 2 giga years ago (Gya) on earth with a concentration of 1-2 % and many organisms had to adapt to the new O_2-containing atmosphere by evolution of metabolic processes (Canfield *et al.*, 2006; Raymond and Blankenship, 2008) after this so called "great oxygenation event" (Holland, 2006). The second increase up to todays 20 % atmospheric O_2 concentration occurred 850 mega years ago (Mya) and was the consequence of the appearance of photosynthetic eukaryotes, like algae and lichens, which increased the photosynthetic productivity on earth by their colonization of land mass (reviewed in Hohmann-Marriott and Blankenship, 2011). Overviews of the increase in atmospheric O_2 and the appearance of organisms performing oxidative photosynthesis are given in Figure 1.

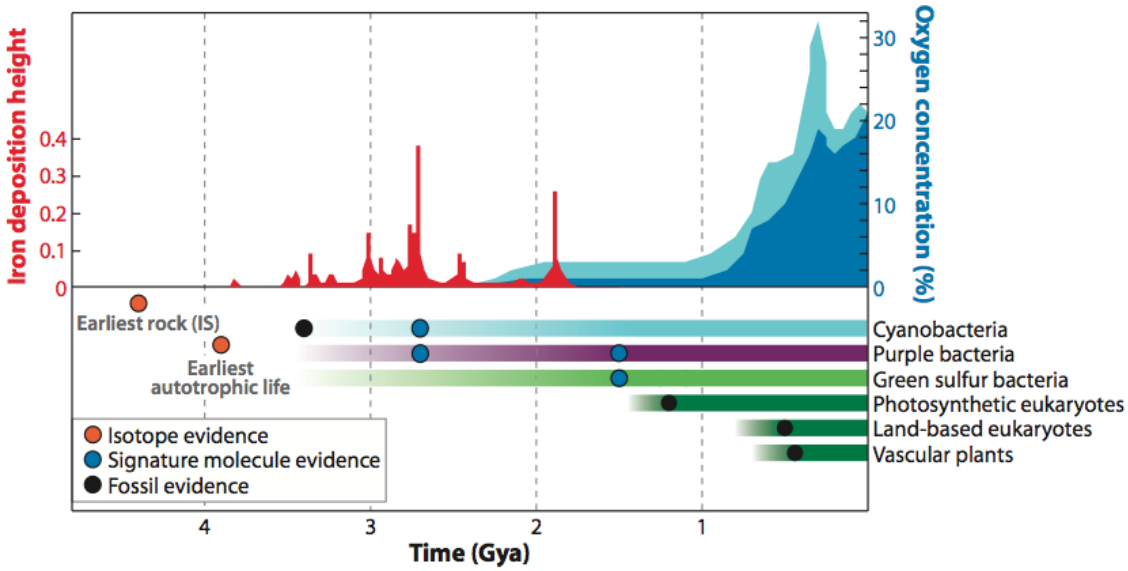

Figure 1: Increase in atmospheric oxygen concentration and appearance of organisms performing oxygenic photosynthesis. Oxygen concentration is shown in blue (minimum concentration: light blue areas, maximum concentration: dark blue areas). Figure is taken from Hohmann-Marriott and Blankenship, 2011.

2.2 Evolution of photosynthetic eukaryotes

The ability of eukaryotes to perform photosynthesis is the consequence of the integration of a cyanobacteria-like progenitor into a eukaryotic host cell, called primary endosymbiosis. The enclosed prokaryote evolved to the chloroplast, the organelle in which photosynthesis takes place (reviewed in Raven and Allen, 2003). The complete integration of the organelle comprised the transfer of most cyanobacterial genome information into the genome of the eukaryotic host cell. To date three ancient lines of photosynthetic eukaryotes are known, including Glaucophytes, Rhodophytes and Chlorophytes (reviewed in Gould *et al.*, 2008). Glaucophytes still show cyanobacterial characteristics like a cyanobacterial peptidoglycan cell wall (Pfanzagl *et al.*, 1996), a carboxysome and a phycobilisome light harvesting complex, which is also used by Rhodophytes (reviewed in Hohmann-Marriott and Blankenship, 2011). Further secondary and tertiary endosymbiotic events, where a photosynthetic eukaryote was integrated into a second eukaryote led to further species as shown **Figure 2** (reviewed in Keeling, 2010).

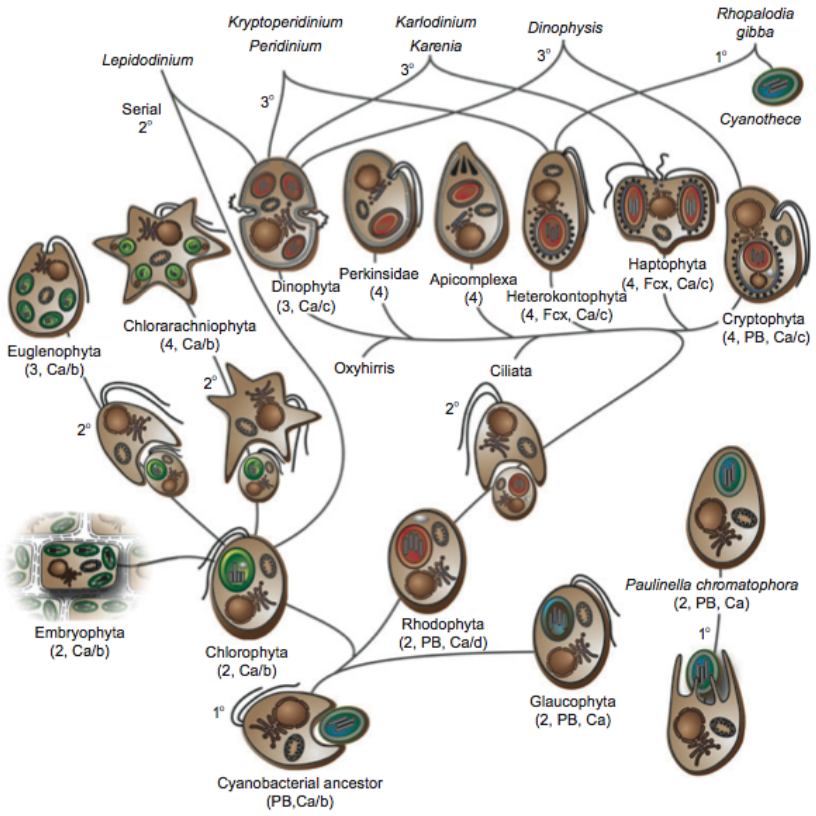

Figure 2: Schematic overview of the evolution of photosynthetic eukaryotes by primary (1°), secondary (2°) and tertiary (3°) endosymbiosis. Chlorophyta, Rhodophyta and Glaucophyta are the result of primary endosymbiosis, where a eukaryotic host cell took up a cyanobacterial ancestor. Figure taken from Gould *et al.*, 2008.

3 Oxygenation reaction of RubisCO and photorespiration

RubisCO initiate the first step of the CBB cycle by the carboxylation of RuBP. The enzyme is one of the most abundant proteins on earth and provides 50 % of the soluble proteins of leaves in plants. This high abundance may be explained by the low catalytic efficiency with a turnover rate of 5 s^{-1} (Tabita *et al.*, 2007). In addition RubisCO is also able to oxygenate RuBP to yield one molecule 3-PGA and one molecule 2-Phosphoglycolate (2-PG). The second molecule is toxic to the organism and has to be recycled by 3-PGA under energy consumption. The initial steps of RubisCO are identical between oxygenation and carboxylation reaction, but the produced enediolate intermediate can react with CO_2 or O_2. This step and the following hydration and cleavage steps are irreversible reactions (Savir *et al.*, 2010). The efficiency of RubisCO is therefore not only determined by reaction velocity, but

also by the specificity to discriminate between O_2 and CO_2. Enhancing the specificity of RubisCO would minimize the loss of carbon and might increase the crop yield (reviewed in Tabita *et al.*, 2008).

3.1 Diversity of RubisCO types

Today three forms of RubisCO (I, II and III) are known which perform the carboxylation reaction of RuBP. A fourth form (IV) is described as a RubisCO-like protein (RLP). RubisCO exist in phototrophic and chemoautotrophic organisms. The most abundant form is RubisCO I that exists in higher plants, eukaryotic algae, cyanobacteria and proteobacteria. RubisCO I is divided in four subclasses IA, IB, IC and ID (Tabita, 1999). The protein set-up (L_8S_8) consists of eight large subunits (50 kDA) that form as four dimers the catalytic core. Top and bottom are covered with four small subunits each (15 kDA). Second form, RubisCO II was found in different types of prokaryota and dinoflagellates (reviewed in Tabita *et al.*, 2008). The structure ($(L_2)_x$) is formed by large subunit dimers, whereby the large subunit shows 30 % sequence identity with the RubisCO I large subunit (Tabita, 1999). RubisCO II offers a worse discrimination specificity between CO_2 and O_2 compared to RubisCO I and forms I and II exist often in parallel in one organism, indicating that RubisCO II is not the major form (reviewed in Tabita *et al.*, 2008). The third RubisCO form (RubisCO III) is archaeal and catalyses the removal of RuBP produced during Purine/Pyrenoide metabolism (Archaea *et al.*, 2004; Sato *et al.*, 2007). This form is highly oxygen sensitive, respectively shows a high affinity to O_2 and exists in anaerobic extremophiles (Finn and Tabita, 2003; Kreel and Tabita, 2007). The fourth clade includes RubisCO-like proteins (RLP) and can be found in organisms that not assimilate CO_2 via the CBB cycle. RLP does not show the catalytic activity of RubisCO forms I to III. The RLP enzyme is part of the Methionine salvage pathway where it catalyses the enolization of the RuBP analog 2,3-diketo-5-methylthiopentyl-1-P, which is very similar to the RubisCO reaction (Ashida *et al.*, 2003; Imker *et al.*, 2007). Furthermore RLP are thought to play a role in thiosulphate oxidation (Hanson and Tabita, 2001, 2003).

3.2 Improvement of RubisCO efficiency

The analysis of 28 different RubisCO enzymes (RubisCO I) including organisms from non green algae, C3 plants, C4 plants, green algae, photosynthetic bacteria and cyanobacteria revealed, that an increase in the specificity to discriminate between CO_2 and O_2 always goes along with an decrease in velocity (Savir *et al.*, 2010). RubisCO enzymes from cyanobacteria for example perform a very fast carboxylation reaction, but exhibit therefore a low specificity. In contrast non green algae, like the extremophile red algae *Galdieria sulphuraria*, use a very specific RubisCO, which performs a slow carboxylation reaction (Savir *et al.*, 2010). RubisCO is thought to be optimally adapted to the different environments, why genetic engineering would only lead to a small improvement in velocity and specificity (Tcherkez *et al.*, 2006). More promising is the focus on the reduction of the 2-PG recycling pathway, known as photorespiration, and the mechanisms to concentrate carbon around RubisCO (Savir *et al.*, 2010; Maurino and Weber, 2012; Peterhansel *et al.*, 2013).

3.3 Photorespiration

Photorespiration allows organism to recycle toxic 2-PG produced by oxygenation reaction of RubisCO to 3-PGA, which can re-enter the CBB cycle (reviewed in Bauwe *et al.*, 2010). This pathway exists in all oxygen-producing photosynthetic organisms. Suggested functions are next to the removal of inhibitory 2-PG (Eisenhut *et al.*, 2008), the minimization of carbon loss due to 2-PG generation (Bauwe *et al.*, 2010), the consumption of energy in the form of ATP and NADPH to avoid photoinhibition (Kozaki and Takeba, 1996) and the production of amino acids as serine and glycine (Bauwe *et al.*, 2010). The photorespiratory cycle involves energy consuming enzymatic steps in three organelles: the chloroplast, the peroxisome and the mitochondrion (Figure 3). Photorespiration is initiated by the oxygenation reaction of RubisCO resulting in the formation of one molecule 3-PGA and one molecule 2-PG out of one molecule RuBP and O_2. To recycle the acceptor molecule RuBP and to detoxify 2-PG, 2-PG phosphatase (PGP) catalyses the production of glycolate, which is further converted to glyoxylate by the glycolate oxidase (GOX)

in the peroxisome. The generated side-product hydrogen peroxide (H_2O_2) has to be removed by a catalase converting one molecule H_2O_2 into one molecule water (H_2O) and ½ molecule O_2. In the subsequent process, one molecule of glycine is generated out of one molecule glyoxylate by a glutamate-glyoxylate aminotransferase (GGT) and a serine-glyoxylate aminotransferase (SGT). In the mitochondrion, the collaboration of a glycine decarboxylase (GDC) and a serine hydroxymethlytransferase (SHMT) yield one molecule serine out of two molecules glycine. Back in the peroxisome, serine is reduced to hydroxypyruvate by the activity of SGT. Thereby the released amino group is used for the production of glycine out of glyoxylate. The following conversion of hydroxypyruvate to glycerate can either be performed by a peroxisomal hydroxypyruvate reductase (HPR1) or its cytosolic isoform (HPR2). In the final step of photorespiration, a glycerate-3-kinase (GLYK) catalyses the mitochondrial reaction of glycerate to 3-PGA, which can re-enter the CBB cycle.

The photorespiratory cycle is closely connected to the nitrogen cycle of the plant. Generated ammonia (NH_3) during the glycine to serine conversion in the mitochondrion enters the glutamine: glutamate cycle in the chloroplast, providing glutamate for glycine production out of glyoxylate (Bauwe *et al.*, 2010). The high flux of metabolites over three different organelles demand for a high number of transporters regulating the metabolite flux over the membrane (reviewed in Eisenhut and Hocken *et al.*, 2015). Today, only three plastidic transporters are known, including the PLGG1 transporter, maintaining the glycolate glycerate transport over the chloroplast membrane (Pick *et al.*, 2013). The DIT 1 and 2 transporters perform the 2-oxoglutarate (2-OG) and glutamate in exchange with malate over the chloroplast membrane (Menzlaff and Flügge, 1993; Weber and Flügge, 2002). A detailed overview of photorespiration, required known and unknown plastididal transporters and the connection to nitrogen and sulfur metabolism is given in the review “Plastidial metabolite transporters integrate photorespiration with carbon, nitrogen, and sulfur metabolism“ by M. Eisenhut and N. Hocken (Cell Calcium, 2014) attached to this work.

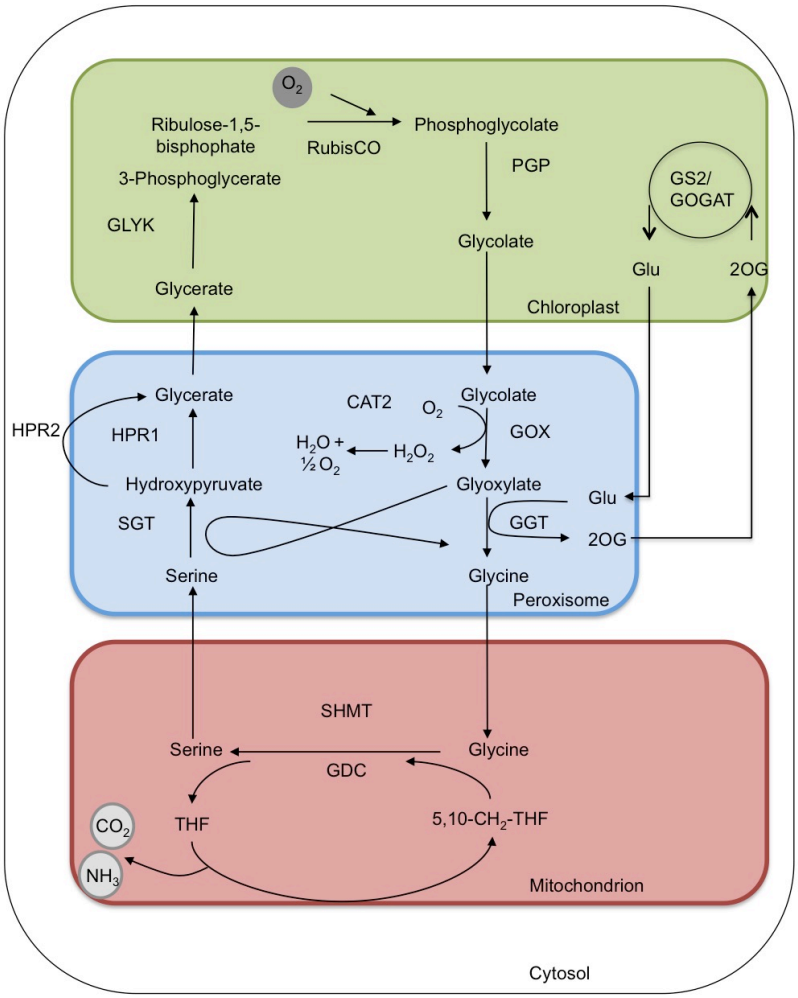

Figure 3: Schematic overview of the photorespiratory pathway. Enzymes involved in detoxification of 2-PG are: 2-PG phosphatase (PGP), Glycolate oxidase (GOX), Catalase 2 (CAT2), Glutamate:glyoxylate reductase (GGT), Serine hydroxymethlytransferase (SHMT), Glycine decarboxylase (GDC), peroxisomal Hydroxypyruvate reductase (HPR1), cytosolic Hydroxypyruvate reductase (HPR2), Glycerate 3-kinase (GLYK), Ribulose-1,5-bisphosphat carboxylase/ oxygenase (RubisCO), ferredoxin- dependent Glutamate synthase (GOGAT) and Glutamine synthease (GS).

3.3.1 Evolution of Glycolate oxidase (GOX)

Phylogenetic analysis of enzymes involved in the photorespiratory pathway and the acquisition of different carbon concentration mechanisms suggest a coevolution of photorespiration and oxygenic photosynthesis in ancient cyanobacteria 2700 Mya ago (Kern *et al.*, 2011; Bauwe *et al.*, 2012; Hagemann *et al.*, 2016). Most photorespiratory proteins have a cyanobacterial or a α-proteobacterial origin (Bauwe *et al.*, 2012). The mixed ancestry of enzymes from chloroplastidial and mitochondrial ancestors led to the assumption of a cyanobacterial origin for the RubisCO and GLYK enzyme and a proteobacterial origin of the GDC proteins, SHMT, HPR and GGT (Hackenberg *et al.*, 2011; Kern *et al.*, 2011, 2013).

The conversion of glycolate to glyoxylate during photorespiration can be catalyzed by two phylogenetic unrelated enzymes: a glycolate dehydrogenase (GlcD) in cyanobacteria and chlorophyta or by a glycolate oxidase (GOX) in all algae, with exclusion to chlorophyta, and plants (reviewed in Esser *et al.*, 2014). The NADPH dependent GlcD enzyme in cyanobacteria and chlorophyta is part of the mitochondrial glycolate pathway, which exhibits the advantage of ATP production (reviewed in Esser *et al.,* 2014). In contrast, the mitochondrial detoxification of 2-PG offers a low capacity compared to the plant-like photorespiratory cycle and leads to a glycolate excretion under high glycolate production conditions (Stabenau and Winkler, 2005). A low rate of photorespiration and glycolate synthesis is reached by a carbon concentrating mechanism in cyanobacteria and chlorophyta that increases the carbon concentration around the RubisCO enzyme to avoid the oxidation reaction (Giordano *et al.*, 2005; Esser *et al.*, 2014).

In contrast, the peroxisomal GOX shows a high capacity to handle large rates of glycolate synthesis, but the conversion of glycolate to glyoxylate is coupled to the production of hydrogen peroxide that has to be removed by a catalase (Hageman *et al.,* 2013). The evolution of a peroxisomal GOX instead of a mitochondrial GlcD is forced by the increased atmospheric oxygen conditions during the appearance of land plants (Esser *et al.*, 2014).

Two hypothesis exist about the phylogenetic origin of the GOX enzyme, whereat it is either of cyanobacterial origin (Eisenhut *et al.*, 2008; Hackenberg *et al.*, 2011; Kern *et al.*, 2011) or derived from an ancient eukaryotic enzyme (Esser *et al.*, 2014).

The first hypothesis is based on the idea that the whole photosynthetic machinery and the photorespiratory cycle in Glaucophytes, Rhodophytes and Chlorophytes derived from cyanobacteria (Eisenhut *et al.*, 2008; Bauwe *et al.*, 2012). Phylogenetic studies including the genome of N_2-fixing cyanobacteria, which are closely related to the primary endosymbiont, and green algae, revealed genes for a GlcD and a plant-like GOX protein in cyanobacteria (Kern *et al.*, 2011). Further BlastP studies of the photorespiratory Arabidopsis GOX2 protein, identified two phylogenetic clades with GOX-like sequences in plantae, algae and cyanobacteria in one clade and with bacterial proteins with a known lactate oxidase (LOX) function in the second clade (Hackenberg *et al.*, 2011). GOX and LOX proteins have a close relationship including a very similar structure of the active site with only few alterations (Hackenberg *et al.*, 2011). The substrates are in both cases short-chain hydroxyl acids and FMN is used as a cofactor (Lindqvist and Brändén, 1989; Maeda-Yorita *et al.*, 1995). The authors conclude, that N_2-fixing cyanobacteria with a low photorespiratory rate due to a carbon concentrating mechanism, used the GlcD with a lower catalytic efficiency for Glycolate detoxification and kept the oxygen consuming LOX protein to protect their nitrogenase from O_2 inactivation (Hackenberg *et al.*, 2011; Kern *et al.*, 2011). The cyanobacterial LOX specified to a GOX enzyme involved in photorespiration after the last common ancestor of the green algae Chlamydomonas and land plant (Hackenberg *et al.*, 2011).

The second hypothesis is based on phylogenetic analysis of the superior gene family of animal and plant GOX enzymes: the (L)-2- hydroxyacid-oxidases ((L)-2-HAOX). The results indicate similar substrate specificity for plant and mammalian (L)-2-HAOX proteins and the authors conclude that all (L)-2-HAOX proteins derived from a common eukaryotic ancestors, where the proteins were already located to the peroxisome due to the existence of a peroxisomal targeting sequence (PTS1) in almost all plant, animal and fungi (L)-2-HAOX proteins. Findings of a lactate oxidase (LOX) in chlorophyta with similar kinetic properties of a cyanobacterial LOX but an unknown function are explained by differential gene loss in the chlorophyta versus the glaucophyta, rhodophyta and charophyta. Chlorophyta retained the LOX gene derived by endosymbiontic gene transfer, where the gene was first encoded on the endosymbiontic genome (cyanobacteria) and then transferred to the host genome. Additionally chlorophyta lost the ancestral eukaryotic (L)-2-

HAOX gene. Glaucophyta, Rhodophyta and Charophyta lost the cyanobacterial LOX gene, but retained the eukaryotic (L)-2-HAOX gene that evolved to the photorespiratory GOX.

A schematic overview of the hypothesis regarding the origin of the photorespiratory GOX is given in Figure 4.

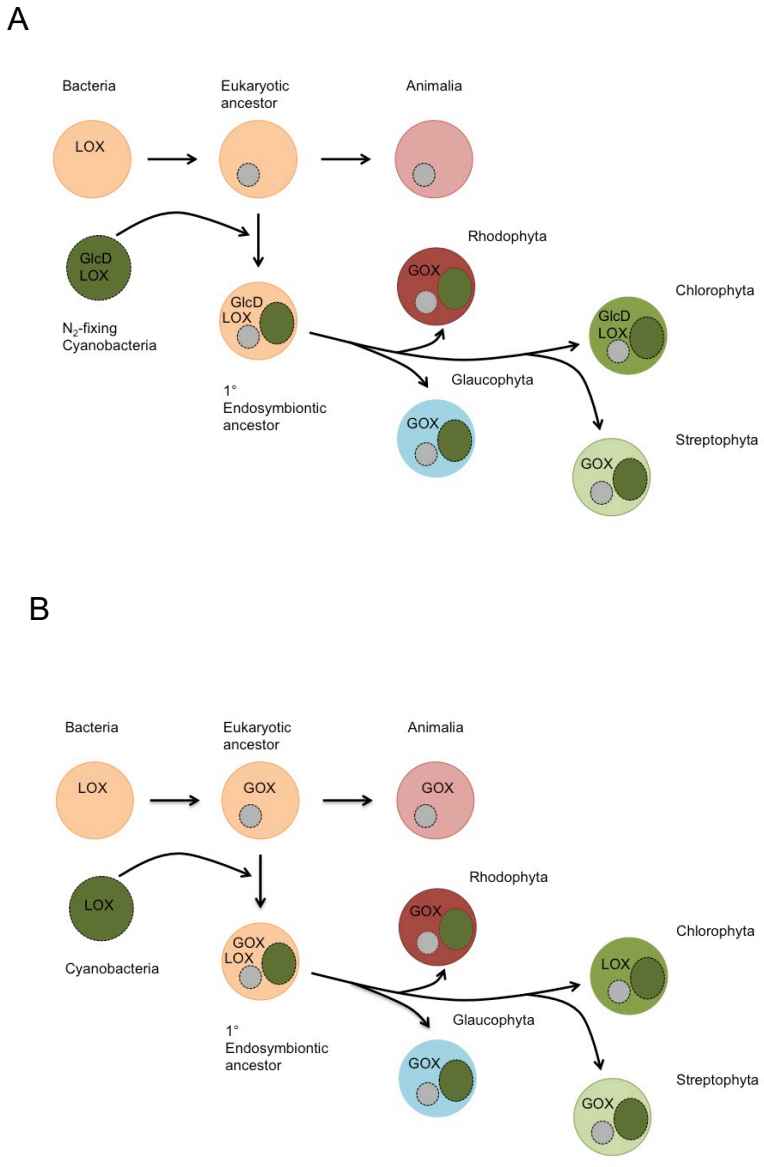

Figure 4: Two different models explaining the phylogenetic origin of the Glycolate oxidase. A: The GOX protein is of cyanobacterial origin and derived from a Lactate oxidase (Eisenhut *et al.*, 2008; Hackenberg *et al.*, 2011; Kern *et al.*, 2011). B: The GOX protein derived from an eukaryotic ancestor and the LOX protein was lost during evolution of Rhodophyta, Glaucophyta and Streptophyta (Esser *et al.*, 2014). Figure modified from Esser *et al.*, 2014.

4 *Cyanidioschyzon merolae* – a red algae model organism

To date only little knowledge exists about the importance of the photorespiratory pathway in red algae. A well-characterized model organism for red algae is *Cyanidioschyzon merolae (C. merolae)*, which is part of the *Cyanidiophyceae*, a group of ancient thermo acidic pre-Rhodophytes (Seckbach, 1995). *Cyanidiophyceae* are composed of three genera containing several species: *Cyanidioschyzon*, *Cyanidium* and *Galdieria* (Seckbach, 1995). *Cyanidioschyzon* is the most original genera with mixed characteristics of cyanobacteria and archaebacteria, a very simple cell structure and the smallest amount of nuclear and chloroplast DNA (Seckbach, 1995; Nozaki *et al.*, 2007). *Cyanidium* offers also a simple cell structure but shows more progressive characteristics (Seckbach, 1995). *Galderia* is the most evolutionary developed genera, which is very close to unicellular red algae and has typical advanced eukaryotic characteristics (Seckbach, 1995). The natural habitat of *Cyanidiophycean* consists of a very high concentration of CO_2, an acidic pH of two to four, high temperatures (up to 57 °C) and only low levels of atmospheric O_2 (reviewed in Seckbach, 1994).

C. merolae is a primitive, photosynthetic eukaryotic organism and often used for studies dealing with the evolution of eukaryotic cells, with a special focus on the evolution of the chloroplast, organelle division, photosynthesis and its related pathways (Zenvirth *et al.*, 1985; Nozaki *et al.*, 2003; Nishida *et al.*, 2004).

C. merolae lives in acidic hot springs and was found near the fumaroles of Campi Flegrei in south Italy (De Luca *et al.*, 1978). The cell has a very simple architecture and is only 2 µm in diameter (reviewed Matsuzaki *et al.*, 2004). So far no cell wall could be detected for these organism (Kuroiwa *et al.*, 1994). The cytoplasm contains one chloroplast, one peroxisome, one mitochondrion and one nucleus (Kuroiwa *et al.*, 1994). The nucleus offers a diameter of 0.6 µm and is surrounded by a nuclear envelope with nuclear pores (Kuroiwa *et al.*, 1994). The chloroplast includes five to ten concentric thylakoid membrane excrescences that exhibit phycobilisomes as light harvesting structures (reviewed in Takahashi *et al.*, 1993). The phycobilisomes contain pigments such as phycocyanin, phycoerythrin and chlorophyll, for that reason *C. merolae* appear blue-green in color (reviewed in Takahashi *et al.*, 1993). The genome is rather small (16 546 747 nucleotides) and distributed among 20

chromosomes, including 5 331 genes, of which 86% are expressed (Matsuzaki *et al.*, 2004; Nozaki *et al.*, 2007). Only 26 genes contain intron structures (Matsuzaki *et al.*, 2004). Next to the nuclear genome, the complete plastid and mitochondrion genome is fully sequenced (Ohta *et al.*, 1998, 2003; Matsuzaki *et al.*, 2004; Nozaki *et al.*, 2007). A schematic overview of the genome size and gene numbers is given in Figure 5. Methods for targeted gene knock-out and transient expression in *C. merolae* are available (Ohnuma *et al.*, 2008; Imamura *et al.*, 2010; Watanabe *et al.*, 2011).

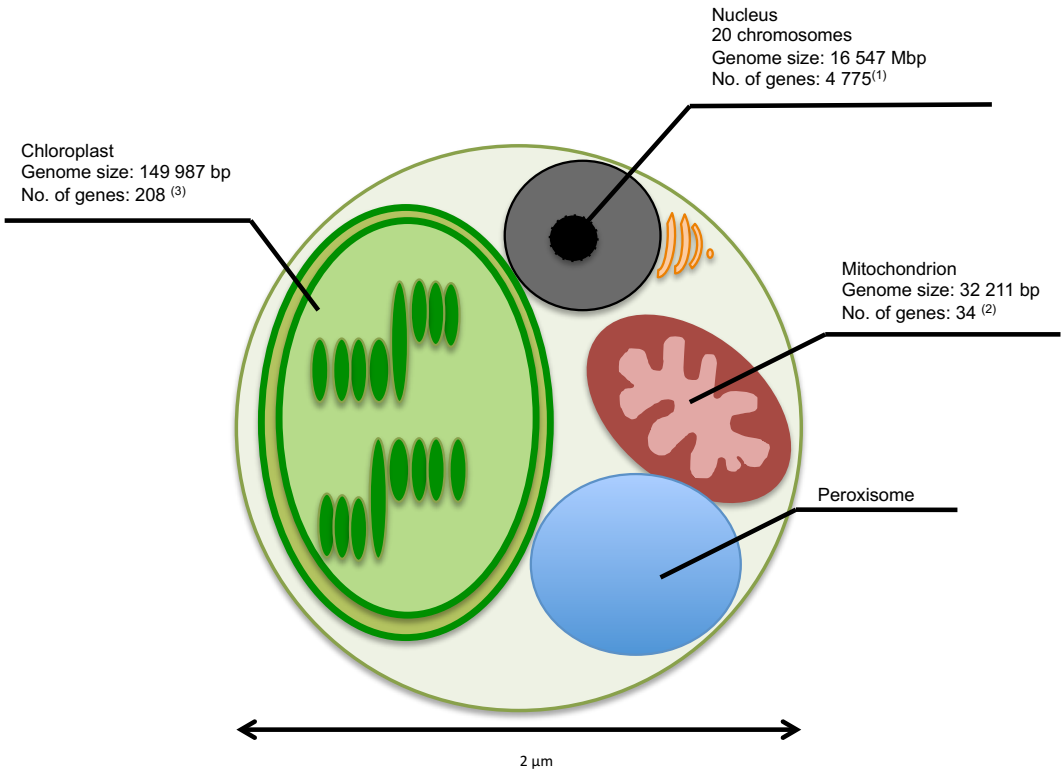

Figure 5: Schematic overview of a *Cyanidioschyzon merolae* cell. Shown are genome size and gene number of the nucleus, the plastid and the mitochondrion. Data taken from Nozaki *et al.*, 2007 (1), Ohta *et al.*, 1998 (2) and Ohta *et al.*, 2003 (3).

REFERENCES:

Archaea M, Finn MW, Tabita FR. 2004. Modified pathway to synthesize Ribulose 1,5-bisphosphate in methanogenic archaea. Journal of bacteriology **186**, 6360–6366.

Ashida H, Saito Y, Kojima C, Kobayashi K, Ogasawara N, Yokota A. 2003. A functional link between RuBisCO-like protein of Bacillus and photosynthetic RuBisCO. Science **302**, 286–290.

Bauwe H, Hagemann M, Fernie AR. 2010. Photorespiration: players, partners and origin. Trends in Plant Science **15**, 330–336.

Bauwe H, Hagemann M, Kern R, Timm S. 2012. Photorespiration has a dual origin and manifold links to central metabolism. Current Opinion in Plant Biology **15**, 269–275.

Canfield DE, Rosing MT, Bjerrum C. 2006. Early anaerobic metabolisms. Philosophical transactions of the Royal Society of London. Series B, Biological sciences **361**, 1819–1834; discussion 1835–1836.

Eberhard S, Finazzi G, Wollman F-A. 2008. The dynamics of photosynthesis. Annual review of genetics **42**, 463–515.

Eisenhut M, Hocken N, Weber APM. 2015. Plastidial metabolite transporters integrate photorespiration with carbon, nitrogen, and sulfur metabolism. Cell Calcium **58**, 98–104.

Eisenhut M, Ruth W, Haimovich M, Bauwe H, Kaplan A, Hagemann M. 2008. The photorespiratory glycolate metabolism is essential for cyanobacteria and might have been conveyed endosymbiontically to plants. PNAS **105**, 17199–17204.

Esser C, Kuhn A, Groth G, Lercher MJ, Maurino VG. 2014. Plant and animal glycolate oxidases have a common eukaryotic ancestor and convergently duplicated to evolve long-chain 2-hydroxy acid oxidases. Molecular Biology and Evolution **31**, 1089–1101.

Finn MW, Tabita FR. 2003. Synthesis of Catalytically Active Form III Ribulose 1 , 5-Bisphosphate Carboxylase / Oxygenase in Archaea. Journal of bacteriology **185**, 3049–3059.

Giordano M, Beardall J, Raven JA. 2005. CO_2 Concentrating Mechanisms in Algae: Mechanisms , Environmental Modulation , and Evolution. Annual Review of Plant Biology. **56**, 99-131.

Gould SB, Waller RF, McFadden GI. 2008. Plastid Evolution. Annual Review of Plant Biology **59**, 491–517.

Hackenberg C, Kern R, Hüge J, Stal LJ, Tsuji Y, Kopka J, Shiraiwa Y, Bauwe H, Hagemann M. 2011. Cyanobacterial lactate oxidases serve as essential partners in N2 fixation and evolved into photorespiratory glycolate oxidases in plants. The Plant cell **23**, 2978–90.

Hagemann M, Fernie AR, Espie GS, Kern R, Eisenhut M, Reumann S, Bauwe H, Weber APM. 2013. Evolution of the biochemistry of the photorespiratory C2 cycle. Plant Biology **15**, 639–647.

Hagemann M, Kern R, Maurino VG, Hanson DT, Weber APM, Sage RF, Bauwe H. 2016. Evolution of photorespiration from cyanobacteria to land plants, considering protein phylogenies and acquisition of carbon concentrating mechanisms. Journal of Experimental Botany, in press.

Hanson TE, Tabita FR. 2001. A ribulose-1,5-bisphosphate carboxylase/oxygenase (RubisCO)-like protein from Chlorobium tepidum that is involved with sulfur metabolism and the response to oxidative stress. Proceedings of the National Academy of Sciences of the United States of America **98**, 4397–4402.

Hanson TE, Tabita FR. 2003. Insights into the stress response and sulfur metabolism revealed by proteome analysis of a *Chlorobium tepidum* mutant lacking the Rubisco-like protein. Photosynthesis Research **78**, 231–248.

Hohmann-Marriott MF, Blankenship RE. 2011. Evolution of photosynthesis. Annu Rev Plant Biol **62**, 515–548.

Holland HD. 2006. The Oxygenation of the Atmosphere and Oceans. Philosophical transactions of the Royal Society of London. Series B, Biological sciences **361**, 903–915.

Imamura S, Terashita M, Ohnuma M, *et al.* 2010. Nitrate assimilatory genes and their transcriptional regulation in a unicellular red alga *Cyanidioschyzon merolae*: Genetic evidence for nitrite reduction by a sulfite reductase-like enzyme. Plant and Cell Physiology **51**, 707–717.

Imker HJ, Fedorov AA, Fedorov E V., Almo SC, Gerlt JA. 2007. Mechanistic diversity in the RuBisCO superfamily: The 'enolase' in the methionine salvage pathway in *Geobacillus kaustophilus*. Biochemistry **46**, 4077–4089.

Keeling PJ. 2010. The endosymbiotic origin, diversification and fate of plastids.

Philosophical transactions of the Royal Society of London. Series B, Biological sciences **365**, 729–48.

Kern R, Bauwe H, Hagemann M. 2011. Evolution of enzymes involved in the photorespiratory 2-phosphoglycolate cycle from cyanobacteria via algae toward plants. Photosynthesis Research **109**, 103–114.

Kern R, Eisenhut M, Bauwe H, Weber a PM, Hagemann M. 2013. Does the *Cyanophora paradoxa* genome revise our view on the evolution of photorespiratory enzymes? Plant biology **15**, 759–768.

Kozaki A, Takeba G. 1996. Photorespiration protects C3 plants from photooxidation. Nature **384**, 557–560.

Kreel NE, Tabita FR. 2007. Substitutions at methionine 295 of *Archaeoglobus fulgidus* ribulose-1,5-bisphosphate carboxylase/oxygenase affect oxygen binding and CO_2/O_2 specificity. Journal of Biological Chemistry **282**, 1341–1351.

Kuroiwa T, Kawazu T, Takahashi H, Suzuki K, Ohta N, Kuroiwa H. 1994. Comparison of Ultrastructures between the Ulta-small Eukaryote *Cyanidioschyzon merolae* and *Cyanidium caldarium*. Cytologia **59**, 149–158.

Lindqvist Y, Brändén CI. 1989. The active site of spinach glycolate oxidase. Journal of Biological Chemistry **264**, 3624–3628.

De Luca P, Taddei R, Barano L. 1978. *Cyanidioschyzon merolae*: a new alga of thermal acidic environments. Webbia **33**, 264–268.

Maeda-Yorita K, Aki K, Sagai H, Misaki H, Massey V. 1995. L-lactate oxidase and L-lactate monooxygenase: Mechanistic variations on a common structural theme. Biochimie **77**, 631–642.

Matsuzaki M, Misumi O, Shin-I T, *et al.* 2004. Genome sequence of the ultrasmall unicellular red alga *Cyanidioschyzon merolae* 10D. Nature **428**, 653–657.

Maurino VG, Weber APM. 2012. Engineering photosynthesis in plants and synthetic microorganisms. Journal of Experimental Botany **64**, 743–751.

Menzlaff E, Flügge UI. 1993. Purification and functional reconstitution of the 2-oxoglutarate/malate translocator from spinach chloroplasts. Biochim. Biophys. Acta **1147**, 13–18.

Nishida K, Misumi O, Yagisawa F, Kuroiwa H, Nagata T, Kuroiwa T. 2004. Triple Immunofluorescent Labeling of FtsZ, Dynamin, and EF-Tu Reveals a Loose Association Between the Inner and Outer Membrane Mitochondrial Division

Machinery in the Red Alga *Cyanidioschyzon merolae*. Journal of Histochemistry and Cytochemistry **52**, 843–849.

Nozaki H, Matsuzaki M, Takahara M, Misumi O, Kuroiwa H, Hasegawa M, Shin-i T, Kohara Y, Ogasawara N, Kuroiwa T. 2003. The Phylogenetic Position of Red Algae Revealed by Multiple Nuclear Genes from Mitochondria-Containing Eukaryotes and an Alternative Hypothesis on the Origin of Plastids. Journal of Molecular Evolution **56**, 485–497.

Nozaki H, Takano H, Misumi O, *et al.* 2007. A 100%-complete sequence reveals unusually simple genomic features in the hot-spring red alga *Cyanidioschyzon merolae*. BMC Biology **5**, 28.

Ohnuma M, Yokoyama T, Inouye T, Sekine Y, Tanaka K. 2008. Polyethylene glycol (PEG)-mediated transient gene expression in a red alga, *Cyanidioschyzon merolae* 10D. Plant and Cell Physiology **49**, 117–120.

Ohta N, Matsuzaki M, Misumi O, Miyagishima SY, Nozaki H, Tanaka K, Shin-i T, Kohara Y, Kuroiwa T, Shin IT. 2003. Complete sequence and analysis of the plastid genome of the unicellular red alga Cyanidioschyzon merolae. DNA Research **10**, 67–77.

Ohta N, Sato N, Kuroiwa T. 1998. Structure and organization of the mitochondrial genome of the unicellular red alga *Cyanidioschyzon merolae* deduced from the complete nucleotide sequence. Nucleic Acids Research **26**, 5190–5198.

Peterhansel C, Krause K, Braun H, Espie GS, Fernie AR, Hanson DT, Keech O, Maurino VG, Mielewczik M, Sage RF. 2013. Engineering photorespiration: current state and future possibilities. Plant biology **15**, 754–8.

Pfanzagl B, Zenker A, Pittenauer E, Allmaier G, Martinez-Torrecuadrada J, Schmid ER, De Pedro MA, Löffelhardt W. 1996. Primary structure of cyanelle peptidoglycan of *Cyanophora paradoxa*: A prokaryotic cell wall as part of an organelle envelope. Journal of Bacteriology **178**, 332–339.

Pick TR, Bräutigam A, Schulz MA, Obata T, Fernie AR, Weber APM. 2013. PLGG1, a plastidic glycolate glycerate transporter, is required for photorespiration and defines a unique class of metabolite transporters. Proceedings of the National Academy of Sciences **110**, 3185–3190.

Raven J, Allen JF. 2003. Genomics and chloroplast evolution: what did cyanobacteria do for plants? Genome biology **4**, 209.

Raymond J, Blankenship RE. 2008. The origin of the oxygen-evolving complex. Coordination Chemistry Reviews **252**, 377–383.

Sato T, Atomi H, Imanaka T. 2007. Archaeal type III RuBisCOs function in a pathway for AMP metabolism. Science **315**, 1003–1006.

Savir Y, Noor E, Milo R, Tlusty T. 2010. Cross-species analysis traces adaptation of Rubisco toward optimality in a low-dimensional landscape. Proceedings of the National Academy of Sciences of the United States of America **107**, 3475–3480.

Seckbach J. 1994. Evolutionary Pathways and Enigmatic Algae: *Cyanidium caldarium* (Rhodophyta) and Related Cells. In: Seckbach J, ed. Dordrecht: Springer Netherlands, 99–112.

Seckbach J. 1995. The First Eukaryotic Cells - Acid Hot-Spring Algae. Journal of Biological Physics **20**, 335–345.

Stabenau H, Winkler U. 2005. Glycolate metabolism in green algae. Physiologia Plantarum **123**, 235–245.

Tabita FR. 1999. Microbial ribulose 1,5-bisphosphate carboxylase/oxygenase: A different perspective. Photosynthesis Research **60**, 1–28.

Tabita FR, Hanson TE, Li H, Satagopan S, Singh J, Chan S. 2007. Function, structure, and evolution of the RubisCO-like proteins and their RubisCO homologs. Microbiology and molecular biology reviews **71**, 576–99.

Tabita FR, Hanson TE, Satagopan S, Witte BH, Kreel NE. 2008. Phylogenetic and evolutionary relationships of RubisCO and the RubisCO-like proteins and the functional lessons provided by diverse molecular forms. Philosophical transactions of the Royal Society of London. Series B, Biological sciences **363**, 2629–2640.

Taiz L, Zeiger E. 2007. *Plant Physiology*. Springer Verlag.

Takahashi H, Suzuki K, Ohta N, Suzuki T, Takano H, Kawano S, Kuroiwa T. 1993. An electrophoretic karyotype of *Cyanidioschyzon merolae*. Cytologia **58**, 477–482.

Tcherkez GGB, Farquhar GD, Andrews TJ. 2006. Despite slow catalysis and confused substrate specificity, all ribulose bisphosphate carboxylases may be nearly perfectly optimized. Proceedings of the National Academy of Sciences of the United States of America **103**, 7246–51.

Watanabe S, Ohnuma M, Sato J, Yoshikawa H, Tanaka K. 2011. Utility of a GFP reporter system in the red alga *Cyanidioschyzon merolae*. The Journal of

general and applied microbiology **57**, 69–72.

Weber A, Flügge U-I. 2002. Interaction of cytosolic and plastidic nitrogen metabolism in plants. Journal of Experimental Botany **53**, 865–874.

Zenvirth D, Volokita M, Kaplan A. 1985. Photosynthesis and inorganic carbon accumulation in the acidophilic alga *Cyanidioschyzon merolae*. Plant Physiology **77**, 237–239.

AIM OF THE THESIS

The photorespiratory pathway originated from cyanobacteria and was adopted by photosynthetic eukaryotes after the integration of a cyanobacterial ancestor into a eukaryotic host cell, known as endosymbiosis (Eisenhut *et al.,* 2008). Studying the photorespiratory metabolism in eukaryotic algae helps to understand the evolutionary steps between the metabolic pathway in cyanobacteria and in plants. The red algal model organism *Cyanidioschyzon merolae* is a primitive, photosynthetic eukaryote in close evolutionary distance to cyanobacteria (Seckbach*,* 1995). The natural habitats of this organism are acidic hot springs results in a high concentration of carbon dioxide (CO_2) in the aqueous phase. Therefore, only a minor importance of photorespiratory metabolism was expected (reviewed in Seckbach, 1994). However, a BlastP analysis revealed that the complete set of enzymes involved in photorespiration is encoded in the genome of *C. merolae*. Interestingly, the photorespiratory glycolate to glyoxylate conversion was supposed to be performed by a glycolate oxidase (GOX) instead of a glycolate dehydrogenase. The employment of a GOX rather than a glycolate dehydrogenase is typical for organisms with high photorespiratory flux (Hackenberg *et al.,* 2011; Kern *et al*., 2011).

The aim of this thesis was to investigate the photorespiratory metabolism in the model red alga *C. merolae* to gain a more detailed insight into the significance and evolution of the photorespiratory metabolism in red algae. Therefore, objectives of this thesis were first to study the general importance of photorespiration in extremophile red algae by the generation and comparative physiological analysis of a GOX knock-out mutant under photorespiratory and non-photorespiratory conditions. The second object was to study changes in gene expression in *C. merolae* as a reaction to a decrease in CO_2 with a special focus on possible compensation mechanisms to deal with the reduction of inorganic carbon.

REFERENCES:

Eisenhut M, Ruth W, Haimovich M, Bauwe H, Kaplan A, Hagemann M. 2008. The photorespiratory glycolate metabolism is essential for cyanobacteria and might have been conveyed endosymbiontically to plants. PNAS **105**, 17199–17204.

Hackenberg C, Kern R, Hüge J, Stal LJ, Tsuji Y, Kopka J, Shiraiwa Y, Bauwe H, Hagemann M. 2011. Cyanobacterial lactate oxidases serve as essential partners in N2 fixation and evolved into photorespiratory glycolate oxidases in plants. The Plant Cell **23**, 2978–90.

Kern R, Bauwe H, Hagemann M. 2011. Evolution of enzymes involved in the photorespiratory 2-phosphoglycolate cycle from cyanobacteria via algae toward plants. Photosynthesis Research **109**, 103–114.

Seckbach J. 1994. Evolutionary Pathways and Enigmatic Algae: *Cyanidium caldarium* (Rhodophyta) and Related Cells. In: Seckbach J, ed. Dordrecht: Springer Netherlands, 99–112.

Seckbach J. 1995. The First Eukaryotic Cells - Acid Hot-Spring Algae. Journal of Biological Physics **20**, 335–345.

MANUSCRIPT I

Plastidial metabolite transporters integrate photorespiration with carbon, nitrogen, and sulfur metabolism

Cell Calcium 58 (2015) 98–104

Contents lists available at ScienceDirect

Cell Calcium

journal homepage: www.elsevier.com/locate/ceca

Review

Plastidial metabolite transporters integrate photorespiration with carbon, nitrogen, and sulfur metabolism

Marion Eisenhut [1], Nadine Hocken [1], Andreas P.M. Weber *

Institute of Plant Biochemistry, Center of Excellence on Plant Sciences (CEPLAS), Heinrich-Heine-University, Universitätsstraße 1, D-40225 Düsseldorf, Germany

ARTICLE INFO

Article history:
Received 26 July 2014
Received in revised form 15 October 2014
Accepted 17 October 2014
Available online 29 October 2014

Keywords:
Photorespiration
Plastid
Transporter
Nitrogen
Sulfur

ABSTRACT

Plant photorespiration is an essential prerequisite for oxygenic photosynthesis. This metabolic repair pathway bestrides four compartments, which poses the requirement for several metabolites transporters for pathway function. However, in contrast to the well-studied enzymatic steps of the core photorespiratory cycle, only few photorespiratory translocators have been identified to date. In this review, we give an overview of established and unknown plastidic transport proteins involved in photorespiration and intertwined nitrogen and sulfur metabolism, respectively. Furthermore, we discuss the evolutionary origin of the dicarboxylate translocators and the recently identified glycolate glycerate translocator.

1. Introduction

The enzyme Ribulose-1,5-bisphosphate carboxylase/oxygenase (Rubisco) is the most abundant protein on earth. It catalyzes the key step of atmospheric carbon dioxide (CO_2) fixation in all photosynthetic organisms, such as cyanobacteria, algae, and plants. Rubisco evolved about 3 billion years ago in an atmosphere with high CO_2 and negligible O_2 concentrations [1]. Thus, its additional activity as oxygenase did not appear. However, as a consequence of oxygenic photosynthesis, atmospheric O_2 concentrations rose and CO_2 concentrations declined, resulting in Rubisco performing both carboxylation and oxygenation reactions. CO_2 fixation results in generation of two molecules 3-phosphoglycerate (3-PGA), which are processed in the Calvin–Benson–Bassham (CBB) cycle. O_2 fixation by Rubisco leads to generation of one molecule 3-PGA and one molecule 2-phosphoglycolate (2-PG) [2]. 2-PG inhibits enzymes, such as triose-phosphate isomerase [3,4] and must thus be detoxified. This metabolic repair process occurs via the photorespiratory pathway, also called C2 or glycolate cycle (reviewed in [5]), which encompasses four different compartments in the plant cell: chloroplast, peroxisome, mitochondrion, and cytosol. The different enzymatic steps (reviewed in [6]) will be discussed in more detail where required. Since mutants deficient in photorespiratory metabolism are typically not viable under ambient CO_2 conditions (reviewed in [7]), this process is an essential partner for oxygenic photosynthesis [8,9]. The primary reason for this basic necessity is still matter of debate. Suggested are following functions: (1) decomposition of inhibitory 2-PG [8], (2) recovery of 75% of carbon retained in 2-PG to 3-PGA [6], (3) consumption of ATP and reduction equivalents, dissipation of excess excitation energy to prevent photoinhibition [10], and (4) production of the amino acids glycine and serine [8,11].

Since the photorespiratory pathway is highly compartmentalized, metabolite shuttles located in the boundary membranes of the contributing organelles are of great importance to connect the compartments and to ensure efficient metabolite flow through the cycle and associated metabolic pathways. So far only several plastidic transporters have been identified while the majority of peroxisomal and mitochondrial transport proteins remains still unknown (reviewed in [12]).

In this review we will focus on the current knowledge about plastidic transporters involved in the photorespiratory processes. In this context will not only consider the core photorespiratory carbon cycle but also the transport proteins involved in photorespiration-associated nitrogen and sulfur metabolism, such as ammonium recycling, and the biosynthesis of sulfurous amino acid and glutathione.

* Corresponding author. Tel.: +49 211 81 12347; fax: +49 211 81 13706.
E-mail address: andreas.weber@hhu.de (A.P.M. Weber).
[1] These authors contributed equally to this work.

http://dx.doi.org/10.1016/j.ceca.2014.10.007
0143-4160/

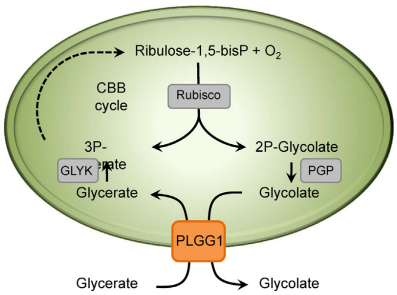

Fig. 1. PLGG1 mediated transport processes in the core photorespiratory carbon cycle. The plastidic glycolate glycerate translocator, PLGG1, is highlighted in an orange box. Abbreviations are: CBB, Calvin–Benson–Bassham; GLYK, glycerate kinase; PGP, phosphoglycolate phosphatase.

2. The plastidic glycolate glycerate translocator PLGG1 is essential for the core photorespiratory carbon cycle

The initial and final reactions of the photorespiratory cycle take place in the chloroplast. Rubisco catalyzes the oxygenation of Ribulose-1,5-bisphosphate and generates one molecule of each, 3-PGA and 2-PG. Since 2-PG acts as inhibitor of several enzymes, such as triosephosphate isomerase [4] and phosphofructokinase [13], 2-PG is rapidly converted into glycolate by phosphoglycolate phosphatase. For further processing, glycolate needs to be shuttled from the chloroplast to the peroxisome. After metabolic turnover in peroxisome and mitochondrion the generated glycerate must be imported into the chloroplast to become phosphorylated by glycerate kinase and eventually reenter the CBB cycle (see Fig. 1). Intriguingly, Howitz and McCarty [14,15] found biochemical evidence that both transport processes, export of glycolate and import of glycerate, are mediated by the same transporter in the chloroplast inner envelope. Using isolated chloroplasts and reconstituted inner envelope fractions from pea, they could furthermore demonstrate that the transport mode is not a strict counter exchange but can proceed either as glycolate/glycerate antiport or as substrate/proton symport, depending on substrate availability [14,16,17].

However, it took almost 30 years to identify the protein on the molecular level. In contrast to the photorespiratory enzymes that could be mainly identified by an elegant forward genetic screen using *Arabidopsis thaliana* (hereafter *Arabidopsis*) as model plant (reviewed in [18]), with the exception of the plastidial dicarboxylate transporter, DiT2.1, mutants defective in transporter function did not show up in the screen. Pick and coworkers [19] chose an alternative approach and employed coexpression analysis, as described in Bordych et al. [20], to identify a candidate protein functioning as glycolate/glycerate transporter in the chloroplast. The selected protein was designated plastidial glycolate glycerate translocator 1, abbreviated as PLGG1 [19]. In order to verify the suggested function, a T-DNA knock out mutant line *plgg1-1* was established and characterized. Mutant plants showed reduced growth and chlorotic leaves under ambient (390 ppm) CO_2 conditions. Importantly, this phenotype could be rescued by growth under elevated CO_2 concentrations (3000 ppm CO_2). Thus, *plgg1-1* fulfilled the criteria for a "photorespiratory phenotype" [19]. Metabolite profiling of the mutant demonstrated glycerate and glycolate accumulation that was both CO_2 and light dependent. Additionally, $^{18}O_2$ labeling of glycolate was enhanced in the mutant while the transfer of label from the glycolate to the glycerate pool was delayed. Further, PLGG1-mediated uptake of glycerate into proteoliposomes reconstituted with recombinant PLGG1 protein was demonstrated. It was concluded that PLGG1 indeed functions as glycolate/glycerate translocator in the chloroplast inner envelope [19]. The *plgg1-1* mutant phenotype demonstrates the essentiality of PLGG1 for the core photorespiratory carbon cycle in plants.

3. The role of DiT1 and DiT2.1 in photorespiratory nitrogen recycling and general nitrogen metabolism

Photorespiration is intimately interfaced with nitrogen metabolism. Catalyzed by the multienzyme system glycine decarboxylase (GDC) and serine hydroxymethyl transferase (SHMT) two molecules glycine are converted into one molecule serine, while CO_2 and ammonium are released in the mitochondrion (reviewed in [21]). The amount of ammonium released by photorespiration can be up to ten fold higher compared to primary assimilation [22]. Nitrogen is a limiting factor in plant growth and ammonium acts as an uncoupler, hence this recycling process is mandatory. Recycling is realized by the photorespiratory nitrogen cycle. To recycle the released ammonium, it must first be shuttled from the mitochondrion into the chloroplast. In this organelle ammonium becomes integrated into the amino acid glutamine by the glutamine synthase (GS). Complementary, two molecules of glutamate are produced by the ferredoxin-dependent glutamate synthase (GOGAT), transferring the amino group from glutamine to 2-oxoglutarate (2-OG) (reviewed in [23]). One molecule glutamate has to re-enter the GS/GOGAT cycle, the second molecule can be utilized in other metabolic pathways. 90% of ammonium consumed in the GS/GOGAT cycle is produced during photorespiration in the mitochondria by the GDC and SHMT [21,23,24] clearly demonstrating the significance of the photorespiratory nitrogen cycle. The importance of the GS/GOGAT cycle is further supported by the observation that mutants in Fd-GOGAT [25] and GS2 [26,27], the plastidial isoform of GS, respectively, display a photorespiratory phenotype. Both, the GS2 and the GOGAT mutant cannot grow under photorespiratory conditions, but survive in conditions that suppress photorespiration [25–27].

Photorespiratory ammonium and the carbon precursor for ammonium-assimilation, 2-OG, which is produced either in the cytosol or in the mitochondria, have to be transported into the chloroplast [28]. In contrast, synthesized glutamate has to leave the chloroplast to function amongst others as an amino-donor in the transamination of glyoxylate to glycine in the peroxisome [6,28]. The simplified photorespiratory nitrogen cycle and involved transport processes are shown in Fig. 2.

3.1. Search for a plastidic ammonium importer

To date it is unknown whether ammonium uptake into the chloroplast occurs as an active or passive process. However, given that during the light the pH of the plastid stroma is higher than that of the cytosol, it is unlikely that passive diffusion of NH_3 across the plastid envelope accounts for the high transport rates required to meet the needs of the photorespiratory pathway. Assuming a cytosolic pH-value of 7.25 and a pK_a-value of 9.25 for NH_4^+ only one out 100 molecules would be in the form of NH_3, while 99 would be in the NH_4^+ form. In the chloroplast stroma, assuming a pH-value of 7.8 in the light, the ratio of NH_3 to NH_4^+ would be approximately four-times higher than in the cytoplasm, which would lead to an outward-directed concentration gradient for NH_3. To date, only ammonium translocators of the ammonium transport (AMT) family have been characterized. In *Arabidopsis* six genes are known encoding AMT1 and AMT2 proteins, with AMT1 functioning as putative high-affinity ammonium transporters [29,30] and AMT2 as ammonium low capacity transporters [31]. However, due to the

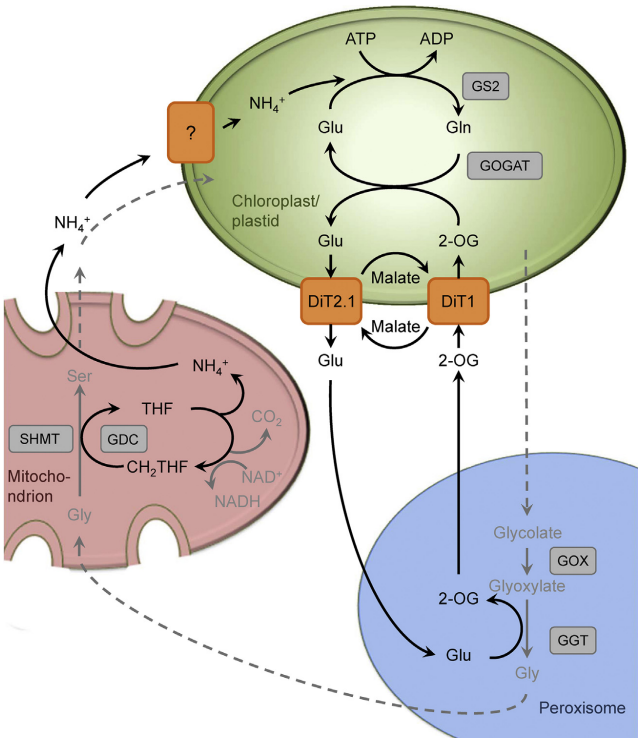

Fig. 2. DiT1 and Dit2.1 mediated transport processes in the photorespiratory nitrogen cycle. The known dicarboxylate transporters DiT1 and DiT2.1 are highlighted in orange boxes. A hypothetical, so far unidentified ammonium transporter is labeled with a question mark. Black arrows mark the photorespiratory nitrogen cycle. Gray arrows indicate the core photorespiratory pathway. Abbreviations of metabolites are: ATP, adenosine triphosphate; ADP, adenosine diphosphate; Glu, glutamate; Gln, glutamine; Gly, glycine; NADH/NAD^+, nicotinamide adenine dinucleotide; NH_4^+, ammonium; 2-OG, 2-oxoglutarate; Ser, serine; THF, tetrahydrofolate; CH_2-THF, methylene-tetrahydrofolate. Enzymes in gray boxes: GDC, glycine decarboxylase; GGT, glutamate:glyoxylate aminotransferase; GOGAT, glutamine synthase/ferredoxin-dependent glutamate synthase; GOX, glycolate oxidase; GS2, glutamate synthase; SHMT, serine hydroxymethyl transferase.

exclusive expression in root and shoot [31–33], and the observation that no member of the AMT family contains a plastid target peptide, we do not consider AMT proteins as candidates. Thus, in case the plastid envelope contains an ammonium transporter it still awaits identification.

3.2. The plastidic dicarboxylate transport system

Initially, the requirement for a plastidic dicarboxylate transport system in photorespiration was established by Somerville and Ogren [34]. They screened ethylmethane sulfonate mutagenized *Arabidopsis* plants for mutants displaying a photorespiratory phenotype under ambient CO_2 conditions (reviewed in [18]). Isolated chloroplasts from of these mutant lines were not able to take up dicarboxylic acids from the medium [34]. It was further shown that purified chloroplast envelope fractions of this mutant were lacking a normally abundant protein with an apparent molecular mass of 45 kDa [35]. Thus, the authors suggested that the lacking protein should have the function of a plastidic dicarboxylic acid transporter and named the mutant accordingly *dct* [34,35]. Further work indicated that at least two transporters with overlapping substrate specificity must be involved in the plastidic dicarboxylic acid transport [36]. The two-translocator model describes the uptake of 2-OG into the chloroplast by a 2-OG/malate translocator (DiT1) and the export of glutamate via a glutamate/malate translocator (DiT2) [28,36]. Since both transporters DiT1 and DiT2.1 use malate as exchange metabolite the net malate transport is zero [28].

The genome of *Arabidopsis* contains three genes encoding DiT proteins: *DiT1*, *DiT2.1* and *DiT2.2*, with *DiT2.1* and *DiT2.2*, being arranged in a tandem array [28]. All *DiT* genes are expressed in leaves and roots, indicating that their function is not only restricted to photorespiration but also rather important in global nitrogen metabolism [37].

3.2.1. DiT1 – the 2-OG/malate translocator

The first component of the two-translocator model is DiT1, which mediates the transport of 2-OG produced in the cytosol or the mitochondrion into the chloroplast in counter exchange for malate [36]. The DiT1 transporter was identified as a component of the plastid envelope with a molecular mass of 45 kDa [38]. The functional characterization of the protein based on the heterologous expression of *DiT1* from spinach, *Arabidopsis*, and maize in yeast revealed a specificity of DiT1 for dicarboxylates such as malate, succinate, fumarate, oxaloacetate, and 2-OG [37,39–42]. Transgenic *DiT1* antisense lines in tobacco showed a photorespiratory phenotype, which confirms the importance of a dicarboxylate transport system under ambient air conditions [39]. Furthermore, a reduced transport capacity for 2-OG as well as impaired

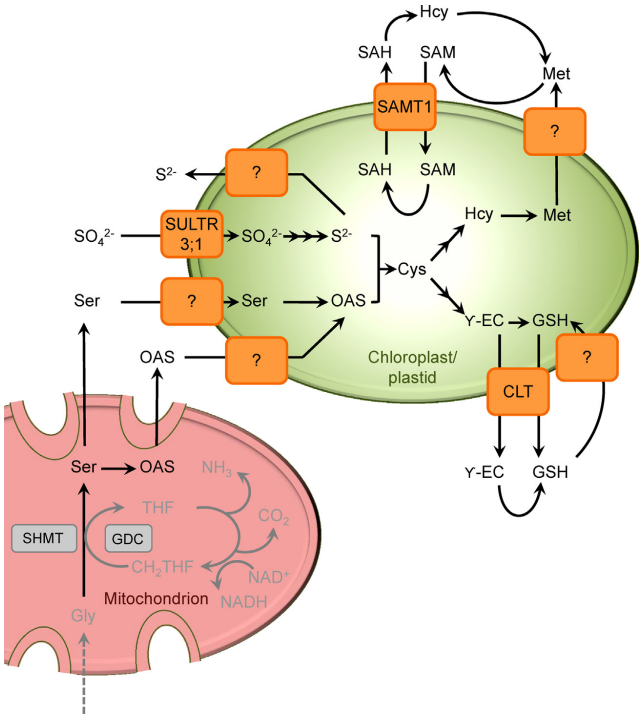

Fig. 3. Plastidic sulfur metabolism and postulated transport processes. The known transporters CLT, SULTR3;1, and SAMT1 are highlighted in orange boxes. Hypothetical, so far unidentified translocators are labeled with a question mark. Black arrows mark the sulfur metabolism. Gray arrows indicate reactions of the core photorespiratory pathway. Abbreviations of metabolites are: Cys, cysteine; GSH, glutathione; γ-EC, γ-glutamylcysteine; Hcy, homocysteine; Met, methionine; OAS, *O*-acetylserine; SAH, *S*-adenosylhomocyteine; SAM, *S*-adenosylmethionine. Enzymes in gray boxes: GDC, glycine decarboxylase; SHMT, serine hydroxymethyl transferase.

amino acid biosynthesis, decreased protein and sugar concentrations in the leaf, accumulation of organic compounds and reduced photosynthetic capacity were observed [39]. Importantly, in a recent study using a T-DNA mutant in *Arabidopsis*, Kinoshita and coworkers [43] could demonstrate that the activity of DiT1 is not only restricted to carbon/nitrogen metabolism but also functions as the long-searched malate valve which exchanges oxaloacetate with malate across the chloroplast envelope.

3.2.2. DiT2.1 – the glutamate/malate translocator

The second component of the two-translocator model is DiT2.1, which mediates the export of glutamate produced in the GS/GOGAT cycle out of the chloroplast in counter exchange for malate [28,36]. The DiT2.1 transporter is specific for the same substrates as DiT1: malate, succinate, fumarate, and 2-OG, but accepts in addition glutamate and aspartate [28].

Map-based cloning of the gene deficient in the *dct* mutant [34] showed that this gene encodes for DiT2.1 [37]. Eventually, it was determined, that the *dct* mutant carries a single point mutation in the *DiT2.1* gene [37].

The photorespiratory phenotype of *dct* indicates an essential function of DiT2.1 as a glutamate/malate transporter under ambient air conditions in the photorespiratory nitrogen recycling. In contrast, the function of its homolog DiT2.2 remains largely elusive. T-DNA knockout mutants in the *DiT2.2* gene did not show any phenotype [37], and DiT2.2 protein reconstituted in liposomes did not show dicarboxylate transport activity [37,41].

4. Chloroplast transporters facilitate integration of photorespiration with sulfur metabolism

Besides its central role in carbon and nitrogen metabolism, photorespiration is also involved in sulfur metabolism. Interestingly, this facet has not gained much attention to date since it is not obvious at first sight. In this section we give an overview on sulfur metabolism in the plastid and discuss how the photorespiratory metabolism is integrated into this pathway (see Fig. 3).

Cellular sulfur assimilation starts by the uptake of sulfate via the sulfate transporter SULTR3;1 [44] into the chloroplast. Next, sulfate is activated and stepwise reduced to sulfide. The sulfite reductase catalyzes the final step in this process. As this enzyme acts ferredoxin-dependent (reviewed in [45]) the chloroplast is the exclusive location for sulfur assimilation. Generated sulfide is used in the chloroplast, mitochondrion and cytosol for cysteine biosynthesis. To allow for sulfide distribution a transporter in the plastid envelope should exist. However, a sulfide exporter has not yet been identified for this compartment. For the cysteine biosynthesis first serine and acetyl-Coenzyme A are converted into *O*-acetylserine (OAS). Then, catalyzed by OAS lyase, this intermediate reacts with sulfide to generate cysteine. The origin of serine entering this reaction is still a matter of debate. Three different pathways in plants produce serine: the glycerate pathway, the phosphorylated

Table 1
Conservation of PLGG1, DiT1, and DiT2.1 in Archaeplastida. Homologous proteins were identified by performing BlastP analyses (e-value higher than e^{-27}) at the National Center for Biotechnology Information (http://blast.ncbi.nlm.nih.gov/Blast.cgi), at the *Cyanidioschyzon merolae* Genome Project (http://merolae.biol.s.u-tokyo.ac.jp/blast/blast.html), at the *Galdieria sulphuraria* Genome Project (http://genomics.msu.edu/cgi-bin/galdieria/blast.cgi), at the *Porphyridium purpureum* Genome Project (http://cyanophora.rutgers.edu/porphyridium/), and at the Cyanophora Genome Project (http://cyanophora.rutgers.edu/cyanophora/). Only proteins were considered that are predicted by TargetP [55] to localize to the chloroplast. –, no homologous protein identified.

	Organism	PLGG1	DiT1	DiT2.1
Embryophyta	*Arabidopsis thaliana*	At1g32080	At5g12860	At5g64290
	Zea mays	GRMZM2G478212 GRMZM5G873519	GRMZM2G383088	GRMZM2G040933
	Sorghum bicolor	SORBIDRAFT_01g027840	SORBIDRAFT_08g016630	SORBIDRAFT_07g029170
	Selaginella moellendorffii	SELMODRAFT_116401[a] SELMODRAFT_85667[a]	SELMODRAFT_129026	SELMODRAFT_267817
	Physcomitrella patens	PHYPADRAFT_190246	PHYPADRAFT_225280 PHYPADRAFT_65687	PHYPADRAFT_225280 PHYPADRAFT_65687
Chlorophyta	*Chlamydomonas rheinhardtii*	CHLREDRAFT_148310	CHLREDRAFT_185488[b]	CHLREDRAFT_185488[b]
	Ostreococcus taurii	Ot01g05990[b]	Ot04g02670[b]	Ot18g00730
Rhodophyta	*Cyanidioschyzon merolae*	CMM067C	–	–
	Galdieria sulphuraria	Gasu_58100	–	–
	Porphyridium purpureum	Porphypu_evm.model.contig_482.13	–	–
Glaucophyta	*Cyanophora paradoxa*	Cyanophora_Contig9040-snap-gene-0.0[a]	–	–

[a] Due to partial sequence, target peptide prediction was impossible.
[b] Mitochondrial localization predicted by TargetP.

pathway, and the photorespiratory pathway (reviewed in [46]). Work with mutants in plastidic phosphoglycerate dehydrogenases demonstrated that the phosphorylated pathway becomes important under conditions with reduced photorespiratory activity [47]. Accordingly it is suggested, that the photorespiratory cycle is the major source of serine in leaves in ambient CO_2, with serine production in mitochondria by the concerted action of GDC and SHMT. This finding implies that either serine or OAS must be shuttled from the mitochondrion into the chloroplast. Indeed, it was demonstrated that mitochondria make the largest contribution to OAS synthesis [48]. Thus, a plastidic importer for serine and/or OAS must exist to facilitate cysteine biosynthesis in the chloroplast. However, this translocator has not yet been identified.

Cysteine on the one hand is required for plastidial protein biosynthesis and on the other hand as a precursor for two central metabolites, the second sulfurous proteinogenic amino acid methionine and the tripeptide glutathione (GSH).

De novo biosynthesis of methionine is likely restricted to plastids, though the final step, the methylation of homocysteine to form methionine, occurs in both chloroplast and cytosol [49]. The predominant share of the methionine pool is converted into the central methyl donor *S*-adenosylmethionine (SAM). Since SAM formation takes only place in the cytosol, methionine must first be exported from the chloroplast into the cytosol, converted into SAM and then transferred back into the chloroplast to function in biosynthetic or regulatory methylation reactions. Plastidic SAM import was described by Ravanel and coworkers [49]. They studied isolated chloroplasts and defined the transport mode as *S*-adenosylhomocyteine (SAH)/SAM counter-exchange. In *Arabidopsis* the protein SAMT1 could be finally identified as the plastidic SAM transporter [50]. Heterologously expressed and reconstituted SAMT1 mediated counter-exchange of SAH with SAM as it was observed earlier with isolated chloroplasts [50].

In most plants the synthesis of the GSH precursor γ-glutamylcysteine (γ-EC) from cysteine occurs exclusively in plastids, while the final enzymatic step, catalyzed by GSH synthetase, takes place in plastids and cytosol [51]. Due to the observation that mutants unable to generate GSH in the chloroplast are viable, the presence of a GSH importer in the chloroplast membrane was postulated [52]. Likewise, γ-EC needs to be exported from the plastid into the cytosol for GSH synthesis. The small protein family of CRT-like transporters (CLT) with three homologous proteins could be identified as transporters facilitating γ-EC and GSH export from the chloroplast in Arabidopsis [53]. By expression of the transporters in *Xenopus* oocytes, uptake of labeled GSH could be demonstrated.

It must be mentioned that sulfur metabolism is plant species specific and differences in compartmentalization occur. Here, we refer to studies performed with *Arabidopsis*.

In conclusion, the de novo biosynthesis of both sulfurous amino acids cysteine and methionine as well as the central antioxidant glutathione are closely linked to photorespiratory serine production.

5. Evolutionary origin of plastidial photorespiratory transporters and distribution among Archaeplastida

Photorespiration likely coevolved with oxygenic photosynthesis in unicellular ancestral cyanobacteria [8]. With the rise of multicompartmented eukaryotic photoautotrophes, the Archaeplastida, the photorespiratory metabolism was distributed over several specialized compartments. Accordingly, translocators had to be employed, which facilitated the metabolite flux through the cycle. It is subject of discussion, what the origin of theses transport proteins is.

To determine the distribution and evolutionary origin of the established photorespiratory transporters PLGG1, DiT1, and DiT2 in the membranes of extant plastids, we searched the genomes of Embryophyta, Chlorophyta, Rhodophyta and Glaucophyta for homologous proteins (see Table 1).

Sequences related to the plastidial glycolate/glycerate transporter PLGG1 from *Arabidopsis* can be detected in all members of the Archaeplastida, including the basal glaucophyte *Cyanophora paradoxa*. This indicates that the gene encoding this transporter was either already present in the common ancestor of the Archaeplastida or was introduced via the cyanobiont in the process of endosymbiosis. Related proteins can be found in a range of bacterial species, archaea, and some fungi but not in metazoa [19]. Remarkably, so far studied green algae, such as *Chlamydomonas rheinhardtii*, show a significant difference in their

photorespiratory pathway. In contrast to higher plants, green algae do not employ peroxisomes and thus perform the glycolate oxidation by glycolate dehydrogenase in mitochondria [3,54]. This difference implies that the mitochondrion needs a transporter comparable to the plastidic PLGG1, facilitating glycolate import and glycerate export. Using the subcellular localization tool TargetP (http://www.cbs.dtu.dk/services/TargetP/ [55]), plastidial and mitochondrial targeting, respectively, of the PLGG1 homologs in *C. rheinhardtii* and *Ostreococcus taurii* were predicted. The PLGG1 homolog from *Volvox carteri*, VOLCADRAFT_121401, was equally predicted to localize to both organelles. Thus, dual targeting of PLGG1 in green algae is conceivable.

The dicarboxylate translocators DiT1 and DiT2 have their closest orthologs in members of the Chlamydiae [56]. Interestingly, they are found only in the green lineage of the Archaeplastida but not in red algae or glaucophytes. This indicates that they have been either acquired by horizontal transfer from Chlamydiae after the separation of the red algae and glaucophytes from the green lineage, or that they have been lost from the former. Generally, orthologs of DiTs are distributed throughout the bacterial kingdom were they frequently function as tricarboxylate transporters [57].

6. Concluding remarks

Photorespiration serves additional important functions in plant metabolism that reach beyond a supportive metabolic repair pathway in oxygenic photosynthesis. It is closely intertwined with several major metabolic functions, such as nitrogen assimilation and sulfur metabolism. Future research is needed to fully understand these interdependences and to discover further, yet unknown metabolic connections. Obviously, a major challenge in this context is the identification of the missing translocators in peroxisomes and mitochondria. With respect to the plastid envelope the main photorespiratory transporters have now been established. However, some postulated translocators, such as the ammonium or serine importer are still awaiting identification.

Conflicts of interest

The authors declare that there are no known conflicts of interest associated with this study.

Acknowledgement

We thank the Deutsche Forschungsgemeinschaft for funding (PROMICS Research Unit FG 1186, WE 2231/8-2, EXC 1028, WE 2231/16-1).

References

[1] E.G. Nisbet, N.V. Grassineau, C.J. Howe, P.I. Abell, M. Regelous, R.E.R. Nisbet, The age of Rubisco: the evolution of oxygenic photosynthesis, Geobiology 5 (2007) 311–335.
[2] W.L. Ogren, G. Bowes, Ribulose diphosphate carboxylase regulates soybean photorespiration, Nat. New Biol. 230 (1971) 159–160.
[3] D.W. Husic, H.D. Husic, N.E. Tolbert, C.B. Clanton Jr., The oxidative photosynthetic carbon cycle or C_2 cycle, Crit. Rev. Plant Sci. 5 (1987) 45–100.
[4] E.G. Norman, B. Colman, Purification and characterization of phosphoglycolate phosphatase from the cyanobacterium *Coccochloris peniocystis*, Plant Physiol. 95 (1991) 693–698.
[5] N.E. Tolbert, The C2 oxidative photosynthetic carbon cycle, Annu. Rev. Plant Physiol. Plant Mol. Biol. 48 (1997) 1–25.
[6] H. Bauwe, M. Hagemann, A.R. Fernie, Photorespiration: players, partners and origin, Trends Plant Sci. 15 (2010) 330–336.
[7] S. Timm, H. Bauwe, The variety of photorespiratory phenotypes – employing the current status for future research directions on photorespiration, Plant Biol. 15 (2013) 737–747.
[8] M. Eisenhut, W. Ruth, M. Haimovich, H. Bauwe, A. Kaplan, M. Hagemann, The photorespiratory glycolate metabolism is essential for cyanobacteria and might have been conveyed endosymbiontically to plants, Proc. Natl. Acad. Sci. U. S. A. 105 (2008) 17199–17204.
[9] H. Bauwe, M. Hagemann, R. Kern, S. Timm, Photorespiration has a dual origin and manifold links to central metabolism, Curr. Opin. Plant Biol. 15 (2012) 269–275.
[10] A. Kozaki, G. Takeba, Photorespiration protects C3 plants from photooxidation, Nature 384 (1996) 557–560.
[11] G.H. Lorimer, The carboxylation and oxygenation of ribulose 1,5-bisphosphate – the primary events in photosynthesis and photorespiration, Annu. Rev. Plant Physiol. Plant Mol. Biol. 32 (1981) 349–383.
[12] M. Eisenhut, T.R. Pick, C. Bordych, A.P. Weber, Towards closing the remaining gaps in photorespiration – the essential but unexplored role of transport proteins, Plant Biol. 15 (2013) 676–685.
[13] L.E. Anderson, Chloroplast and cytoplasmic enzymes. II. Pea leaf triosephosphate isomerases, Biochim. Biophys. Acta 235 (1971) 237–244.
[14] K.T. Howitz, R.E. McCarty, Substrate-specificity of the pea chloroplast glycolate transporter, Biochemistry 24 (1985) 3645–3650.
[15] K.T. Howitz, R.E. McCarty, Solubilization, partial-purification, and reconstitution of the glycolate glycerate transporter from chloroplast inner envelope membranes, Plant Physiol. 96 (1991) 1060–1069.
[16] K.T. Howitz, R.E. McCarty, Kinetic characteristics of the chloroplast envelope glycolate transporter, Biochemistry 24 (1985) 2645–2652.
[17] X.K. Young, R.E. McCarty, Assay of proton-coupled glycolate and D-glycerate transport into chloroplast inner envelope membrane-vesicles by stopped-flow fluorescence, Plant Physiol. 101 (1993) 793–799.
[18] C.R. Somerville, An early Arabidopsis demonstration. Resolving a few issues concerning photorespiration, Plant Physiol. 125 (2001) 20–24.
[19] T.R. Pick, A. Bräutigam, M.A. Schulz, T. Obata, A.R. Fernie, A.P. Weber, PLGG1, a plastidic glycolate glycerate transporter, is required for photorespiration and defines a unique class of metabolite transporters, Proc. Natl. Acad. Sci. U. S. A. 110 (2013) 3185–3190.
[20] C. Bordych, M. Eisenhut, T.R. Pick, C. Kuelahoglu, A.P. Weber, Co-expression analysis as tool for the discovery of transport proteins in photorespiration, Plant Biol. 15 (2013) 686–693.
[21] H. Bauwe, U. Kolukisaoglu, Genetic manipulation of glycine decarboxylation, J. Exp. Bot. 54 (2003) 1523–1535.
[22] A.J. Keys, I.F. Bird, M.J. Cornelius, P.J. Lea, R.M. Wallsgrove, B.J. Miflin, Photorespiratory nitrogen cycle, Nature 275 (1978) 741–743.
[23] B. Hirel, P.J. Lea, Ammonia assimilation, in: P.J. Lea (Ed.), Plant Nitrogen, Springer Verlag, Berlin, 2001, pp. 79–99.
[24] A. Wingler, P.J. Lea, W.P. Quick, R.C. Leegood, Photorespiration: metabolic pathways and their role in stress protection, Philos. Trans. R. Soc. Lond. B: Biol. Sci. 355 (2000) 1517–1529.
[25] C.R. Somerville, W.L. Ogren, Inhibition of photosynthesis in Arabidopsis mutants lacking leaf glutamate synthase activity, Nature 286 (1980) 257–259.
[26] R.D. Blackwell, A.J.S. Murray, P.J. Lea, Inhibition of photosynthesis in barley with decreased levels of chloroplastic glutamine-synthetase activity, J. Exp. Bot. 38 (1987) 1799–1809.
[27] R.M. Wallsgrove, J.C. Turner, N.P. Hall, A.C. Kendall, S.W.J. Bright, Barley mutants lacking chloroplast glutamine-synthetase – biochemical and genetic analysis, Plant Physiol. 83 (1987) 155–158.
[28] A. Weber, U.I. Flügge, Interaction of cytosolic and plastidic nitrogen metabolism in plants, J. Exp. Bot. 53 (2002) 865–874.
[29] S. Gazzarrini, L. Lejay, A. Gojon, O. Ninnemann, W.B. Frommer, N. von Wirén, Three functional transporters for constitutive, diurnally regulated, and starvation-induced uptake of ammonium into Arabidopsis roots, Plant Cell 11 (1999) 937–948.
[30] S.R. Rawat, S.N. Silim, H.J. Kronzucker, M.Y. Siddiqi, A.D. Glass, AtAMT1 gene expression and NH_4^+ uptake in roots of *Arabidopsis thaliana*: evidence for regulation by root glutamine levels, Plant J. 19 (1999) 143–152.
[31] N. von Wiren, S. Gazzarrini, A. Gojon, W.B. Frommer, The molecular physiology of ammonium uptake and retrieval, Curr. Opin. Plant Biol. 3 (2000) 254–261.
[32] M. Mayer, U. Ludewig, Role of AMT1;1 in NH_4^+ acquisition in *Arabidopsis thaliana*, Plant Biol. 8 (2006) 522–528.
[33] L. Yuan, D. Loque, S. Kojima, et al., The organization of high-affinity ammonium uptake in Arabidopsis roots depends on the spatial arrangement and biochemical properties of AMT1-type transporters, Plant Cell 19 (2007) 2636–2652.
[34] S.C. Somerville, W.L. Ogren, An *Arabidopsis thaliana* mutant defective in chloroplast dicarboxylate transport, Proc. Natl. Acad. Sci. U. S. A. 80 (1983) 1290–1294.
[35] S.C. Somerville, C.R. Somerville, A mutant of Arabidopsis deficient in chloroplast dicarboxylate transport is missing a envelope protein, Plant Sci. Lett. 37 (1985) 217–220.
[36] K.C. Woo, U.I. Flügge, H.W. Heldt, A 2-translocator model for the transport of 2-oxoglutarate and glutamate in chloroplasts during ammonia assimilation in the light, Plant Physiol. 84 (1987) 624–632.
[37] P. Renné, U. Dressen, U. Hebbeker, D. Hille, U.I. Flügge, P. Westhoff, A.P.M. Weber, The Arabidopsis mutant *dct* is deficient in the plastidic glutamate/malate translocator DiT2, Plant J. 35 (2003) 316–331.
[38] E. Menzlaff, U.I. Flügge, Purification and functional reconstitution of the 2-oxoglutarate malate translocator from spinach-chloroplasts, Biochim. Biophys. Acta 1147 (1993) 13–18.
[39] J. Schneidereit, R.E. Hausler, G. Fiene, W.M. Kaiser, A.P. Weber, Antisense repression reveals a crucial role of the plastidic 2-oxoglutarate/malate translocator DiT1 at the interface between carbon and nitrogen metabolism, Plant J. 45 (2006) 206–224.

[40] Y. Taniguchi, J. Nagasaki, M. Kawasaki, H. Miyake, T. Sugiyama, M. Taniguchi, Differentiation of dicarboxylate transporters in mesophyll and bundle sheath chloroplasts of maize, Plant Cell Physiol. 45 (2004) 187–200.
[41] M. Taniguchi, Y. Taniguchi, M. Kawasaki, et al., Identifying and characterizing plastidic 2-oxoglutarate/malate and dicarboxylate transporters in *Arabidopsis thaliana*, Plant Cell Physiol. 43 (2002) 706–717.
[42] A. Weber, E. Menzlaff, B. Arbinger, M. Gutensohn, C. Eckerskorn, U.I. Flügge, The 2-oxogutarate malate translocator of chloroplast envelope membranes – molecular-cloning of a transporter containing a 12-helix motif and expression of the functional protein in yeast-cells, Biochemistry 34 (1995) 2621–2627.
[43] H. Kinoshita, J. Nagasaki, N. Yoshikawa, et al., The chloroplastic 2-oxoglutarate/malate transporter has dual function as the malate valve and in carbon/nitrogen metabolism, Plant J. 65 (2011) 15–26.
[44] M.J. Cao, Z. Wang, M. Wirtz, R. Hell, D.J. Oliver, C.B. Xiang, SULTR3;1 is a chloroplast-localized sulfate transporter in *Arabidopsis thaliana*, Plant J. 73 (2013) 607–616.
[45] H. Takahashi, S. Kopriva, M. Giordano, K. Saito, R. Hell, Sulfur assimilation in photosynthetic organisms: molecular functions and regulations of transporters and assimilatory enzymes, Annu. Rev. Plant Biol. 62 (2011) 157–184.
[46] R. Ros, J. Muñoz-Bertomeu, S. Krueger, Serine in plants: biosynthesis, metabolism, and functions, Trends Plant Sci. (2014), http://dx.doi.org/10.1016/j.tplants.2014.06.003, July 3, pii: S1360-1385(14)00146-0 [Epub ahead of print].
[47] R.M. Benstein, K. Ludewig, S. Wulfert, S. Wittek, T. Gigolashvili, H. Frerigmann, M. Gierth, U.I. Flügge, S. Krueger, Arabidopsis phosphoglycerate dehydrogenase1 of the phosphoserine pathway is essential for development and required for ammonium assimilation and tryptophan biosynthesis, Plant Cell 25 (2013) 5011–5029.
[48] F.H. Haas, C. Heeg, R. Queiroz, A. Bauer, M. Wirtz, R. Hell, Mitochondrial serine acetyltransferase functions as a pacemaker of cysteine synthesis in plant cells, Plant Physiol. 148 (2008) 1055–1067.
[49] S. Ravanel, M.A. Block, P. Rippert, et al., Methionine metabolism in plants: chloroplasts are autonomous for de novo methionine synthesis and can import *S*-adenosylmethionine from the cytosol, J. Biol. Chem. 279 (2004) 22548–22557.
[50] F. Bouvier, N. Linka, J.C. Isner, J. Mutterer, A.P. Weber, B. Camara, Arabidopsis SAMT1 defines a plastid transporter regulating plastid biogenesis and plant development, Plant Cell 18 (2006) 3088–3105.
[51] A. Wachter, S. Wolf, H. Steininger, J. Bogs, T. Rausch, Differential targeting of GSH1 and GSH2 is achieved by multiple transcription initiation: implications for the compartmentation of glutathione biosynthesis in the Brassicaceae, Plant J. 41 (2005) 15–30.
[52] M. Pasternak, B. Lim, M. Wirtz, R. Hell, C.S. Cobbett, A.J. Meyer, Restricting glutathione biosynthesis to the cytosol is sufficient for normal plant development, Plant J. 53 (2008) 999–1012.
[53] S.C. Maughan, M. Pasternak, N. Cairns, et al., Plant homologs of the *Plasmodium falciparum* chloroquine-resistance transporter, PfCRT, are required for glutathione homeostasis and stress responses, Proc. Natl. Acad. Sci. U. S. A. 107 (2010) 2331–2336.
[54] Y. Nakamura, S. Kanakagiri, K. Van, W. He, M.H. Spalding, Disruption of a glycolate dehydrogenase gene in a high-CO2-requiring mutant of *Chlamydomonas reinhardtii*, Can. J. Bot. 83 (2005) 796–809.
[55] O. Emanuelsson, H. Nielsen, S. Brunak, G. von Heijne, Predicting subcellular localization of proteins based on their N-terminal amino acid sequence, J. Mol. Biol. 300 (2000) 1005–1016.
[56] H.M. Tyra, M. Linka, A.P. Weber, D. Bhattacharya, Host origin of plastid solute transporters in the first photosynthetic eukaryotes, Genome Biol. 8 (2007) R212.
[57] I.G. Janausch, E. Zientz, Q.H. Tran, A. Kröger, G. Unden, C4-dicarboxylate carriers and sensors in bacteria, Biochim. Biophys. Acta 1553 (2002) 39–56.

Authors' contribution to manuscript I:

M. Eisenhut and N. Hocken (Rademacher) contributed equally to this work

Nadine Hocken (Rademacher): Wrote the manuscript (mainly chapter 1,2 and 3), performed BlastP analysis and designed figures.

Marion Eisenhut: Wrote manuscript (mainly chapter 1,4 and 5).

Andreas Weber: Participated in drafting the manuscript.

MANUSCRIPT II

Photorespiratory glycolate oxidase is essential for survival of the red alga *Cyanidioschyzon merolae* under ambient CO_2 conditions

Journal of Experimental Botany Advance Access published March 19, 2016

Journal of Experimental Botany
doi:10.1093/jxb/erw118
This paper is available online free of all access charges (see http://jxb.oxfordjournals.org/open_access.html for further details)

RESEARCH PAPER

Photorespiratory glycolate oxidase is essential for the survival of the red alga *Cyanidioschyzon merolae* under ambient CO_2 conditions

Nadine Rademacher[1], Ramona Kern[2], Takayuki Fujiwara[3], Tabea Mettler-Altmann[1], Shin-ya Miyagishima[3,4], Martin Hagemann[2], Marion Eisenhut[1] and Andreas P.M. Weber[1,*]

[1] Institute of Plant Biochemistry, Cluster of Excellence on Plant Sciences (CEPLAS), Heinrich Heine University, Universitätsstraße 1, 40225 Düsseldorf, Germany
[2] University Rostock, Department Plant Physiology, Albert-Einstein-Straße 3, 18059 Rostock, Germany
[3] Division of Symbiosis and Cell Evolution, National Institute of Genetics, 1111 Yata, Mishima 411–8540, Shizuoka, Japan
[4] Japan Science and Technology Agency, CREST, 4-1-8 Honcho, Kawaguchi 332-0012, Saitama, Japan

* Correspondence: andreas.weber@hhu.de

Received 18 December 2015; Accepted 29 February 2016

Editor: Christine Raines, University of Essex

Abstract

Photorespiration is essential for all organisms performing oxygenic photosynthesis. The evolution of photorespiratory metabolism began among cyanobacteria and led to a highly compartmented pathway in plants. A molecular understanding of photorespiration in eukaryotic algae, such as glaucophytes, rhodophytes, and chlorophytes, is essential to unravel the evolution of this pathway. However, mechanistic detail of the photorespiratory pathway in red algae is scarce. The unicellular red alga *Cyanidioschyzon merolae* represents a model for the red lineage. Its genome is fully sequenced, and tools for targeted gene engineering are available. To study the function and importance of photorespiration in red algae, we chose glycolate oxidase (GOX) as the target. GOX catalyses the conversion of glycolate into glyoxylate, while hydrogen peroxide is generated as a side-product. The function of the candidate GOX from *C. merolae* was verified by the fact that recombinant GOX preferred glycolate over L-lactate as a substrate. Yellow fluorescent protein-GOX fusion proteins showed that GOX is targeted to peroxisomes in *C. merolae*. The GOX knockout mutant lines showed a high-carbon-requiring phenotype with decreased growth and reduced photosynthetic activity compared to the wild type under ambient air conditions. Metabolite analyses revealed glycolate and glycine accumulation in the mutant cells after a shift from high CO_2 conditions to ambient air. In summary, or results demonstrate that photorespiratory metabolism is essential for red algae. The use of a peroxisomal GOX points to a high photorespiratory flux as an ancestral feature of all photosynthetic eukaryotes.

Key words: Evolution, glycolate oxidase, knockout mutant, metabolites, photorespiration, red alga.

Introduction

The enzyme Rubisco catalyses the first step in photosynthetic carbon fixation by adding one molecule of carbon dioxide (CO_2) to the acceptor molecule ribulose 1,5–bisphosphate (RuBP). The resulting two molecules of 3-phosphoglycerate

(3-PGA) are fed into the Calvin–Benson cycle for the production of sugar molecules. Beside the carboxylation reaction, Rubisco also catalyses the oxygenation of RuBP in the presence of oxygen (O_2). In this case, one molecule of 3-PGA and one of 2-phosphoglycolate (2-PG) are generated (Ogren and Bowes, 1971). 2-PG is detrimental to cellular metabolism, inhibiting enzymatic reactions such as those of triose-phosphate isomerase (Husic *et al.*, 1987; Norman and Colman, 1991). Thus, 2-PG is rapidly converted to 3-PGA by the photorespiratory pathway, which is distributed between the chloroplast, peroxisome, mitochondrion, and cytosol in plants (Somerville, 2001; Bauwe *et al.*, 2010). This pathway has nine enzymatic steps that convert two molecules of 2-PG into one molecule of 3-PGA at the expense of ATP and NADPH.

In addition to its metabolic repair function, photorespiratory metabolism is suggested to protect against acceptor limitation (Heber and Krause, 1980; Kozaki and Takeba, 1996; Takahashi *et al.*, 2007). The essential role of photorespiration under ambient CO_2 conditions is demonstrated by the lethality of mutants with a completely impaired photorespiratory metabolism. These mutants display a photorespiratory, high-carbon-requiring (HCR) phenotype. That is, the mutants become chlorotic and fade under ambient, low CO_2 concentrations. High CO_2 concentrations typically suppress this phenotype (Somerville, 2001). So far, mutants displaying an HCR phenotype have been identified in plants, including *Zea mays* (Zelitch *et al.*, 2009) and *Arabidopsis thaliana* (Voll *et al.*, 2006; Engel *et al.*, 2007; Schwarte and Bauwe, 2007; Timm *et al.*, 2011), the green alga *Chlamydomonas reinhardtii* (Suzuki *et al.*, 1999; Nakamura *et al.*, 2005), and the cyanobacterium *Synechocystis* sp. strain PCC 6803 (Eisenhut *et al.*, 2008).

Photorespiration had already evolved in cyanobacteria, the first organisms performing oxygenic photosynthesis, and exists in all primary endosymbiotic lineages of algae as well as in plants today (Eisenhut *et al.*, 2008; reviewed in Bauwe *et al.*, 2010; Kern *et al.*, 2013). Owing to increasing O_2 concentrations in the atmosphere, the photorespiratory pathway needed to be optimized to deal with the enhanced oxygenation activity of Rubisco and resulting enhanced flux through the pathway. This was achieved in the plant-type photorespiratory pathway by recruiting a glycolate oxidase (GOX) instead of a glycolate dehydrogenase (GlcD) for the photorespiratory glycolate-to-glyoxylate conversion (Kehlenbeck *et al.*, 1995). GOX has a much higher maximal rate (V_{max}) than GlcD and is most efficient in an environment with a high O_2 partial pressure, which enables the quick degradation of the GOX by-product hydrogen peroxide (H_2O_2) by catalase in the peroxisome (reviewed in Hagemann *et al.*, 2013). Thus, the use of GOX in peroxisomes can be considered an indicator of high photorespiratory flux in the optimized plant-type photorespiratory pathway (Kehlenbeck *et al.*, 1995; Hagemann *et al.*, 2013).

It has been postulated that photorespiratory metabolism is essential for all organisms that perform oxygenic photosynthesis and that it evolved very early among cyanobacteria (Eisenhut *et al.*, 2008; Bauwe *et al.*, 2010; Hagemann *et al.*, 2010; Hagemann *et al.*, 2016). However, to date no detailed studies on photorespiration in the other two branches of the Archaeplastida besides Chloroplastida, namely the Glaucophyta and Rhodophyta, have been performed. The red alga *Cyanidioschyzon merolae* serves as a model organism for the Rhodophyta. This unicellular alga is characterized by a simple eukaryotic cell structure with each cell having a single nucleus, mitochondrion, chloroplast, and peroxisome. Its small and minimally redundant 16 Mbp genome is completely known (Matsuzaki *et al.*, 2004) and methods for targeted gene knockout and protein localization are available (Ohnuma *et al.*, 2008; Imamura *et al.*, 2010). *C. merolae* is an extremophile and can tolerate temperatures up to 57°C and pH values <2 (Seckbach, 1995). At this acidic pH, the vast majority of inorganic carbon is present as CO_2 in the aquatic environment. Given that the acidophilic and acidotolerant algae manage to maintain a neutral pH inside the cells (Zenvirth *et al.*, 1985; Gimmler *et al.*, 1988; Colman and Balkos, 2005), the natural pH gradient must allow the diffusive uptake of CO_2 into the cytoplasm, where CO_2 is captured/accumulated in the form of HCO_3^-. A carbonic anhydrase recovers the CO_2 and provides it to Rubisco for fixation. Importantly, red algal Rubisco has the highest specificity for CO_2 over O_2 (Uemura *et al.*, 1997) measured so far.

In this study we tested the hypothesis that photorespiratory metabolism is essential in the red alga *C. merolae.* We focused on red algal GOX, which also allowed us to investigate the hypothesis that plant-type photorespiratory metabolism evolved early in photosynthetic eukaryotes. To this end, we generated and physiologically characterized a mutant with the candidate GOX knocked out. The mutant displayed an HCR phenotype and accumulated glycolate upon a shift from high to low (ambient) CO_2 conditions. Together with the findings that the enzyme localized to the peroxisomal matrix and that recombinant GOX displayed plant-like enzymatic features, we conclude that in the evolutionary basal lineage of red algae, the photorespiratory pathway is already functioning in the plant-type mode. This indicates a high photorespiratory flux before the colonization of terrestrial environments by photosynthetic eukaryotes.

Material and methods

Strains and culture conditions

C. merolae 10D was used as the wild-type (WT) strain in this study. For the generation of the Δ*gox* mutant, the M4 mutant, deficient in uracil synthesis, was used (Minoda *et al.*, 2004). Cells were cultivated in 2× modified Allen's (2×MA) medium (pH 2; Minoda *et al.*, 2004) in glass vessels at 40°C, and aerated with high CO_2 concentrations (5% CO_2 in air, HC) or low CO_2 concentrations (0.04% CO_2 in air, LC) under continuous white light (90 µmol photons m^{-2} s^{-1}). The growth medium for the M4 mutant was supplemented with 500 µg ml^{-1} uracil.

For the CO_2 shift experiment, *C. merolae* WT and the Δ*gox* mutant strains were cultivated in a multicultivator system (Photon System Instruments, Drasov, Czech Republic) at 90 µmol photons m^{-2} s^{-1} light and 40°C. For growth rate calculation, OD_{720} measurements were performed every hour over the experimental time by the multicultivator system.

Quantitative real-time PCR

Samples for RNA extraction were taken 0 h, 3 h, and 24 h after the shift from HC to LC conditions, as well as 24 h after the shift back to

HC. RNA extraction was performed using the EURx GeneMatrix Universal RNA Purification Kit (Roboklon, Berlin, Germany) following manufacturer's instruction for RNA cell extraction. DNase treatment was carried out using RQ1 RNA-Free DNase and cDNA synthesis was performed using M-MLV Reverse Transcriptase, RNase (H−), Point Mutant (Promega, Fitchburg, WI, USA). A MESA BLUE MasterMix for SYBR® Assay (Eurogentec, Seraing, Liège, Belgium) was employed for the quantitative (q)RT assay. The primers used for qRT-PCR were qRT-CmGOX-fw and qRT-CmGOX-rev (efficiency 2.0) for amplification of the *CmGOX* (*CMQ436C*) transcript and qRT-CmrbcL-fw and qRT-CmrbcL-rev (efficiency 2.1). The red algal homologue of the constitutively expressed gene *TIP-41-like* (*At4g34270*) in *A. thaliana* (Czechowski *et al.*, 2005) was used as a reference gene. We designated this gene, *CMM193C*, as *CmBLACK* and applied it as a reference for ΔΔCt analysis using the primers qRT-CmBlack-fw and qRT-CmBlack-rev (efficiency 2.2). Primer sequences are listed in Supplementary Table S1. qRT-PCR was performed with the StepOne Plus Real-Time system (Applied Biosystems, Waltham, MA, USA). Mean normalized expression was calculated from three biological replicates, including three technical replicates, following the instructions of Simon (2003).

Subcellular localization studies

The CmGOX coding sequence was amplified using Phusion High Fidelity DNA Polymerase (New England Biolabs, Ipswich, MA, USA), P1 forward primer (*Mfe*I restriction site), P2 reverse primer (*Nco*I restriction site), and *C. merolae* genomic DNA as the template. The PCR product was ligated into the pJET2.1 vector system (ThermoFisher Scientific, Waltham, MA, USA) for amplification and sequencing. For localization studies in *Nicotiana benthamiana*, pUBN-YFP-Dest (Grefen *et al.*, 2010) was used as the final vector for fusion of CmGOX with an N-terminal yellow fluorescent protein (YFP) tag. Expression of the fusion protein was under the control of the constitutive *UBIQUITIN 10* promoter. Transformation of *N. benthamiana* was carried out using *Agrobacterium tumefaciens* strain GV3101. For peroxisomal co-localization studies, *A. tumefaciens* cells containing a vector for expression of the cyan fluorescent protein (CFP) fused with the C-terminal peroxisomal target signal 1 (PTS1) were co-infiltrated into the leaf. The CFP::PTS1 construct was used as a peroxisomal-targeted fluorescent marker (Linka *et al.*, 2008). Protoplast isolation and microscopic analysis were performed 2 d after infiltration using a Zeiss LSM 510 Meta laser microscope as described in Breuers *et al.* (2012).

For localization studies in *C. merolae*, the *UBIQUITIN 10* promoter of the pUBN-YFP-Dest vector was exchanged for the *apcC* promoter. To this end, the *apcC* promoter region was synthesized by Phusion PCR using the pCG1 vector (Watanabe *et al.*, 2011) as the template and the primer P3 (*Pme*I restriction site) and P4 (*Spe*I restriction site). The vector pJET2.1 (ThermoFisher Scientific) was used for subcloning. Transformation of *C. merolae* was performed as described by Ohnuma *et al.* (2008). Microscopic analysis was carried out 1 d after transformation using the Zeiss LSM 780 laser microscope. Primer sequences are listed in Supplementary Table S1.

Δgox mutant generation

To inactivate the *CmGOX* gene, the *CmGOX* (*CMQ436C*) locus was replaced by the *C. merolae URA* gene by homologous recombination. The *CmGOX* genomic region was amplified with the primers GOX_KO_F1 and GOX_KO_R1. The amplified DNA was cloned into the pQE80 vector (Qiagen, Hilden, Germany) using the In-Fusion HD Cloning Kit (Clontech, Mountain View, CA, USA). The 3′ portion, vector, and 5′ portion of *CmGOX* was amplified with the primers GOX_KO_F2 and GOX_KO_R2 and then the *URA* gene amplified with URA_F and URA_R was inserted by In-Fusion Cloning. The *CmGOX* genomic region with the *URA* insert was amplified from the vector by PCR with primers GOX_KO_F3 and GOX_KO_R3 and was transformed into *C. merolae* M4, a derivative of *C. merolae* 10D, which has a mutation in the *URA* gene (Minoda *et al.*, 2004). Transformation and selection of the gene knockouts were performed as described (Imamura *et al.*, 2010; Fujiwara *et al.*, 2015). The occurrence of the recombination events in the *CmGOX*-knockout strains was confirmed by PCR with the primer sets GOX_KO_F4/GOX_KO_R4 and GOX_KO_F5/GOX_KO_R5. Absence of *CmGOX* transcripts in the knockout lines was verified by RT-PCR analysis using the primers GOX_KO_F2 and GOX_KO_R2. Transcripts from the *CMQ432C* locus adjacent to *CmGOX* were amplified using the primers CMQ432C-F and CMQ432C-R as a control. Primer sequences are given in Supplementary Table S1.

Metabolite extraction and analysis

Centrifugation was used to harvest 10 ml cells (4°C, 5 min, 3000 RCF) and the resulting pellets were frozen in liquid nitrogen. For metabolite extraction, the pellets were resuspended in ethanol (70% v/v, including 50 µM ribitol as internal standard), using acid-washed glass beads for cell disruption by vortexing (3 × 1 min, 4°C, maximum speed). The extraction mix was centrifuged (4°C, 2 min, 16 000 RCF) and the supernatant was analysed by gas chromatography coupled to a time-of-flight mass spectrometer (7200 GC-QTOF; Agilent Technologies, Santa Clara, CA, USA) according to Fiehn and Kind (2007). Peak areas for all compounds were analysed using the Mass Hunter Software (Agilent) and curated manually if necessary.

For the analysis of glycine and serine, the same extract was derivatized by AccQ-Tag Ultra Reagent Powder (Waters Corporation, Milford, MA, USA) according to the manufacturer's instructions and separated at 60°C and a flow of 0.7 ml min^{-1} on an AccQ-Tag™ Ultra Column 2.1 × 100 mm and particle size 1.7 µm (Waters Corporation) using the 10% AccQ-Tag™ Ultra Eluent A (Waters Corporation) and acetonitrile as eluent B (0–0.54 min, 0.1% B; 0.54–5.74 min, 0.1–9.1% B; 5.74–7.74 min, 9.1–21.2% B; 7.74–8.04 min, 21.2–59.6% B and maintained for 0.6 min; 8.64–8.73 min, 59.6–95% B and maintained for 0.27 min; 9.0–9.1 min, 95–100% B and maintained for 0.1 min). Derivatized compounds were detected at 260 nm. For this purpose a 1290 UHPLC system coupled to diode array detector from Agilent was used.

Photosynthetic rate measurement

Cultivation of WT and the Δ*gox* #46 mutant was performed under continuous light (80 µmol photons m^{-2} s^{-1}) at 28°C. Cells were precultivated at 5% CO_2. Twenty-four hours before measurements, cultures were adjusted to a cell density of OD_{750} of 0.7 and shifted to either HC (bubbling with 5% CO_2) or LC conditions (bubbling with ambient air containing 0.04% CO_2). Cells were then collected by centrifugation (4000 rpm, 5 min, room temperature), washed, and resuspended in CO_2-free 2×MA growth medium to a final OD_{750} of 1. The oxygen production of 3 ml of this cell culture was used to quantify the photosynthetic rate at 28°C and a saturating light intensity of 120 µmol photons m^{-2} s^{-1}, using a Clark electrode (Oxygraph System; Hansatech, Norfolk, England). To determine the CO_2-dependent photosynthetic rate, sodium hydrogen bicarbonate ($NaHCO_3$) was stepwise added to a final saturating concentration of 257 µM. Oxygraph Plus software (Hansatech) and Prism (GraphPad Software, La Jolla, CA, USA) was used for data analysis.

Chlorophyll a determination

To analyse chlorophyll *a* (Chl *a*) concentration, 1 ml of cell culture was centrifuged (2 min, 16 000 RCF, room temperature) and 900 µl supernatant was exchanged by methanol (100% v/v). The suspension was incubated for 10 min at 65°C and measured at OD_{665}. The extinction value (extinction coefficient of 78.74l g^{-1} cm^{-1}) was

multiplied by 12.7 to calculate the Chl *a* content in micrograms per millilitre (Meeks and Castenholz, 1971).

Heterologous expression of CmGOX and enzyme assay

To generate a CmGOX overexpressing *Escherichia coli* strain, the coding sequence was amplified by PCR using genomic DNA from *C. merolae*, gene-specific primers with added cleavage sites (CMQ436C-EcoRI-fw and CMQ436C-SalI-rv; Supplementary Table S1), Taq Polymerase Mastermix (Qiagen), and proof-reading Elongase enzyme (ThermoFisher Scientific). The resulting 1182 bp fragment was cloned into the pGemT-vector (Promega). After sequence confirmation (Seqlab, Göttingen, Germany), the coding sequence was cloned into the expression vector IBA43+ in frame with the N-terminal His-tag using *Eco*RI/*Sal*I and subsequently transformed into the *E. coli* strain BL21 DE3. To improve the folding of the recombinant protein, the CmGOX-overexpressing *E. coli* strain was co-transformed with the pG-KJE8 plasmid coding for five chaperones (Takara, Ohtsu, Japan).

E. coli BL21 cells containing IBA43+-CmGOX and pG-KJE8 were grown in lysogeny broth medium supplemented with plasmid-specific antibiotics, L-arabinose, and tetracycline (0.05% and 0.5 ng ml^{-1} final concentration) to an OD_{750} of 0.6 at 30°C. CmGOX expression was induced by the addition of 200 µg l^{-1} anhydrotetracycline and the cells were incubated for 16 h at 30°C. The fusion protein was purified via the N-terminal His-tag using Ni-NTA Sepharose according to the protocol of the supplier (ThermoFisher Scientific). All purification steps were performed at 4°C. The cells were harvested and resuspended in homogenization buffer (20 mM Tris-HCl, pH 8.0, containing 500 mM NaCl, 1 mM DTT, and 0.1 mM FMN). Proteins were extracted by ultrasonic treatments (4 × 30 s, 90 W) in ice. Soluble protein extracts were used for affinity chromatography on Ni-NTA Sepharose using the homogenization buffer supplemented with 40–80 mM imidazole as washing buffers. The elution buffer contained 300 mM imidazole. The elution fractions were combined and desalted using PD-10 columns (GE Healthcare, Little Chalfont, UK). Finally, the recombinant enzymes were dissolved in 20 mM Tris-HCl, pH 8.0, containing 1 mM DTT, and 0.1 mM FMN. The eluted proteins were checked regarding purity using SDS-PAGE. Protein concentration was determined using Bradford's method with bovine albumin as the standard protein (Bradford, 1976).

The purified and desalted recombinant His-tagged protein was used for enzyme assays with a Hansatech oxygen electrode as described in detail by Hackenberg *et al.* (2011).

Results

The genome of C. merolae *contains single copy genes for all enzymes of the plant-type photorespiratory pathway*

We first performed BLASTP analyses using the BLAST tools of both the *C. merolae* Genome Project (http://merolae.biol.s.u-tokyo.ac.jp/blast/blast.html;Matsuzaki *et al.*, 2004) and the National Center for Biotechnology Information (http://blast.ncbi.nlm.nih.gov/Blast.cgi), to identify in *C. merolae* proteins homologous to the photorespiratory enzymes in *A. thaliana*. The query and match proteins from *A. thaliana* and *C. merolae*, respectively, are listed in Supplementary Table S2. As a result, we identified the full protein repertoire of a plant-type photorespiratory pathway in *C. merolae* (Fig. 1). In contrast to *A. thaliana* and other land plants, single copy genes and not gene families encode the photorespiratory enzymes. For the majority, the *A. thaliana* query and the identified *C. merolae* proteins were the best reciprocal BLAST hits. We were unable to identify a protein homologous with the glycolate dehydrogenase that acts in the photorespiratory pathway of *Chlorophyta* such as *C. reinhardtii* (Nakamura *et al.*, 2005). This suggests that the glycolate-to-glyoxylate converting step is probably catalysed by GOX in *Rhodophyta* such as *C. merolae*. In accordance with the predicted GOX activity, we identified a catalase (Fig. 1) that is needed to decompose the H_2O_2, which is generated as a side-product of GOX activity.

CmGOX has a higher affinity for glycolate than L*-lactate*

To verify the enzymatic activity of the putative GOX from *C. merolae,* the coding gene was heterologously expressed in *E. coli*. The purified His-tagged protein (see Supplementary Fig. S1) was used for enzymatic assays, in which the O_2 consumption was determined depending on the substrates L-lactate or glycolate. Like the homologous protein from the plant *A. thaliana*, CmGOX catalysed the oxidation of both substrates, L-lactate and glycolate (Fig. 2). The low K_m value for glycolate (0.9 ± 0.2 mM) and significantly higher K_m value for L-lactate (14.9 ± 3.0 µM) clearly support the hypothesis that the gene *CMQ436C* encodes an oxidase with higher affinity for glycolate than L-lactate. The V_{max} for L-lactate (3.3 ± 0.3 µmol min^{-1} mg^{-1}) was twice as high as that for glycolate (1.5 ± 0.3 µmol min^{-1} mg^{-1}). The occurrence of GOX in *C. merolae* suggests high flux through the photorespiratory pathway, as found in vascular plants.

CmGOX is localized in the matrix of peroxisomes

Typically, GOX proteins reside in the peroxisomal matrix, where the critical GOX catalysis by-product H_2O_2 is efficiently decomposed by the activity of catalase. The CmGOX protein sequence contains a putative peroxisome targeting sequence (SKL) at the C-terminus (Matsuzaki *et al.*, 2004). To experimentally determine the actual subcellular localization, we generated GOX protein variants that were fused with an N-terminal YFP-domain. For expression in *C. merolae* cells, the YFP::CmGOX construct was set under the control of the strong *apcC* promoter, which has been shown to be suitable for protein localization studies in *C. merolae* (Watanabe *et al.*, 2011). Fluorescence microscopy demonstrated that the YFP::CmGOX resides in the peroxisome in *C. merolae* (Fig. 3A). To improve the resolution, we alternatively expressed the YFP::CmGOX construct under control of the *UBIQUITIN 10* promoter in tobacco leaves. The overlap of the peroxisomal marker (CFP::PTS1, Linka *et al.*, 2008) signal and the YFP::CmGOX signal in protoplasts confirmed the localization of CmGOX in the peroxisomal matrix (Fig. 3B).

The amount of CmGOX *transcript increases under LC conditions*

To examine if transcript amounts of *CmGOX* responded to changes in CO_2 availability, the *CmGOX* steady state

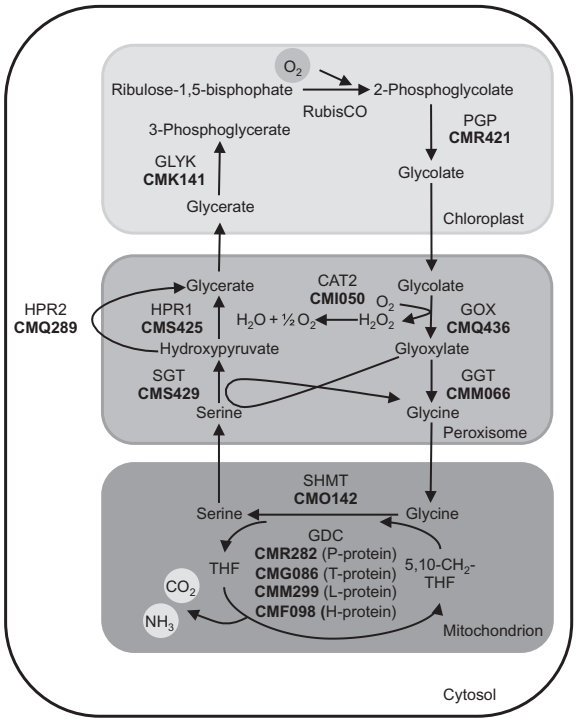

Fig. 1. Schematic view of the photorespiratory pathway in *C. merolae*. Candidate proteins in *C. merolae* were identified by BLAST analysis. Corresponding protein identifiers (acc. to *C. merolae* Genome Project, http://merolae.biol.s.u-tokyo.ac.jp/;Matsuzaki *et al.*, 2004) are shown in bold. The enzymes are CAT2: catalase 2; GDC: glycine decarboxylase; GGT: glutamate:glyoxylate aminotransferase; GLYK, glycerate 3-kinase; GOX, glycolate oxidase; HPR1, peroxisomal hydroxypyruvate reductase 1; HPR2, cytosolic hydroxypyruvate reductase 2; PGP, 2-PG phosphatase; Rubisco, ribulose-1,5-bisphosphate carboxylase/oxygenase; SHMT, serine hydroxymethyl transferase; SGT, serine:glyoxylate aminotransferase.

transcript level was analysed in *C. merolae* WT cells cultivated under photorespiration-suppressing HC conditions and after a shift to photorespiration-stimulating LC conditions. *CmGOX* transcript abundance increased 100-fold 3 h after the shift to LC in comparison to constant HC conditions. After 24 h under LC conditions, the *CmGOX* transcript level returned to the low amounts typical of HC-grown cells (Fig. 4A). We observed a comparable abundance pattern for the gene encoding the large subunit of Rubisco (*CmRBCL*). The transcript level significantly increased 3-fold 3 h after the shift to LC, while it was similar to the HC value after 24 h in LC conditions (Fig. 4B).

Deletion of CmGOX *causes an HCR phenotype and perturbations in photorespiratory metabolism*

To study the importance of photorespiration and especially the function of the GOX protein for *C. merolae,* we generated Δ*gox* knockout mutant lines. Mutant generation was performed as described by Imamura *et al.* (2010). The *CmGOX* coding sequence was exchanged for the *URA5.3* marker gene via homologous recombination (Fig. 5A), conferring uracil autotrophy to the otherwise uracil auxotrophic M4 mutant strain. Correct recombination events were verified for the mutant lines Δ*gox* #43, #45, and #46 by PCR using genomic DNA as the template (Fig. 5B). Because *CmGOX* transcripts could not be detected for Δ*gox* #43 and Δ*gox* #46 (Fig. 5C) at the mRNA level, we chose these as the knockout mutant lines for further analyses.

To gain insight into the impact of *CmGOX* deletion on the metabolism of *C. merolae* we performed a CO_2 shift experiment, in which WT and the knockout mutant lines Δ*gox* #43 and Δ*gox* #46 were pre-cultivated under HC conditions, shifted to LC conditions for 24 h, and then shifted back to HC conditions for another 24 h. Under HC conditions, the growth performance of WT and mutants was not significantly different (Fig. 6). The shift towards LC conditions led to almost fully impaired growth in the Δ*gox* #43 and Δ*gox* #46 mutants, whereas WT cells continued growing. After the shift back to HC conditions, all cultures resumed growth and no difference in growth rates could be detected (Fig. 6). Chl *a* concentrations did not significantly differ between WT

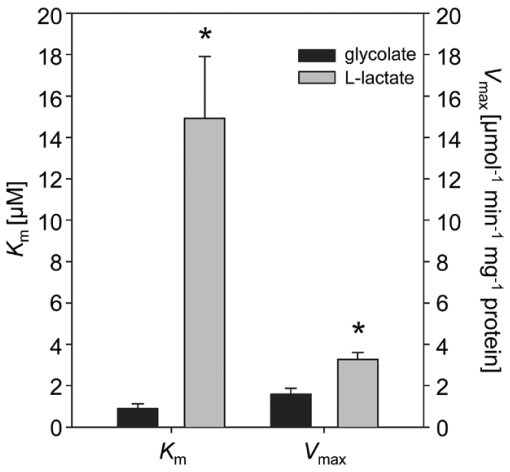

Fig. 2. Biochemical characterization of recombinant CmGOX. The K_m and V_{max} values of CmGOX for the substrates glycolate and L-lactate were calculated by non-linear regression following the Michaelis–Menten kinetic implemented in SigmaPlot 11.0. The means of at least two independent enzyme preparations ± SD are given. Asterisks indicate significant differences ($P < 0.05$) determined with the two-tailed Student's t-test.

and mutant cells (Supplementary Fig. S2). Reduced growth of the Δ*gox* #43 and Δ*gox* #46 mutants was also observed when they were grown on solid medium under LC compared to HC conditions (Supplementary Fig. S3). Thus, the deletion of *CmGOX* resulted in an HCR phenotype, indicating an important role for GOX activity under ambient air conditions in *C. merolae*.

During the shift experiment we took samples and performed a targeted metabolite analysis. Samples were taken before (0 h), 3 h, and 24 h after the shift to LC, and 24 h after the re-shift to HC conditions. When grown continuously under HC conditions, glycolate levels were below the detection limit. Importantly, 3 h after the shift to LC, glycolate had accumulated to a level at which it could be measured. Its concentration was two to four times higher in Δ*gox* mutant lines than in WT. After 24 h at LC, glycolate levels declined slightly in all cultures but were still significantly elevated in the mutants compared to WT. When the cultures were allowed to recover for 24 h under HC conditions, glycolate was only detectable in the Δ*gox* mutant lines but not in WT cells (Fig. 7). Glycine-to-serine conversion in mitochondria is a central step in the photorespiratory pathway (see Fig. 1). In the WT we observed significant increases in both the glycine and the serine levels 3 h after the shift to LC conditions (Supplementary Fig. S4A, B). The Δ*gox* mutants showed a different metabolic response.

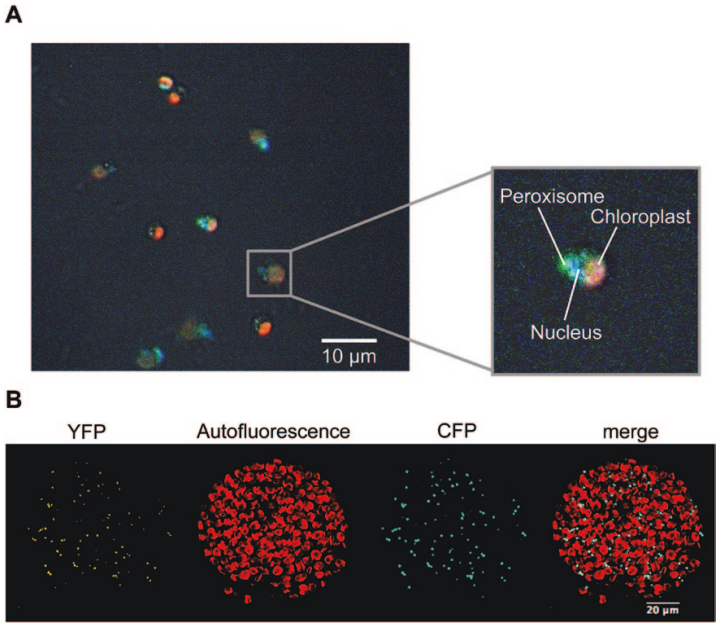

Fig. 3. Subcellular localization studies of CmGOX. (**A**) Localization of CmGOX in *C. merolae*. Red: chloroplast autofluorescence; blue: DAPI-stained nucleus; green: YFP signal from YFP::CmGOX construct. *C. merolae* cells were transformed 24 h before microscopic analysis. (**B**) Localization of CmGOX in tobacco protoplasts. From left to right: YFP signal of YFP::CmGOX construct, chlorophyll autofluorescence, CFP signal as peroxisomal marker (CFP::PTS1), and merge of all three pictures. Microscopic analyses were performed with protoplasts isolated from transiently transformed *N. benthamiana* leaves.

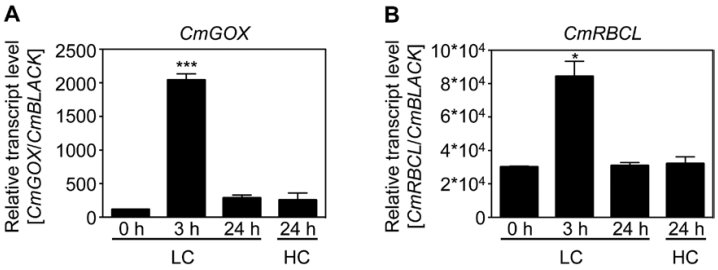

Fig. 4. Effect of shift in CO_2 concentrations on transcript levels of *CmGOX* (**A**) and *CmRBCL* (**B**). Samples were taken before a shift from HC (5% CO_2) to LC (0.04% CO_2) conditions, 3 h and 24 h after the shift, and 24 h after a shift back to HC conditions. Shown is the mean normalized expression of three biological replicates including three technical replicates and the mean normalized standard error. *CmBLACK* (*CMM193C*) was used as the reference gene for Ct analysis. Significant differences to initial transcript levels (LC, 0 h) were analysed by a two-tailed Student's t-test (***$P < 0.001$).

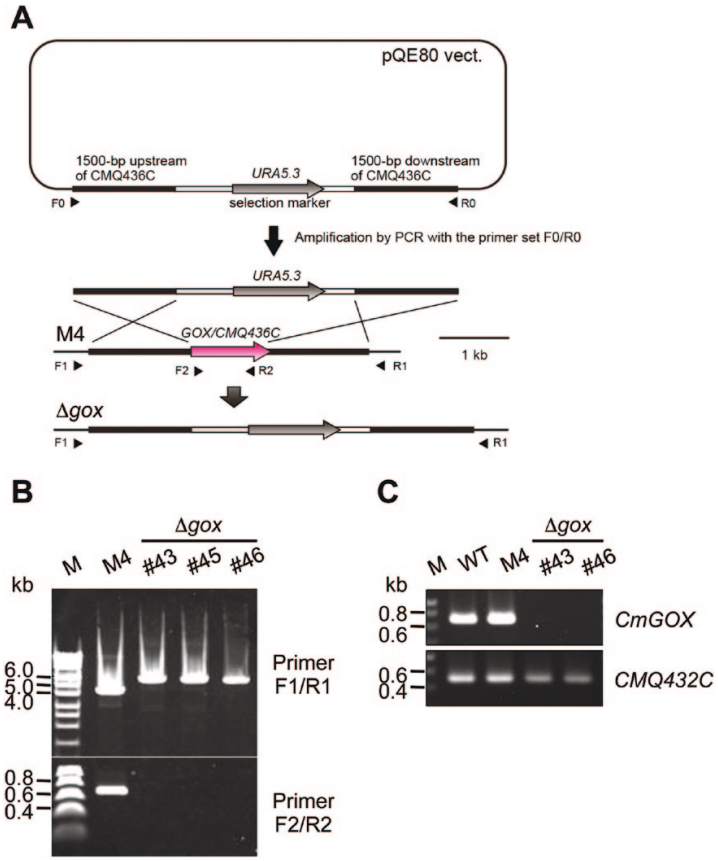

Fig. 5. Generation of a Δ*gox* knockout mutant in *C. merolae*. (**A**) Schematic presentation of the strategy to generate a knockout mutant for *CmGOX*. For detailed information see 'Materials and methods'. (**B**) Verification of Δ*gox* mutant lines #43, #45, and #46. PCR was performed on genomic DNA of the M4 background mutant and the Δ*gox* mutant lines #43, #45, and #46 with primers flanking the *CmGOX* upstream and downstream regions (F1/R1) and the *CmGOX* coding region (F2/R2), respectively. Expected fragment sizes were F1/R1: 4.5 kb (M4), 6 kb (Δ*gox*); F2/R2: 0.66 kb (M4), – (Δ*gox*). (**C**) Verification of absence of *CmGOX* transcripts in the Δ*gox* knockout lines #43 and #46. RT-PCR analysis was performed on cDNA isolated from WT, M4 background mutant, and the Δ*gox* mutant lines #43 and #46 with primers flanking the *CmGOX* coding region (F2/R2). Transcripts from the *CMQ432C* locus adjacent to the *CmGOX* locus were used as a control. Expected fragment sizes are *CmGOX*: 698 bp; *CMQ432C*: 520 bp.

Glycine concentration was already higher under HC conditions in the mutants cells compared to WT, and increased by 2-fold 3 h after the shift to LC, and by 3-fold 24 h after the shift. After 24 h recovery under HC conditions, glycine levels were still elevated in the mutants (Supplementary Fig. S4A). Serine levels had the opposite response and were lower in the Δ*gox* #43 and Δ*gox* #46 mutants than in the WT. A statistically significant difference was observed 3 h after the LC shift, with serine levels of only 40% compared to the WT levels (Supplementary Fig. S4B). For the photorespiratory intermediate glycerate we did not detect significant differences between WT and mutant lines (Supplementary Fig. S4C). With respect to sugars we detected a significant decline in glucose levels 24 h after LC treatment in all strains. After 24 h HC treatment, the values fully recovered (Supplementary Fig. S4D). Fructose concentrations were also reduced in the WT 24 h after the shift to LC conditions, but were not affected in the mutant lines by changes in CO_2 availability (Supplementary Fig. S4E).

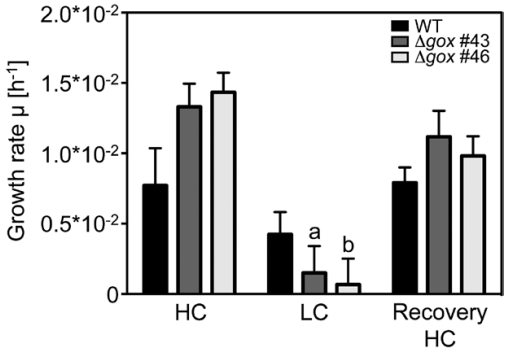

Fig. 6. Growth rate of WT cells and Δ*gox* mutant line #43 and #46 grown for 24 h under HC conditions (5% CO_2), 24 h under LC conditions (0.04% CO_2), and returned for 24 h to HC conditions. OD_{720} measurements were performed every hour by the Multi-Cultivator system (Photons System Instruments). Shown are means of three biological replicates with standard error. Significant differences to initial growth (HC) within one cell line were determined with a two-tailed Student's t-test and are indicated by *a* ($P < 0.01$) and *b* ($P < 0.001$). Significant differences between the mutant and corresponding WT values could not be detected by t-test.

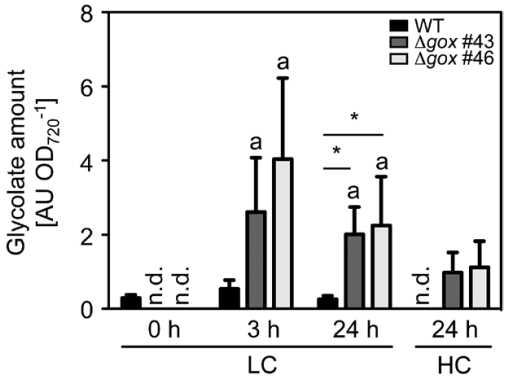

Fig. 7. Glycolate levels of WT and Δ*gox* mutants #43 and #46 during the CO_2 shift experiment. Glycolate levels of the different strains were determined by GC-MS before the shift from HC (5% CO_2) to LC (0.04% CO_2) conditions, 3 h and 24 h after the shift to LC, and after a 24 h recovery phase under HC conditions. Shown are means of four biological replicates and standard errors. n.d., not detectable. Significant differences were analysed by the non-parametric Mann–Whitney test. Significant differences to initial glycolate levels (HC) within one cell line are indicated by *a* ($P < 0.05$). Significant differences between the mutant and corresponding WT values are indicated by an asterisk ($P < 0.05$).

The Δgox *mutant has inhibited photosynthetic activity*

We investigated the impact of *CmGOX* deletion on photosynthetic activity by determining O_2 production in increasing HCO_3^- concentrations (Fig. 8). WT cells grown under either HC or LC conditions had a V_{max} of 14 μmol O_2 h^{-1} per mg Chl *a* (Table 1). However, WT cells grown under HC conditions had a higher apparent K_m (K_m = 13.9 μM) compared to WT cells grown under LC conditions (K_m = 9.1 μM), which means that LC-grown cells were quicker to reach the maximal photosynthetic rate (Table 1). However, this difference was not significant. In comparison to WT, the Δ*gox* #46 mutant line showed a significantly lower maximal photosynthetic rate, and reduced but not significantly different K_m values (Table 1, Fig. 8). Mutant cells grown under LC conditions had a higher V_{max} (V_{max} = 10.3 μmol O_2 h^{-1} per mg Chl *a*) than mutant cells grown under HC conditions (V_{max} = 8.6 μmol O_2 h^{-1} per mg Chl *a*). The different growth conditions resulted in different K_m values (HC K_m = 8.4 μM; LC K_m = 4.9 μM; Table 1), as was the case for the WT.

Discussion

The red alga *C. merolae* lives in acidic and hot aquatic habitats, which are naturally low in CO_2. The solubility of CO_2

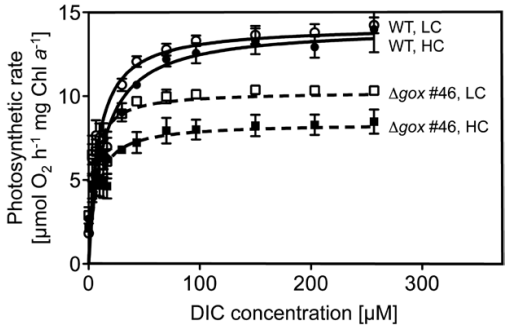

Fig. 8. Photosynthesis rates of WT and Δ*gox* #46 mutant at increasing concentrations of externally supplied dissolved inorganic carbon (DIC). Cells were cultivated under HC conditions (5% CO_2) and O_2 evolution was measured using a Clark electrode. For LC measurements, cells were shifted for 24 h to LC conditions (0.04% CO_2). The photosynthetic rate was analysed according to increasing DIC concentration in the medium. Fitting analysis was performed using the Michaelis–Menten Kinetic (Prism 5) on the basis of three biological replicates each.

Table 1. *Effect of CO_2 concentration on photosynthetic rates (V_{max}) and C_i affinities (K_m) of WT and Δgox #46 cells.*

	HC		LC	
	WT	**Δgox #46**	**WT**	**Δgox #46**
V_{max} [µmol O_2 h^{-1} Mg^{-1} Chl *a*]	14.12 ± 0.49	**8.58 ± 1.62**	14.20 ± 0.49	**10.31 ± 0.60**
K_m [µM]	13.94 ± 4.75	8.42 ± 7.69	9.069 ± 3.60	4.85 ± 2.68

Results are presented as mean values ± SD from three independent determinations each. Significant differences (two-tailed Student's t-test, $P < 0.01$) between WT and Δ*gox* #46 mutant are given in bold. Within one line results for HC and LC conditions were not significantly different.

and its diffusion coefficient is up to four magnitudes lower in water than in air (reviewed in Moroney *et al.*, 2013). Consequently, the red algal Rubisco evolved a characteristically high specificity for CO_2, which is indicative of low CO_2 concentrations at the site of Rubisco activity (Savir *et al.*, 2010). Despite its optimized Rubisco, red algae have been suggested to execute a carbon concentrating mechanism (CCM) that enhances the CO_2 concentration near Rubisco (Zenvirth *et al.*, 1985; Giordano *et al.*, 2005). This raises the question of whether the survival of *C. merolae* under ambient conditions depends on photorespiratory metabolism. The importance of photorespiration in this organism has not been investigated to date.

The red alga *C. merolae* harbours a photorespiratory pathway that appears to be more similar to that of land plants than to *C. reinhardtii,* as revealed by BLAST analysis. All photorespiratory enzymes known from land plants, including catalase, are encoded in the genome of *C. merolae* and are homologous to the plant-type photorespiratory proteins (Supplementary Table S2). In contrast to land plants, all enzymes are encoded by single genes in the small and minimally redundant genome of *C. merolae*. Besides the enzymes catalysing the conversion of the photorespiratory intermediates, transporters shuttling the intermediates between the different organelles play a central role in photorespiratory metabolism in photosynthetic eukaryotes (reviewed in Eisenhut *et al.*, 2013). Among the few photorespiratory transporters identified to date, only the plastidic glycolate glycerate translocator PLGG1 (Pick *et al.*, 2013) is encoded in the genome of *C. merolae.* Homologues for the two plastidic carboxylate translocators DiT1 and DiT2 (Weber and Flügge, 2002; Renné *et al.*, 2003), which are involved in photorespiratory nitrogen recycling, do not exist in *C. merolae* (reviewed in Eisenhut *et al.*, 2015). We did not identify any proteins in *C. merolae* that were homologous with enzymes of the bacterial-type glycerate pathway, as found in cyanobacteria (Eisenhut *et al.*, 2006). We were also unable to identify a GlcD-type glycolate dehydrogenase. Thus, we hypothesized that the candidate GOX protein identified in our study catalyses the conversion of glycolate to glyoxylate in *C. merolae*, which supports previous phylogenetic analyses by Kern *et al.* (2013).

Our analysis revealed that *C. merolae* and probably all *Rhodophyta* perform a plant-like glycolate-to-glyoxylate conversion via a specific GOX in the peroxisome. Heterologous expression of the candidate GOX from *C. merolae* revealed a higher affinity for glycolate than for L-lactate (Fig. 2), and thus supported the likely usage of a GOX for the conversion of glycolate to glyoxylate during photorespiration. We could furthermore demonstrate that, as in plants, CmGOX resides in the peroxisome (Fig. 3), which is a prerequisite for it to function as a photorespiratory GOX. Given that the employment of a GOX is indicative of high flux through the photorespiratory pathway (Kehlenbeck *et al.*, 1995; Hagemann *et al.*, 2013), we suggest that, similar to plants, photorespiratory flux is high in the red alga *C. merolae*. In has previously been assumed that algae such as *C. reinhardtii*, which use a CCM, are characterized by low photorespiratory flux rates (Birmingham *et al.*, 1982). Indeed, glycolate-to-glyoxylate conversion by GlcD in the mitochondria of *C. reinhardtii* meets these low-flux requirements (Kehlenbeck *et al.*, 1995; Nakamura *et al.*, 2005). Moreover, in *Chlorophyceae* such as *C. reinhardtii*, the reduction of hydroxypyruvate and the transaminase steps occur in the mitochondria, and not in the peroxisomes (Atteia *et al.*, 2009). Accordingly, peroxisomes do not seem to be involved in photorespiration in *Chlorophyceae*, which could be the result of a different peroxisomal enzyme repertoire in this algal lineage (Stabenau, 1974; Stabenau *et al.*, 1993).

Further support for the involvement of CmGOX in the photorespiratory pathway in *C. merolae* was provided by gene expression analysis. *CmGOX* transcript amounts strongly increased 3 h after the shift to photorespiratory conditions (Fig. 4A). The 100-fold increase of the *CmGOX* transcript level coincided with accumulation of glycolate in WT cells 3 h after the shift to LC conditions (Fig. 7). It must be mentioned that an increase in transcript abundance does not necessarily lead to a proportional increase in protein abundance, as, for example, demonstrated for *C. reinhardtii* (Mettler *et al.*, 2014). However, the transcriptional response indicates that *C. merolae* quickly senses a change in the CO_2 environment. Comparably, genes for CCM components and photorespiratory enzymes are upregulated in the chlorophyte *C. reinhardtii* (Fang *et al.*, 2012). However, it is not known how oxygenic phototrophs sense alterations in CO_2 concentrations (Raven, 2006). The accumulation of photorespiratory intermediates such as 2-PG (Haimovich-Dayan *et al.*, 2015) and glycolate (Hackenberg *et al.*, 2012) could serve as signals that trigger the enhanced expression of the CCM genes among cyanobacteria under LC conditions.

The plant-like photorespiratory GOX is essential for survival of *C. merolae* under ambient conditions, as demonstrated by the occurrence of the HCR phenotype in the Δ*gox* knockout mutants. Mutant growth almost completely stopped after a shift from 5% CO_2 to ambient air, whereas it quickly recovered when mutant cells were shifted back to HC conditions (Fig. 6, Supplementary Fig. S3). This behaviour is typical for the HCR phenotype (Somerville, 2001). However, in contrast to a plant HCR phenotype, we did not observe a chlorotic phenotype in the Δ*gox* mutants after the shift to

LC conditions (Supplementary Fig. S2). A further argument for the function of photorespiratory GOX is the accumulation of glycolate in the Δ*gox* knockout mutant lines under LC conditions. A 24 h recovery phase in HC was not sufficient to reduce the amount of glycolate below detectable levels in the Δ*gox* mutants, in contrast to what was observed for the WT (Fig. 7). Similarly, the GlcD mutant in *C. reinhardtii* showed a 4-fold higher accumulation of glycolate compared to the WT (Nakamura *et al.*, 2005). The same was true for a GOX mutant in *Zea mays*, which showed an 11-fold higher glycolate level after 25 h in ambient air compared to the stable glycolate level in WT plants (Zelitch *et al.*, 2009).

Furthermore, the photosynthetic performance of Δ*gox* knockout mutants was affected (Fig. 8, Table 1). WT cells showed similar maximal photosynthetic rates when grown under HC or LC conditions, but enhanced CO_2 affinity was found under LC conditions, as has been previously reported (Zenvirth *et al.*, 1985). Although not significant, cells of the mutant Δ*gox* #46 showed an enhanced affinity towards CO_2 compared to the WT cells. However, maximal photosynthetic activity was significantly reduced in the mutant, which is likely the result of toxic effects due to the impaired photorespiratory pathway. For example, accumulation of the photorespiratory intermediates 2-PG (Norman and Colman, 1991) and glycine (Eisenhut *et al.*, 2007) is known to inhibit growth and photosynthesis.

In conclusion, all obtained results support the hypothesis that *C. merolae* has a plant-type photorespiratory pathway, which is an indication for high photorespiratory flux in red algae. A plant-like photorespiratory metabolism with recruitment of peroxisomal GOX to improve the bottleneck reaction glycolate-to-glyoxylate conversion is an early evolutionary strategy to adapt to increasing O_2 concentrations in the atmosphere. These findings are contrary to earlier assumptions that the plant-like photorespiration pathway appeared late and only among streptophytic green algae, which was discussed to be a crucial step for the later colonization of the continents by land plants (e.g. Becker, 2013).

Supplementary data

Supplementary material is available at *JXB* online.

Table S1. Oligonucleotides used in this study.

Table S2. List of *A. thaliana* photorespiratory enzymes and identified homologous proteins in *C. merolae*.

Figure S1. Purification of recombinant CmGOX.

Figure S2. Chl *a* concentrations of WT and Δ*gox* mutants #43 and #46 during the CO_2 shift experiment.

Figure S3. CO_2-dependent growth of WT and Δ*gox* mutants #43 and #46.

Figure S4. Metabolite levels of WT and Δ*gox* mutants #43 and #46 during the CO_2 shift experiment.

Acknowledgments

The technical assistance of Samantha Kurz, Maria Graf, Elisabeth Klemp, Klaudia Michl, and Katrin Weber is greatly appreciated. Maria Graf is also acknowledged for her technical expertise in method development. Our work on photorespiration was supported by grants from the DFG (Deutsche Forschungsgemeinschaft) in the frame of the Forschergruppe FOR 1186 – Promics (WE 2231/8-2).

References

Atteia A, Adrait A, Brugiere S, *et al*. 2009. A proteomic survey of *Chlamydomonas reinhardtii* mitochondria sheds new light on the metabolic plasticity of the organelle and on the nature of the alpha-proteobacterial mitochondrial ancestor. Molecular Biology and Evolution **26,** 1533–1548.

Bauwe H, Hagemann M, Fernie AR. 2010. Photorespiration: players, partners and origin. Trends in Plant Science **15,** 330–336.

Becker B. 2013. Snow ball earth and the split of Streptophyta and Chlorophyta. Trends in Plant Science **18,** 180–183.

Birmingham BC, Coleman JR, Colman B. 1982. Measurement of photorespiration in algae. Plant Physiology **69,** 259–262.

Bradford M. 1976. A rapid and sensitive method for the quantitation of microgram quantities of protein utilizing the principle of protein-dye binding. Analytical Biochemistry **72,** 248–254.

Breuers FKH, Bräutigam A, Geimer S, Welzel U, Stefano G, Renna L, Brandizzi F, Weber APM. 2012. Dynamic remodeling of the plastid envelope membranes – a tool for chloroplast envelope in vivo localizations. Frontiers in Plant Science **3,** 1–10.

Colman B, Balkos KD. 2005. Mechanism of inorganic carbon acquisition in two *Euglena* species. Canadian Journal of Botany **83,** 865–871.

Czechowski T, Stitt M, Altmann T, Udvardi MK. 2005. Genome-wide identification and testing of superior reference genes for transcript normalization. Plant Physiology **139,** 5–17.

Eisenhut M, Bauwe H, Hagemann M. 2007. Glycine accumulation is toxic for the cyanobacterium *Synechocystis sp.* strain PCC 6803, but can be compensated by supplementation with magnesium ions. FEMS Microbiology Letters **277,** 232–237.

Eisenhut M, Hocken N, Weber APM. 2015. Plastidial metabolite transporters integrate photorespiration with carbon, nitrogen, and sulfur metabolism. Cell Calcium **58,** 98–104.

Eisenhut M, Kahlon S, Hasse D, Ewald R, Lieman-Hurwitz J, Ogawa T, Ruth W, Bauwe H, Kaplan A, Hagemann M. 2006. The plant-like c2 glycolate cycle and the bacterial-like glycerate pathway cooperate in phosphoglycolate metabolism in cyanobacteria. Plant Physiology **142,** 333–342.

Eisenhut M, Pick TR, Bordych C, Weber AP. 2013. Towards closing the remaining gaps in photorespiration – the essential but unexplored role of transport proteins. Plant Biology **15,** 676–685.

Eisenhut M, Ruth W, Haimovich M, Bauwe H, Kaplan A, Hagemann M. 2008. The photorespiratory glycolate metabolism is essential for cyanobacteria and might have been conveyed endosymbiontically to plants. PNAS **105,** 17199–17204.

Engel N, van den Daele K, Kolukisaoglu U, Morgenthal K, Weckwerth W, Parnik T, Keerberg O, Bauwe H. 2007. Deletion of glycine decarboxylase in Arabidopsis is lethal under nonphotorespiratory conditions. Plant Physiology **144,** 1328–1335.

Fang W, Si Y, Douglass S, Casero D, Merchant SS, Pellegrini M, Ladunga I, Liu P, Spalding MH. 2012. Transcriptome-wide changes in *Chlamydomonas reinhardtii* gene expression regulated by carbon dioxide and the CO_2-concentrating mechanism regulator CIA5/CCM1. The Plant Cell **24,** 1876–1893.

Fiehn O, Kind T. 2007. Metabolite profiling in blood plasma. Metabolomics - Methods in Molecular Biology **358,** 3–17.

Fujiwara T, Kanesaki Y, Hirooka S, Era A, Sumiya N, Yoshikawa H, Tanaka K, Miyagishima S-Y. 2015. A nitrogen source-dependent inducible and repressible gene expression system in the red alga *Cyanidioschyzon merolae*. Frontiers in Plant Science **6,** 1–10.

Gimmler H, Kugel H, Liebfritz D, Mayer A. 1988. Cytoplasmic pH of *Dunaliella parva* and *Dunaliella acidophila* as monitored by in vivo 31P-NMR spectroscopy and the DMO method. Physiologia Plantarum **74,** 521–530.

Giordano M, Beardall J, Raven JA. 2005. CO_2 concentrating mechanism in algae: mechanisms, environmental modulation, and evolution. Annual Review of Plant Biology **56,** 99–131.

Grefen C, Donald N, Hashimoto K, Kudla J, Schumacher K, Blatt MR. 2010. A ubiquitin-10 promoter-based vector set for fluorescent protein tagging facilitates temporal stability and native protein distribution in transient and stable expression studies. Plant Journal **64,** 355–365.

Hackenberg C, Huege J, Engelhardt A, Wittink F, Laue M, Matthijs HC, Kopka J, Bauwe H, Hagemann M. 2012. Low carbon acclimation in carboxysome-less and photorespiratory mutants of the cyanobacterium *Synechocystis sp.* strain PCC 6803. Microbiology **158,** 398–413.

Hackenberg C, Kern R, Hüge J, Stal LJ, Tsuji Y, Kopka J, Shiraiwa Y, Bauwe H, Hagemann M. 2011. Cyanobacterial lactate oxidases serve as essential partners in N_2 fixation and evolved into photorespiratory glycolate oxidases in plants. The Plant Cell **23,** 2978–90.

Hagemann M, Eisenhut M, Hackenberg C, Bauwe H. 2010. Pathway and importance of photorespiratory 2-phosphoglycolate metabolism in cyanobacteria. Advances in Experimental Medicine and Biology **675,** 91–108.

Hagemann M, Fernie AR, Espie GS, Kern R, Eisenhut M, Reumann S, Bauwe H, Weber APM. 2013. Evolution of the biochemistry of the photorespiratory C2 cycle. Plant Biology **15,** 639–647.

Hagemann M, Kern R, Maurino VG, Hanson DT, Weber APM, Sage RF, Bauwe H. 2016. Evolution of photorespiration from cyanobacteria to land plants considering protein phylogenies and acquisition of carbon concentrating mechanisms. Journal of Experimental Botany , in press.

Haimovich-Dayan M, Lieman-Hurwitz J, Orf I, Hagemann M, Kaplan A. 2015. Does 2-phosphoglycolate serve as an internal signal molecule of inorganic carbon deprivation in the cyanobacterium *Synechocystis sp*. PCC 6803? Environmental Microbiology **17,** 1794–1804.

Heber U, Krause GH. 1980. Open question - what is the physiological role of photorespiration. Trends in Biochemical Sciences **5,** 32–34.

Husic DW, Husic HD, Tolbert NE, Clanton CBJ. 1987. The oxidative photosynthetic carbon cycle or C2 cycle. Critical Reviews in Plant Sciences **5,** 45–100.

Imamura S, Terashita M, Ohnuma M, *et al*. 2010. Nitrate assimilatory genes and their transcriptional regulation in a unicellular red alga *Cyanidioschyzon merolae*: Genetic evidence for nitrite reduction by a sulfite reductase-like enzyme. Plant and Cell Physiology **51,** 707–717.

Kehlenbeck P, Coyal A, Tolbert NE. 1995. Factors affecting development of peroxisomes and glycolate metabolism among algae of different evolutionary lines of Prasinophyceae. Plant Physiology **109,** 1363–1370.

Kern R, Eisenhut M, Bauwe H, Weber APM, Hagemann M. 2013. Does the *Cyanophora paradoxa* genome revise our view on the evolution of photorespiratory enzymes? Plant Biology **15,** 759–768.

Kozaki A, Takeba G. 1996. Photorespiration protects C3 plants from photooxidation. Nature **384,** 557–560.

Linka N, Theodoulou FL, Haslam RP, Linka M, Napier JA, Neuhaus HE, Weber AP. 2008. Peroxisomal ATP import is essential for seedling development in *Arabidopsis thaliana*. Plant Cell **20,** 3241–3257.

Matsuzaki M, Misumi O, Shin-I T, *et al*. 2004. Genome sequence of the ultrasmall unicellular red alga *Cyanidioschyzon merolae* 10D. Nature **428,** 653–657.

Meeks JC, Castenholz RW. 1971. Growth and photosynthesis in an extreme thermophile, *Synechococcus lividius* (Cyanophya). Archives of Microbiology **78,** 25–41.

Mettler T, Mühlhaus T, Hemme D, *et al*. 2014. Systems analysis of the response of photosynthesis, metabolism, and growth to an increase in irradiance in the photosynthetic model organism *Chlamydomonas reinhardtii*. The Plant Cell **26,** 2310–2350.

Minoda A, Sakagami R, Yagisawa F, Kuroiwa T, Tanaka K. 2004. Improvement of culture conditions and evidence for nuclear transformation by homologous recombination in a red alga, *Cyanidioschyzon merolae* 10D. Plant and Cell Physiology **45,** 667–671.

Moroney JV, Jungnick N, DiMario RJ, Longstreth DJ. 2013. Photorespiration and carbon concentrating mechanisms: two adaptations to high O_2, low CO_2 conditions. Photosynthesis Research **117,** 121–131.

Nakamura Y, Kanakagiri S, Van K, He W, Spalding MH. 2005. Disruption of the glycolate dehydrogenase gene in the high-CO_2-requiring mutant HCR89 of *Chlamydomonas reinhardtii*. Canadian Journal of Botany **83,** 820–833.

Norman EG, Colman B. 1991. Purification and characterization of phosphoglycolate phosphatase from the cyanobacterium *Coccochloris peniocystis*. Plant Physiology **95,** 693–698.

Ogren WL, Bowes G. 1971. Ribulose diphosphate carboxylase regulates soybean photorespiration. Nature New Biology **230,** 159–160.

Ohnuma M, Yokoyama T, Inouye T, Sekine Y, Tanaka K. 2008. Polyethylene glycol (PEG)-mediated transient gene expression in a red alga, *Cyanidioschyzon merolae* 10D. Plant and Cell Physiology **49,** 117–120.

Pick TR, Brautigam A, Schulz MA, Obata T, Fernie AR, Weber APM. 2013. PLGG1, a plastidic glycolate glycerate transporter, is required for photorespiration and defines a unique class of metabolite transporters. Proceedings of the National Academy of Sciences U S A **110,** 3185–3190.

Raven JA. 2006. Sensing inorganic carbon: CO_2 and HCO_3^-. Biochemical Journal **395,** e5–e7.

Renné P, Dreßen U, Hebbeker U, Hille D, Flügge UI, Westhoff P, Weber APM. 2003. The Arabidopsis mutant dct is deficient in the plastidic glutamate/malate translocator DiT2. Plant Journal **35,** 316–331.

Savir Y, Noor E, Milo R, Tlusty T. 2010. Cross-species analysis traces adaptation of Rubisco toward optimality in a low-dimensional landscape. Proceedings of the National Academy of Sciences U S A **107,** 3475–3480.

Schwarte S, Bauwe H. 2007. Identification of the photorespiratory 2-phosphoglycolate phosphatase, PGLP1, in Arabidopsis. Plant Physiology **144,** 1580–1586.

Seckbach J. 1995. The first eukaryotic cells - acid hot-spring algae. Journal of Biological Physics **20,** 335–345.

Simon P. 2003. Q-Gene: processing quantitative real-time RT-PCR data. Bioinformatics **19,** 1439–1440.

Somerville CR. 2001. An early Arabidopsis demonstration. Resolving a few issues concerning photorespiration. Plant Physiology **125,** 20–24.

Stabenau H. 1974. Verteilung von Microbody-Enzymen aus Chlamydomonas in Dichtegradienten [Distribution of microbody enzymes in density gradients]. Planta **118,** 35–42.

Stabenau H, Winkler U, Säftel W. 1993. Localization of glycolate dehydrogenase in two species of *Dunaliella*. Planta **191,** 362–364.

Suzuki K, Mamedov TG, Ikawa T. 1999. A mutant of *Chlamydomonas reinhardtii* with reduced rate of photorespiration. Plant and Cell Physiology **40,** 792–799.

Takahashi S, Bauwe H, Badger M. 2007. Impairment of the photorespiratory pathway accelerates photoinhibition of photosystem II by suppression of repair but not acceleration of damage processes in Arabidopsis. Plant Physiology **144,** 487–494.

Timm S, Florian A, Jahnke K, Nunes-Nesi A, Fernie AR, Bauwe H. 2011. The hydroxypyruvate-reducing system in Arabidopsis: multiple enzymes for the same end. Plant Physiology **155,** 694–705.

Uemura K, Anwaruzzaman, Miyachi S, Yokota A. 1997. Ribulose-1,5-bisphosphate carboxylase/oxygenase from thermophilic red algae with a strong specificity for CO_2 fixation. Biochemical and Biophysical Research Communications **233,** 568–571.

Voll LM, Jamai A, Renné P, Voll H, McClung CR, Weber APM. 2006. The photorespiratory Arabidopsis *shm1* mutant is deficient in SHM1. Plant Physiology **140,** 59–66.

Watanabe S, Ohnuma M, Sato J, Yoshikawa H, Tanaka K. 2011. Utility of a GFP reporter system in the red alga *Cyanidioschyzon merolae*. The Journal of General and Applied Microbiology **57,** 69–72.

Weber A, Flügge UI. 2002. Interaction of cytosolic and plastidic nitrogen metabolism in plants. Journal of Experimental Botany **53,** 865–874.

Zelitch I, Schultes NP, Peterson RB, Brown P, Brutnell TP. 2009. High glycolate oxidase activity is required for survival of maize in normal air. Plant Physiology **149,** 195–204.

Zenvirth D, Volokita M, Kaplan A. 1985. Photosynthesis and inorganic carbon accumulation in the acidophilic alga *Cyanidioschyzon merolae*. Plant Physiology **77,** 237–239.

SUPPLEMENTARY MATERIAL

Photorespiratory glycolate oxidase is essential for survival of the red alga *Cyanidioschyzon merolae* under ambient CO_2 conditions

Nadine Rademacher, Ramona Kern, Takayuki Fujiwara, Tabea Mettler-Altmann, Shin-ya Miyagishima, Martin Hagemann, Marion Eisenhut, Andreas PM Weber

Table S1: Oligonucleotides used in this study. Restriction sites are given in bold. Underlines indicate adaptor sequences for In-Fusion reaction.

Oligonucleotide	**Sequence (5´ -> 3`)**
P1	ccacaattgATGGTTGAGAAGCCAGC
P2	ccaccatggGCTCAGAGTTTGCTCTGC
P3	ccagtttaaacTTACAATACCGATAGATGAGTTTCGA
P4	ccaactagtGGTCAACGAACGAAGAAACACA
qRT-CmGOX-fw	GCCTAGCAGTTGATGGCGA
qRT-CmGOX-rev	CCCGAACGACGAGATCTCTC
qRT-CmBlack-fw	TCACGCAAAACAACATCCAT
qRT-CmBlack-rev	TCAACAGCGTTGAATCGAAG
qRT-CmrbcL-fw	GTGCCACAGCTAACCGTGTA
qRT-CmrbcL-rev	AGCGGTTTGAAGAGGACCAC
CMQ436C-EcoRI-fw	**GAATTC**ATGGTTGAGAAGCCAGCAG
CMQ436C-SalI-rv	**GTCGAC**TTAGAGTTTGCTCTGCATC
GOX_KO_F1	ACCATCACCATCACGTCGAGAACTGGAACTTGTCC
GOX_KO_R1	AAGCTCAGCTAATTACGATGTTGCAGTGCGTACG
GOX_KO_F2	AGTCAGCTGCTAGGGTGAGCGCAGGCTGGAG
GOX_KO_R2	TTCGCCCCTCAGTTCCTCTACTTTGTTTCGAATACTGGTAAAACAA
URA_F	GAACTGAGGGGCGAACGCA
URA_R	CCCTAGCAGCTGACTGTATC
GOX_KO_F3	GTCGAGAACTGGAACTTGTCC
GOX_KO_R3	CGATGTTGCAGTGCGTACG
GOX_KO_F4	CGCAGGCATTCAGGGCAG
GOX_KO_R4	CGCGTGATGGATCGCATTGC

GOX_KO_F5	CGTTTCGACGTCTACGCTTCC
GOX_KO_R5	CTCGAGGCAGTCGATGGTG
CMQ432C-F	TCTACGCTGCCGGAGATTG
CMQ432C-R	GCCATACCAAAGCCAGAACG

Table S2: List of *A. thaliana* photorespiratory enzymes and identified homologous proteins in *C. merolae*.

Photorespiratory enzyme	***A. thaliana***	***C. merolae***	**Identity (%)**	**Similarity (%)**
2-PG phosphatase*	AT5G36700	CMR421C	56	68
Glycolate oxidase	AT3G14420	CMQ436C	59	78
	AT4G18360		59	76
	AT3G14415		59	77
Catalase 2	AT4G35090	CMI050C	61	76
Serine:glyoxylate aminotransferase*	AT2G13360	CMS429C	51	68
Glutamate:glyoxylate aminotransferase*	AT1G23310	CMM066C	38	54
T-protein*	AT1G11860	CMG086C	43	59
	AT1G60990		21	39
P-protein	AT4G33010	CMR282C	56	69
	AT2G26080		56	70
H-protein	AT2G35370	CMF098C	50	67
	AT2G35120		52	68
	AT1G32470		51	66
L-protein	AT3G17240	CMM299C	58	74
	AT1G48030		58	74
Serine hydroxymethyl transferase*	AT4G37930	CMO142C	62	78
Hydroxypyruvate reductase 1*	AT1G68010	CMS425C	56	74
Hydroxypyruvate	AT1G79870	CMQ289C	39	55
reductase 2	AT1G68010		38	54
Glycerate kinase*	AT1G80380	CMK141C	37	53

*best bidirectional hit

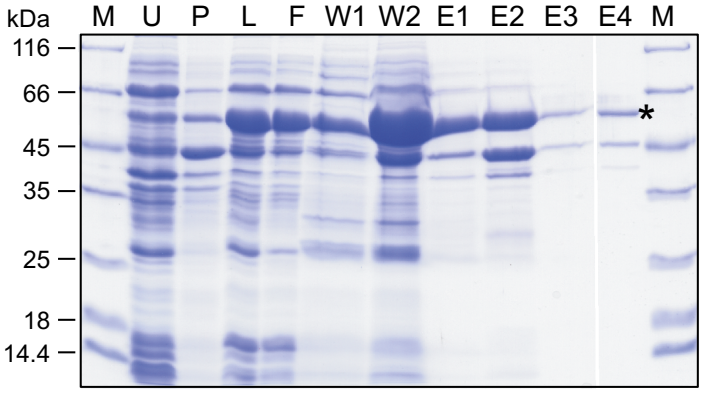

Figure S1: Purification of recombinant CmGOX. N-terminally His-tagged CmGOX (*) was purified via Ni-NTA- affinity chromatography. The desalted elution fraction (E4) was used for *in vitro* enzyme assays of putative GOX/LOX activity. M, Protein Molecular weight marker; U, uninduced crude cell extract; P, Cell-debris obtained after cell disruption and centrifugation; L, Lysat; F, Flow-through of lysat; W1 and W2, Washing flow-through; E1-E3, Elution fractions, which were combined and desalted using PD-10 columns giving E4.

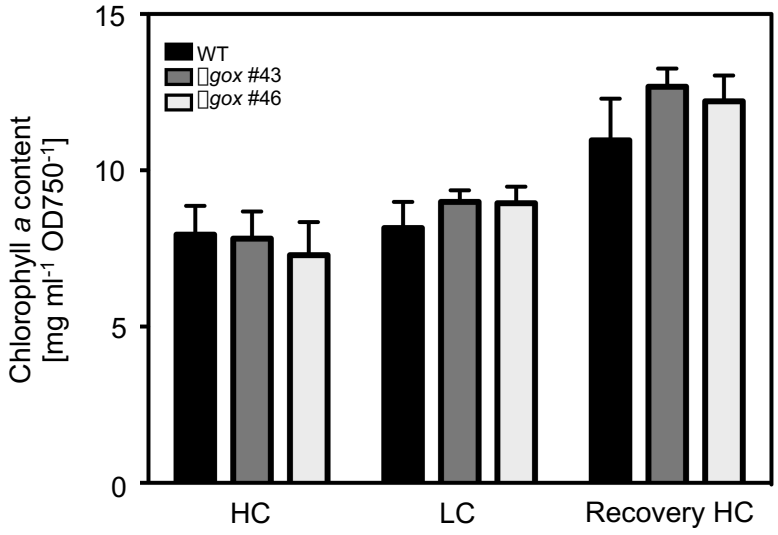

Figure S2: Chlorophyll *a* concentrations of WT and Δ*gox* mutants #43 and #46 during the CO_2 shift experiment. No significant differences ($P < 0.05$) were determined with the two-tailed Student´s t-test.

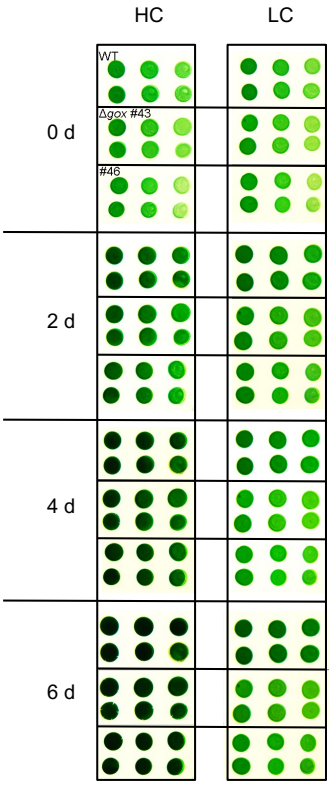

Figure S3: CO_2-dependent growth of WT and Δ*gox* mutants #43 and #46. All cell lines were pre-cultured in 2xMA medium for 1 d under HC conditions. Then cultures were adjusted to a cell density OD_{750} of 2.5, 0.83 and 0.28 and spotted onto a starch bed on solidified 2xMA plates. The plates were incubated for 4 d under HC conditions and continuous light (20 µmol photons m^{-2} s^{-1}) and then shifted to LC conditions. Growth was photographically documented after 0, 2, 4 and 6 d.

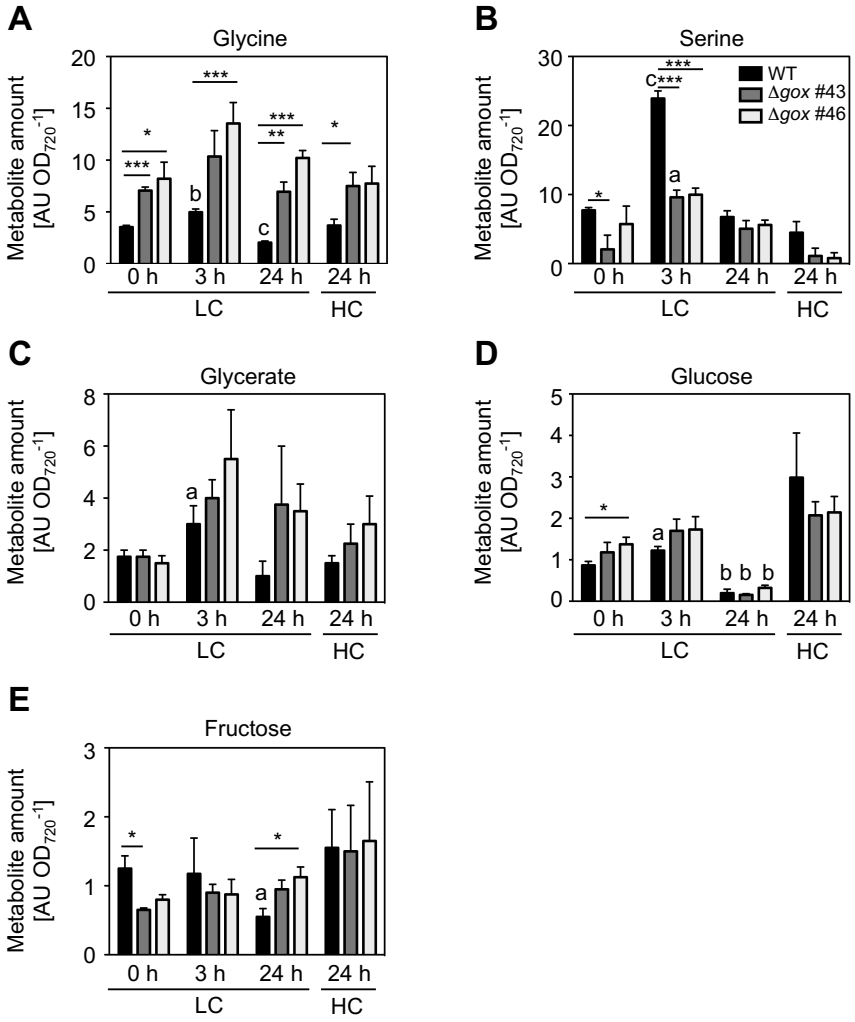

Figure S4: Metabolite levels of WT and Δ*gox* mutants #43 and #46 during the CO_2 shift experiment. Glycine (A), serine (B), glycerate (C), glucose (D), and fructose (E) levels of WT and Δ*gox* mutants #43 and #46 were determined by GC-MS and HPLC, respectively, before (0 h), 3 h and 24 h after the shift from HC (5% CO_2) to LC (0.04% CO_2) conditions, and after a 24 h recovery phase under HC conditions. Shown are mean values and standard errors of four biological replicates. Significant differences between lines were determined with the two-tailed Student´s t-test and are indicated as: $P < 0.05$ (*), $P < 0.01$ (**), $P < 0.001$ (***). Significant differences to initial levels (LC, 0 h) are indicated as: a ($P < 0.05$), b ($P < 0.01$) and c ($P < 0.001$).

Authors' contribution to manuscript II:

Nadine Rademacher: Wrote the manuscript, performed *Cyanidioschyzon merolae* culture cultivation, BlastP analysis, qRT analysis, subcellular localization studies, metabolite extraction and analysis, photosynthetic rate measurement and chlorophyll a determination.

Ramona Kern: Performed heterologous expression of CmGOX and enzyme assay.

Takayuki Fujiwara: Performed Δ-gox mutant generation and phenotypic characterization.

Tabea Mettler-Altmann: Helped with the set-up of metabolite extraction protocol for *Cyanidioschyzon merolae*, coordinated UHPLC and GC-MS analysis.

Shin-ya Miyagishima: Supervised Δ-gox mutant generation.

Martin Hagemann: Supervised experimental design for photosynthetic measurements.

Marion Eisenhut: Participated in drafting the manuscript, supervised general experimental design.

Andreas Weber: Participated in drafting the manuscript and helped with experimental design.

MANUSCRIPT III

(DRAFT)

Transcriptional response of the extremophile red alga
Cyanidioschyzon merolae to changes in CO_2 concentrations

Transcriptional response of the extremophile red algae *Cyanidioschyzon merolae* to changes in CO_2 concentrations

Nadine Rademacher[1]. Thomas Wrobel[1], Alessandro W. Rossoni[1], Marion Eisenhut[1], Samantha Kurz[1], Andrea Bräutigam[2], Andreas P.M. Weber[1*]

[1]Institute of Plant Biochemistry, Cluster of Excellence on Plant Sciences (CEPLAS), Heinrich Heine University, Universitätsstraße 1, 40225 Düsseldorf, Germany
[2]Leibniz-Institut für Pflanzengenetik und Kulturpflanzenforschung (IPK), Corrensstraße 3, 06466 Stadt Seeland, OT Gatersleben, Germany

E-mail addresses:
Nadine.Rademacher@hhu.de
Thomas.Wrobel@hhu.de
Alessandro.Rossoni@hhu.de
M. Eisenhut@hhu.de
Samantha.Kurz @hhu.de
brauetigam@IPK-gatersleben.de
Andreas.Weber@hhu.de

*corresponding author:
Andreas P. M. Weber
andreas.weber@hhu.de
Phone: +49 211 81-12347
Fax: not available

Abstract

Cyanidioschyzon merolae (*C. merolae*) is an acidophilic red alga growing in a natural high carbon dioxide (CO_2) environment. Despite high aqueous CO_2 concentrations and high affinity of Ribulose-1,5-bisphosphate carboxyase/oxygenase for CO_2, fitness of *C. merolae* relies on a functional photorespiratory metabolism. In this publication we tested the effect of reduced CO_2 conditions on the transcriptome of *C. merolae*. To this end we performed a high carbon to low carbon shift experiment with wild-type cells and analyzed the transcriptomic data with a special focus on changes in transcript abundances of genes involved in the photorespiratory and energy metabolism. Moreover, we made use of the generated transcriptome data set to identify possible components of a carbon concentrating mechanism (CCM) based on the assumption that photorespiratory genes and possible candidate genes involved in a CCM should be co-expressed. According to this analysis one bicarbonate transport protein and two α- carbonic anhydrases showed enhanced transcript levels under reduced CO_2 conditions and might thus belong to a low CO_2 conditions compensation mechanism. Localization studies of transient transformed *C. merolae* cells and tobacco protoplast demonstrated a cytosolic localization of both carbonic anhydrases. In total transcriptional analysis revealed with an exception to photorespiratory genes only minor changes as a response to reduced CO_2 concentrations.

Introduction

Photoautotrophic organisms represent the main biomass producers on earth by the conversion of inorganic carbon into organic carbon compounds and oxygen by utilization of light energy, water and mineral nutrients. This process called photosynthesis evolved in cyanobacteria about 2.7 billion years ago in an almost oxygen (O_2) free atmosphere and exists today in all oxygenic photosynthesis performing organisms due to endosymbiosis (reviewed in Hohmann-Marriott and Blankenship, 2011).

Photosynthesis is initialized by the fixation of one molecule carbon dioxide (CO_2) to the acceptor molecule ribulose-1,5-bisphosphate by the ribulose-1,5-bisphosphate carboxylase oxygenase, short RubisCO. The produced two molecules of 3-phosphoglycerate (3-PGA) are fed into the Calvin-Benson-Bassham cycle (CCB) for sugar production and recycling of the acceptor molecule. Next to the carboxylation reaction, RubisCO also performs an oxygenation reaction where O_2 is added to the acceptor molecule resulting in one molecule of 3-PGA and 2-phosphoglycolate (2-PG) each. The latter is toxic for the organism and has to be detoxified to 3-PGA in the photorespiratory pathway under consumption of energy and nitrogen and release of one molecule CO_2, to minimize loss of carbon for the organism. The ability of RubisCO to perform both, the carboxylation and the oxygenation reaction makes the ratio of CO_2 to O_2 next to the enzyme an important factor for the efficiency of photosynthesis. RubisCO is one of the most abundant enzymes on earth and differs in reaction velocity and substrate specificity between the different lineages (Savir *et al.*, 2010). Basically, a higher specificity for CO_2 decreases velocity, while an increase in velocity goes along with a decline in specificity (Savir *et al.*, 2010). Cyanobacteria for example have a very fast RubisCO with only low specificity, while C3 and C4 plants RubisCO achieve a higher specificity by the loss of velocity (Savir *et al.*, 2010). RubisCO enzymes of extremophile red algae like *Galderia parta* and *Cyanidium caldarium* exhibit a very high specificity and thereby a low velocity (Uemura *et al.*, 1997). Next to the enzyme properties, the CO_2 concentration around RubisCO has a strong influence on the carboxylation to oxygenation reaction rate. Therefore many organisms employ a carbon concentrating mechanism (CCM) to enhance the CO_2 accumulation around RubisCO. A CCM uses biophysical or

biochemical methods to accumulate directly or indirectly inorganic carbon in the photosynthetic tissue, which is released as CO_2 around RubisCO to increase the carboxylation rate (Giordano *et al.*, 2005; Raven *et al.*, 2012). The existence of a CCM could be shown for cyanobacteria, most algae and aquatic plants, as well as for C4 and Crassulacean acid metabolism (CAM)-plants (reviewed in Raven *et al.*, 2008). CCM is an energy consuming pathway that can either be a constitutive pathway like the C3/C4 decarboxylation cycle preceding to RubisCO in C4 or CAM plants or an active transport process of CO_2, HCO_3^- and H^+ across the membrane, which is enhanced under lower CO_2 conditions as shown for cyanobacteria and some algae (reviewed in Raven *et al.*, 2008). Cyanobacteria accumulate HCO_3^- in the cytosol. The diffusion into the carboxysome and the conversion back to CO_2 by carbonic anhydrases (CAs) within in the carboxysome enables an enrichment of CO_2 up to 1,000-fold in close proximity to RubisCO to efficiently reduce the oxygenation reaction (Badger and Price, 2003; Eisenhut *et al.*, 2007). An analogue to the cyanobacterial micro-compartment carboxysome is the pyrenoid in many but not all CCM-performing green algae (reviewed in Giordano *et al.*, 2005).

Organisms employing a CCM still depend on photorespiration to survive in today's atmosphere. The close relation between CCM and photorespiration suggest an early evolution of CCM together with the evolution of the photorespiratory cycle in cyanobacteria (Hagemann *et al.*, 2016). However, the question whether genes involved in CCMs have been endosymbiotically transferred from cyanobacteria to photosynthetic eukaryotes, as it could be shown for some photorespiratory enzymes, is still open (Eisenhut *et al.*, 2008; Kern *et al.*, 2011; Hagemann *et al.*, 2016). CCMs of most algae lineages differ in structural components and mechanisms compared to the cyanobacterial CCM (Raven *et al.*, 2008). The ancient Glaucophyte *Cyanophora paradoxa* for example exhibits carboxysome like structures in the chloroplast similar to cyanobacteria and an enhanced cellular affinity towards inorganic carbon under carbon limiting conditions (Burey *et al.*, 2007; Fathinejad *et al.*, 2008). However, homologs of the cyanobacterial carboxysome proteins could not be identified in the genome of *Cyanophora paradoxa*, which makes the existence of a CCM questionable (Price *et al.*, 2012; Hagemann *et al.*, 2016).

Thermoacidic algae, like the red alga *Galdieria sulphuraria,* encode for a RubisCO enzyme with a high specificity for CO_2 (Savir *et al.,* 2010). The closely related red

algae *Cyanidioschyzon merolae* (*C. merolae*) is able to handle temperatures up to 57 °C and an acidic pH of 2 in the growth medium (Seckbach, 1995). Their challenge is to deal with CO_2 as single C_i species at an acidic pH and the general low amount of available CO_2 for photosynthesis due to the reduced solubility of CO_2 at high temperatures. A further limiting factor for the growth in an acidic environment is the ability to maintain a neutral pH inside the cells. *C. merolae* is able to maintain an inner cellular neutral pH of 6.35 to 7.10 in a range of a changing extracellular pH of 1.5 to 7.5, while photosynthesis is most efficient at a low extracellular pH and decreases at a neutral pH (Zenvirth *et al.*, 1985). This indicates CO_2 to be the only C_i species taken up from the external medium by *C. merolae*. Recently it could be shown that despite the high CO_2 concentration in its natural habitat, *C. merolae* performs the plant-like photorespiratory cycle, which is indispensable for the growth under natural conditions (Rademacher *et al.,* 2016). Furthermore, a CCM composed of a carbon uptake system is postulated to be located in the chloroplast envelope membrane, to transport carbon entering the neutral cytoplasm as CO_2 by diffusion over the plasma membrane into the chloroplast for the accumulation around RubisCO (Zenvirth *et al.*, 1985).

C. merolae is a single cell model organism, which is used for studies of early photosynthesis and photorespiration evolution. The genome is fully sequenced and small with only 16 Mbp (Matsuzaki *et al.*, 2004). Techniques for targeted gene knock-out and transient transformation for localization studies are available (Minoda *et al.*, 2004; Imamura *et al.*, 2010; Watanabe *et al.*, 2011). To date, carbon transport proteins and functional CAs have not been identified on molecular level in *C. merolae*. It could be shown that genes encoding CCM components in the green alga *Chlamydomonas reinhardtii* (*C. reinhardtii*) are co-regulated with genes involved in photorespiration to coordinate the acclimation to carbon limited conditions (Fang *et al.*, 2012). Here, we analyzed changes in transcript abundances in *C. merolae* wild-type (WT) cells due to a shift from high to low carbon concentrations with a special focus on the general energy metabolism. Additionally, we searched the transcriptomic data set for possible candidates constituting a CCM in *C. merolae.*

Material and methods

Cyanidioschyzon merolae cultivation:
C. merolae 10D WT cells were cultivated in 2x modified Allen's growth medium at 30 °C temperature, bubbled with 5% CO_2 (HC) at 90 µE m^{-2} s^{-1}light in a Multi-Cultivator MC 1000-OD (Photon Systems Instruments). For low carbon conditions, cultures were bubbled with ambient air (0.04% CO_2 – LC).

Experimental set-up of carbon shift experiment:
Three independent biological replicates of *C. merolae* WT cells were cultivated for 24 h under HC conditions with an initial OD_{750} = 0.7 (90 mL). After 24 h cells were shifted for 24 h to LC and afterwards shifted back to HC for a 24 h recovery phase. Samples of 5 mL volume for RNA extraction were taken directly after the shift to LC (LC 0 h), 3 h after shifting to LC (LC 3 h) and 24 h after shift to LC (LC 24 h) and 24 h after a recovery phase in HC (HC 24 h).

TruSeq RNA library preparation and transcriptome generation:
For RNA extraction 5 ml culture (OD720 ≈ 1) were centrifuged for 5 min at 4 °C (3,000 rpm) and the cell pellet snap-frozen. RNA extraction was performed using the universal RNA purification kit (roboklon) following the protocol for cell extraction.
Library preparation was performed using the TruSeq RNA Sample Prep Kit v2 (Illumina). RNA integrity, sequencing library quality and fragment size were checked on a 2100 Bioanalyzer (Agilent). Library quantification was carried out by the Biologisch-Medizinisches Forschungszentrum (BMFZ, Heinrich Heine University, Düsseldorf). Average library size was 320 bp with equimolar pooling (2 nM). Paired-end (PE) sequencing included two lanes with 12 samples, supplied with different adapter sequences (Illumina Index kit), per pool and delivered two 470M reads with a sequencing read type of two times 100 bp (Beckman Coulter Genomics). Beckman Coulter Genomics performed primary quality control and data demultiplexing.

Read mapping and gene expression profiling

The genomic sequence of *Cyanidioschyzon merolae* strain 10D (ASM9120v1) (Matsuzaki *et al.*, 2004), as well as its latest annotated reference transcriptome (ASM9120v1.30.gtf) (Nozaki *et al.*, 2007) were retrieved from the ENSEMBL database (Yates *et al.*, 2015).

The resulting 726,326,434 Illumina PE-reads (~18.4 Million PE-reads per sample on average) were aligned to the reference transcriptome of *Cyanidioschyzon merolae* strain 10D using RSEM (Li and Dewey, 2011). RSEM was run in very-sensitive mode and yielded ~18.4 Million mapped PE-reads per sample on average (60.72% overall alignment rate). Although gapped alignments are not supported, Bowtie2 (Langmead and Salzberg, 2012) was chosen over Bowtie1 (Langmead *et al.*, 2009) as read mapping algorithm due to faster computation. Gapped alignments were suppressed through the command line input. Gibbs sampling (Geman and Geman, 1984) (--calc-pme) was used to calculate posterior mean expression estimates within 95% credibility intervals (--calc-ci). Gibbs sampling was iterated 500 times (--gibbs-burnin 500).

Data Analysis:

Differential gene expression was analyzed via the DeSeq2 package (Love *et al.*, 2014) using default settings and different time points as experimental structure. A *P*-value of 0.05 was chosen as significance threshold after correction for multiple testing via the Benjamini Hochberg algorithm (Benjamini and Hochberg, 1995). For kmeans clustering FPKM values were normalized to their average and clustering was performed for 1 to 50 clusters. The ratio between the sum of square errors (SSE) within the clusters and the total SSE was calculated to determine a suitable number of clusters. Kmeans clustering was carried out 10,000 times for 10 clusters and the clustering with the best SSE ratio was used for further analysis.

The functional categorization of all genes in the *C. merolae* genome was performed by comparing their protein sequence to Arabidopsis TAIR10 (http://www.arabidopsis.org/) using the standalone version of NCBI BLASTP (2.2.31+) with standard settings. The Mapman categorization (Thimm *et al.,* 2004)was performed on basis of the Arabidopsis genes with the MAPMAN dataset for TAIR10. The functional enrichment was performed on Mapman categories

reduced to their first level and a custom categorization (Bräutigam unpublished) using Fishers exact tests. All *P*-values were corrected for multiple testing via the Benjamini Hochberg algorithm (Benjamini and Hochberg, 1995).
All statistic analyses were carried out in R (3.2.3 "Wooden Christmas-Tree"). The parsing and association of the BLAST results were performed in perl (v5.16.2). Heatmaps were created using the heatmap.2 from the gplots package. All other figures were created using ggplot2 (both accessible via CRAN).
Reads for specific pathway analysis were mapped against the *C. merolae* genome (Matsuzaki *et al.*, 2004) using the CLC Genomics server (Qiagen) and normalized to reads per kilobase per million mapped reads (RPKM). Fold change analysis were performed for all known genes involved in photorespiration, light reaction and energy metabolism regarding changes from 0 h LC to 3 h LC, 3 h LC to 24 h LC, and 0 h LC to 24 h recovery in HC. Significant differences were tested on single reads using One-way Anova test including a Newman-Keuls post-test (Prism 5, GraphPad software).

Identification of possible candidate genes involved in a carbon concentrating mechanism:
Identification of CAs in the genome of *C. merolae* were performed by BlastP analysis with protein sequences of known α-, β-, and γ CAs of *Arabidopsis thaliana (A. thaliana)* (Fabre *et al.*, 2007) and *C. reinhardtii* (Tirumani *et al.*, 2014) against the *C. merolae* database (Matsuzaki et al., 2004). Maximum Likelihood phylogenetic tree analysis including MUSCLE alignment was performed using the phylogeny.fr platform (phlogeny.fr; Castresana, 2000; Edgar, 2004; Chevenet *et al.*, 2006; Anisimova and Gascuel, 2006; Dereeper *et al.*, 2008; Guindon *et al.*, 2010). To identify possible carbon transporters, protein sequences of known carbon transporters in the cyanobacterium *Synecchocystis* sp. PCC 6803 were used for BlastP analysis (Eisenhut et al., 2007).

Constructs for α- carbonic anhydrases localization:
For subcellular localization of α-CA1 (CmT416) and α-CA2 (CmI270) in *Nicotiana benthamiana* protoplasts and *C. merolae* cells two constructs were generated for each protein with either an N- or a C- terminal YFP-fusion. Gene sequences were

amplified by PCR on genomic DNA from *C. merolae* and cloned into the pUBN-YFP or pUBC-YFP vector using gateway technology and pDONR207 for subcloning (Grefen *et al.*, 2010). Primer sequences are shown in Supplementary Table 1. All constructs were under the control of the *Ubiquitin10* promoter.

Transformation of *N. benthamiana* was carried out using the *Agrobacterium tumefaciens* (*A. tumefaciens*) strain GV3101. Protoplast isolation and microscope analysis was performed 2 d after infiltration using a Zeiss LSM 510 Meta laser microscope as described in Breuers *et al.*, 2012. Transient transformation of *C. merolae* cells was performed as described by Ohnuma *et al.*, 2008. Microscope analysis was perfomed 24 h after transformation with a Zeiss LSM780 microscope.

Results

Mapping of reads against the C.merolae genome revealed an incomplete assembled transcriptome data set of C. merolae.

Mapping of reads on the transcriptome revealed only 60% successful mapped reads. In order to test the source of the low alignment rate, all Illumina PE-reads were mapped against the reference genome (Matsuzaki *et al.*, 2004; Nozaki *et al.*, 2007) with TopHat2 (Kim *et al.*, 2013) in very-sensitive mode. As a result, an overall alignment rate of 92.1 % was obtained, hinting towards a yet unexploited coding capacity within the transcriptome of *C. merolae strain 10D* that could be added to the passed efforts (Supplementary table S6).

Reduction in CO_2 concentrations results in immediate and delayed reactions in gene expression

To analyze changes on transcriptional level due to shifts in the aqueous CO_2 concentrations, we performed a HC-LC-HC shift experiment. Principle component analysis (PCA) of all four conditions (0 h, 3 h and 24 h after the shift to LC and 24 h recovery time in HC) revealed a common behavior for all biological replicates before the shift to LC and 3 h after the shift to LC (Supplementary Figure 1). The transcriptional response after 24 h under LC conditions and the 24 h recovery time under HC conditions was more diverse (Supplementary Figure 1). A full recovery to the initial state was not reached after 24 h in HC (Supplementary Figure 1). The

specific transcriptional response of all genes is shown in Figure 1 clustered in 10 different possible reaction types. The number of clusters was determined using a graph showing the sum of squares divided by the total sum of squares per number of clusters (Supplementary Figure 2). Corresponding heat maps are given in Supplementary Figures 3 and 4. A general classification can be done in groups containing genes with a high expression level under HC conditions, showing an immediate reaction in transcription in the first 3 h after the shift to LC (Figure 1, cluster number 3, 4, 6, 7, and 8), or a delayed reaction in the long-term adaption phase 3 to 24 h after the shift (Figure 1, cluster number 2). The second group of clusters includes genes with a low expression under HC conditions and can be divided in clusters containing genes with an immediate change in transcription level (Figure 1, cluster number 5 and 9) or a delayed response in transcription (Figure 1, cluster number 1 and 5). Only cluster 7 and 9 contain genes that show a full recovery in their transcription rate after 24 h in HC.

A general analysis of significant changes in gene transcription between all four conditions: 0 h LC, 3 h LC, 24 h LC and 24 h recovery in HC, revealed most significant transcript alterations in the immediate reaction phase (LC 0 h to LC 3 h) (Figure 2C) and the delayed reaction phase (LC 3 h and LC 24 h, Figure 2D). Only few changes occurred in the recovery phase (LC 24 h to HC 24 h, Figure 2E). A full recovery on transcriptional level was not reached by most of the genes after 24 h under HC conditions (Figure 2 A).

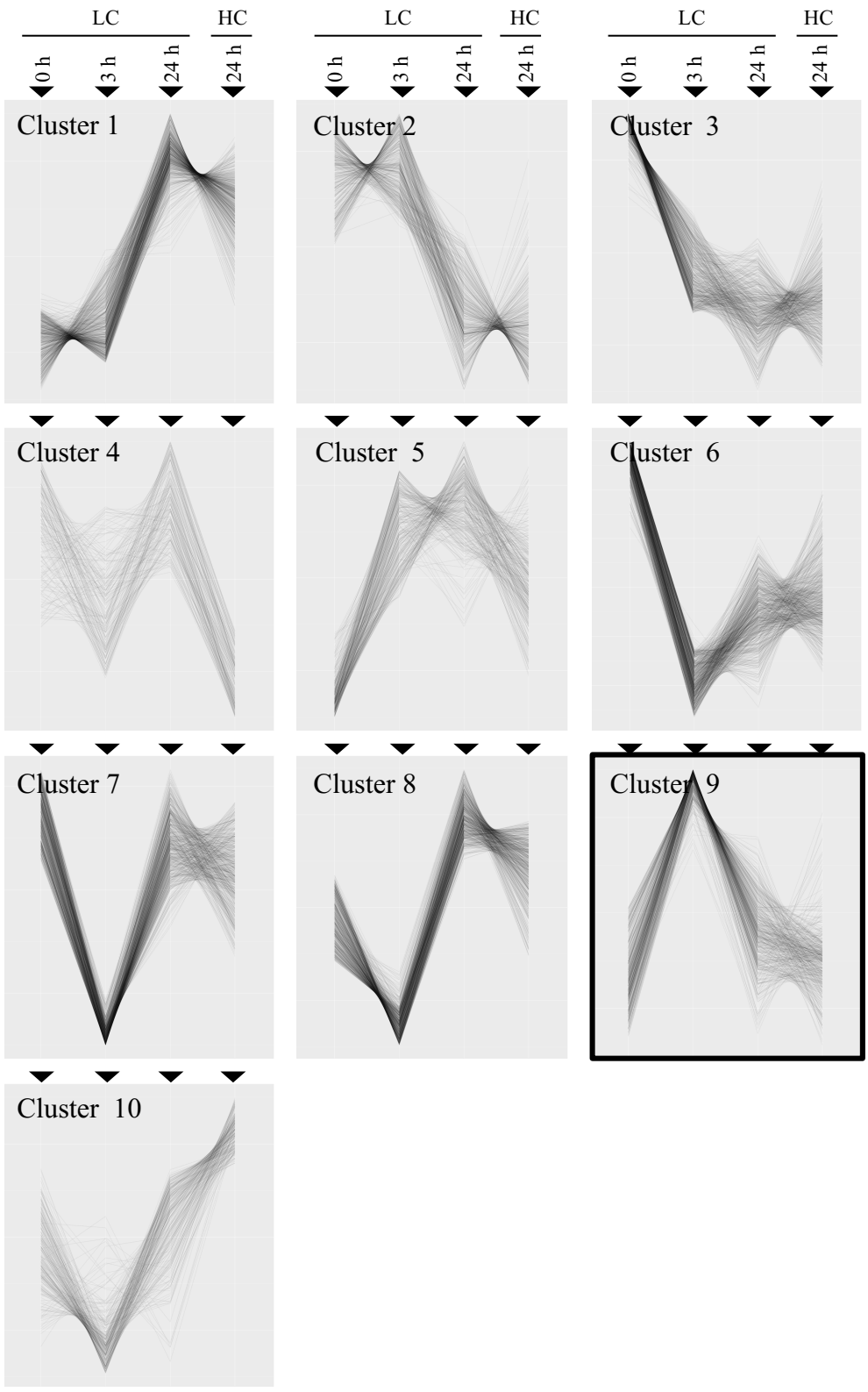

Figure 1: K-means clustering of gene expression directly after the shift to ambient air conditions (LC 0 h), 3 h after the shift to LC (LC 3 h), 24 h after the shift to LC (LC 24 h) and 24 h after recovery phase in HC (HC 24 h). Gray lines represent the expression pattern of each single gene. Black framed cluster number 9 contains all photorespiratory genes.

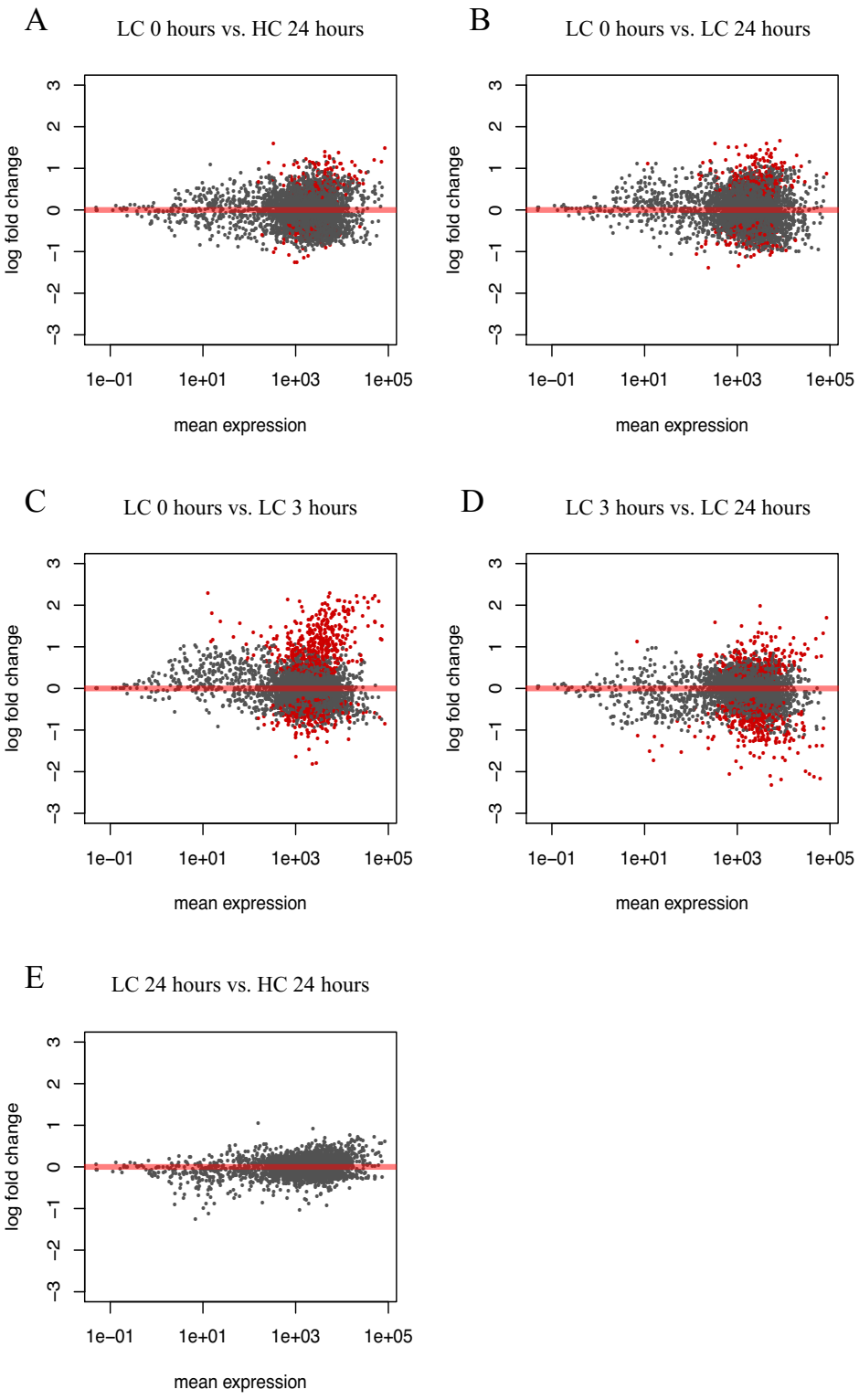

Figure 2: Changes of transcript abundances between two different conditions: LC 0 h vs. HC 24 h (A), LC 0 h vs. LC 24 h (B), LC 0 h vs. LC 3 h (C), LC 3 h vs LC 24 h (D) and LC 24 h vs. HC 24 h (E). Red line indicates 0-fold change between both conditions. Red dots indicate genes with a significant difference in gene expression.

Severe changes in the expression of genes involved in photorespiration and only minor changes in the expression level of the energy metabolism

Functional analysis of transcriptional changes within pathways could not identify severe changes in the transcript amount of distinct groups (Supplementary Figure 5, 6, 7, 8, 9, Supplementary Table S3). Only the transcript amount of genes involved in photorespiration adopted half of the transcript amount of genes involved in photosynthesis 3 h after the shift to LC (Figure 4). Already 24 h in LC led to a decrease in the photorespiratory transcript level. Noticeable is the high amount of not assigned genes or genes with an unknown function (Figure 4).

A detailed analysis of genes involved in photorespiration revealed that *C. merolae* reacted with a significantly enhanced expression of genes encoding for the main enzymes of the photorespiratory cycle immediately 3 h after a shift from HC to LC (Figure 3A). Only the gene encoding for the peroxisomal catalase (CAT2) showed no significant increase in the expression. The long-term acclimation to LC (3 h to 24 h after the shift) included a uniform down regulation of the transcript level, which was still enhanced compared to HC conditions (Figure 3B). A full recovery of all photorespiratory transcript levels, including no significant differences to the initial HC transcript levels, was reached 24 h after the shift back to HC (Figure 3C). Genes involved in the energy metabolism, like glycolysis, pyruvate metabolism, oxidative and reductive Pentose-phosphate pathway (PPP) and citric acid cycle (TCA) did not show a comparable unique up or down regulation on the transcriptional level in comparison to photorespiration. However, genes with a significant down-regulation on the transcriptional level could be found in all four pathways still after 24 h recovery time in HC (Supplementary Figures 5, 6, 7, 8). Genes encoding for proteins involved in light reaction (Photosystem II, Photosystem I, Antenna proteins and Phycobilisomes) showed a general up-regulation in their expression as a reaction to LC conditions, which was still present after 24 h recovery in HC (Supplementary Figure 9)

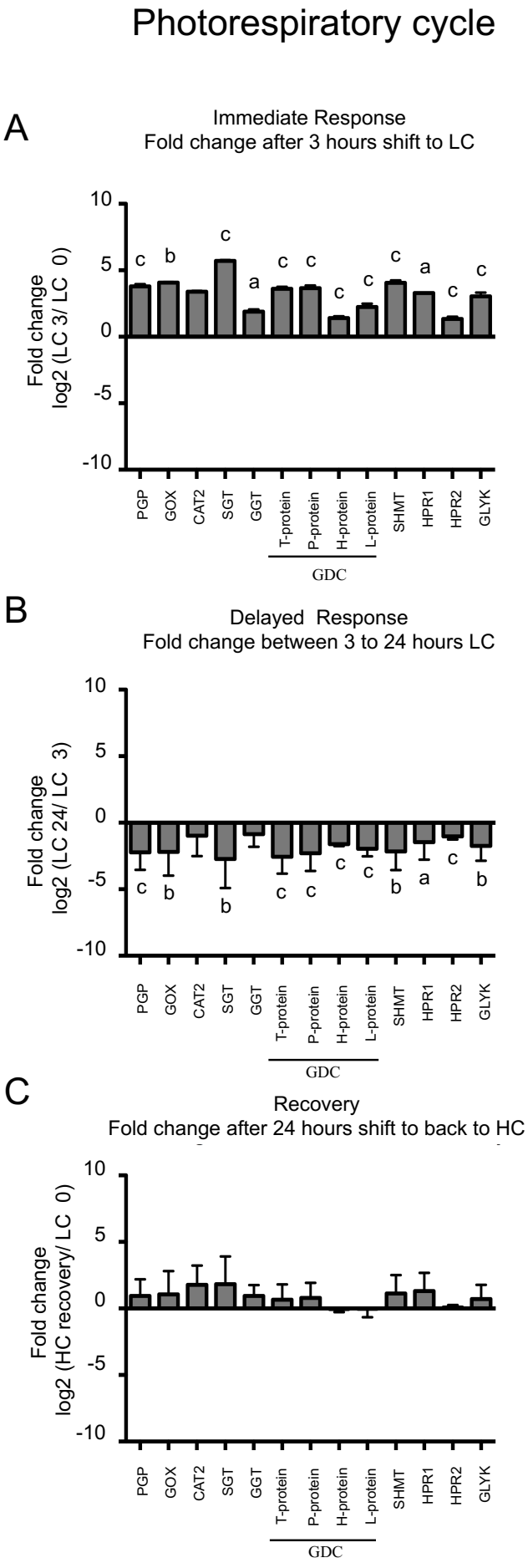

Figure 3: Transcriptional response of photorespiratory genes in response to changing CO_2 conditions. Data show fold-changes in transcript abundances of genes encoding for main photorespiratory enzymes between different sampling point: 0 h LC vs. 3 h LC, 3 h LC vs. 24 h LC and 0 h LC vs. 24 h recovery in HC). Significant differences between two conditions are shown as a ($p<0.5$), b ($p<0.1$) and c ($p<0.01$). Photorespiratory enzymes: 2 PG phosphatase (PGP), Glycolate oxidase (GOX), Catalase 2 (CAT2), Serine: glyoxylate aminotransferase (SGT), Glutamate: glyoxylate aminotransferase (GGT), Glycine decarboxylase (GDC), Serine hydroxymethyltransferase, peroxisomal Hydroxypyruvate reductase (HPR1), cytosolic Hydroxypyruvate reductase, Glycine decarboxylase (GLYK).

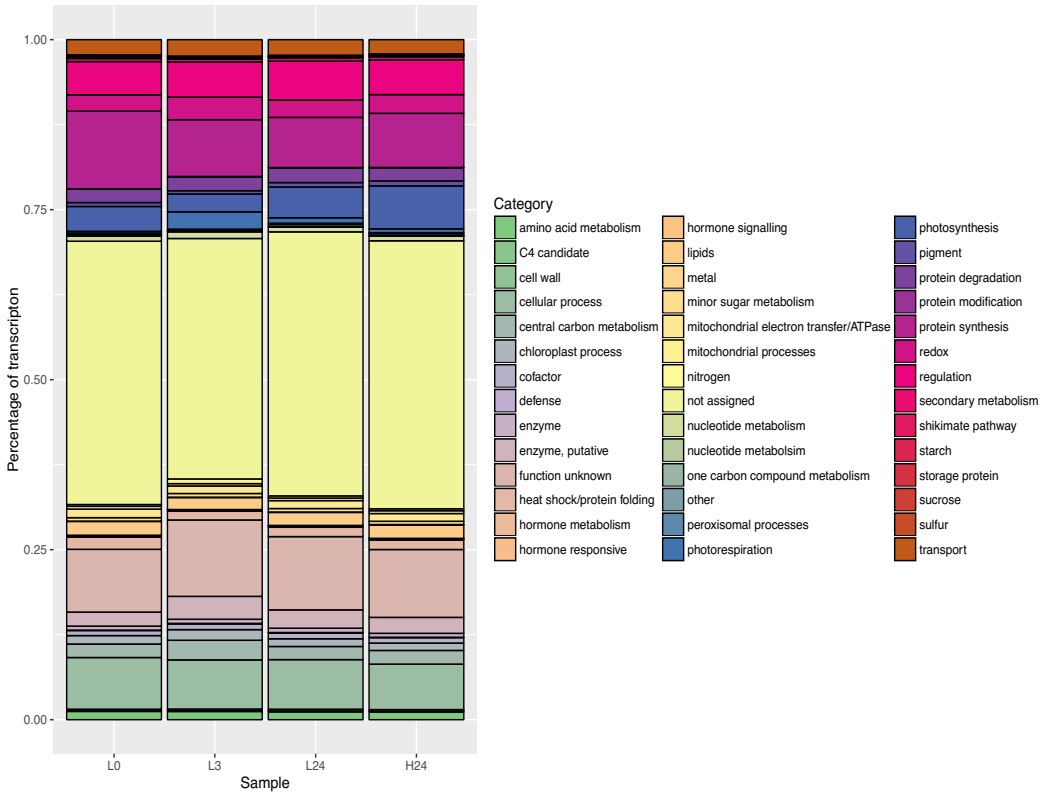

Figure 4: Comparison of gene expression dynamics in superior pathway categories shown for 0 h, 3 h and 24 h after the shift to LC and 24 h recovery phase under HC conditions.

Carbonic anhydrases and a HCO_3^- transporter are co-expressed with photorespiratory enzymes

Carbonic anhydrases play an important role in nearly all CCM performing organisms by catalyzing the CO_2 to HCO_3^- equilibrium (Raven *et al.,* 2012). Identification of CA homologs helps to proof the hypothesis of a possible CCM in *C. merolae*.

While at an acidic pH of 2 the only available Ci species is CO_2, aqueous carbon exists at a neutral pH as CO_2 and bicarbonate (HCO_3^-) in equal amounts. To make HCO_3^- also usable as carbon source for the RubisCO enzyme, CAs are often used to convert HCO_3^- to usable CO_2 (Raven *et al.,* 2012). BlastP analysis with known α-, β-, and γ-CAs of *A. thaliana* against the *C. merolae* genome (http://merolae.biol.s.u-tokyo.ac.jp/blast/blast.html;Matsuzaki *et al.,* 2004) revealed two possible α-CAs: α-CA1 (CmT416) and α-CA2 (CmI270). BlastP analysis with the α-type CA CAH3 of *C. reinhardtii* resulted in identical hits. The search for a *C. merolae* β-CA did not yield any results using sequences of β-CAs of the cyanobacterium *Synechocystis*, the green alga *C. reinhardtii* and the plant *A. thaliana*. A γ-CA (CmM052) was already identified in the *C. merolae* genome by Gawryluk and Gray, 2010.

In silico analysis of both α-CAs revealed a high similarity of both proteins with an amino acid sequence identity of 90% and a similarity of 92% (NCBI Blast). The α-CA1 protein has a 100 amino acids long extension at the N-terminus compared to α-CA2, which includes a 22 amino acids long transmembrane region (predicted by SOSUI, http://harrier.nagahama-i-bio.ac.jp/sosui/; Hirokawa *et al.*, 1998). A distinct target peptide in the protein sequence of α-CA1 and α-CA2 for the chloroplast or another organelle could not be identified (TargetP, ChloroP target sequence prediction tool - http://www.cbs.dtu.dk/services/TargetP/; Emanuelsson *et al.*, 1999, 2000).

All three CAs are expressed in *C. merolae* under LC and HC conditions. For the γ-CA (CmM052) gene only minor changes after the shift to LC conditions were detectable. Genes encoding for α-type CA showed a strong increase in the first 3 h after the shifting to LC. Notably, the α-CA1 gene, with the extension at the N-terminus, had a minor transcript level compared to the second α-type CA under HC conditions. After the shifting to LC the α-CA1 gene transcript increased up to 2,500 fold, while α-CA2 showed a significant, but smaller increase in transcript level (Figure 5). Compared to 3 h after the shift, the transcript level of all CAs encoding

genes decreased in the following 21 h LC, but were still not fully recovered after 24 h in HC (Figure 5).

BlastP analysis of known HCO_3^- transport proteins of *C. reinhardtii* revealed only one hypothetical HCO_3^- transporter in *C. merolae* as a homolog to the high-light induced gene3 (HLA3) HCO_3^- transporter induced under limiting CO_2 conditions (Supplementary Table S3) (Tirumani *et al.*, 2014). The corresponding gene CMN251C showed the same transcription pattern as the photorespiratory genes and a high increase in transcript 3 h after the shifting to LC conditions (Figure 1 Cluster 9). Further analysis revealed a homologous protein (CMS091C) for the chloroplast envelope proteins (CCP1 and CCP2) with HCO_3^- transporter function in the chloroplast membrane in *C. reinhardtii* (Supplementary Table S3) (Tirumani *et al.*, 2014). CMS091C does not cluster together with the photorespiratory genes. The transcription pattern is grouped in Cluster 6 (Figure 1) and is annotated as member of the mitochondrial carrier family.

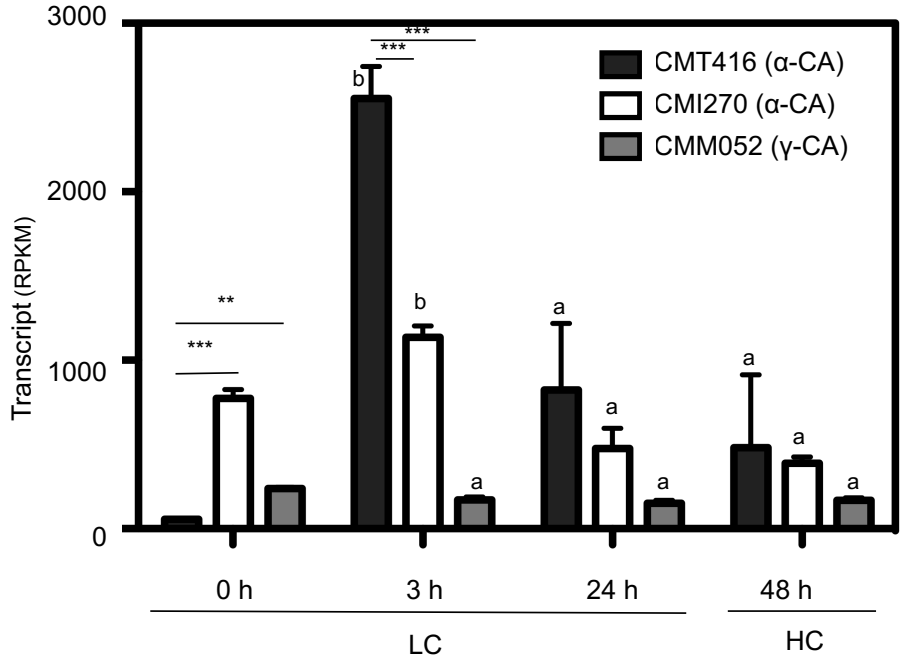

Figure 5: Transcript level of CmT416, CmI270 and CmM052 encoding for possible carbonic anhydrases in *C. merolae* 0 h, 3 h and 24 h after the shift to low carbon conditions (LC) and 24 h recovery phase in high carbon concentration (HC). Significant differences within the same conditions between different carbonic anhydrases are indicated as ** ($p<0.01$) and *** ($p<0.001$). Significant changes for the same gene between 0 h after shift to LC and later timer points are indicated as a ($p<0.05$) and b ($p<0.01$).

Localization studies of carbonic anhydrases in tobacco and C. merolae revealed a cytosolic expression.

To fulfill a function in a CCM, both α-CAs of *C. merolae* should be either localized in the chloroplast to support RubisCO with CO_2 as supposed by Zenvirth *et al.*, 1985 or in the cytosol to increase the amount of CO_2 for the diffusion over the chloroplast membrane. Localization constructs were designed with an N- or a C-terminal fusion to the yellow fluorescent protein (YFP) to avoid masking of an unidentified peptide target signal. Figure 6A shows the results of a transient transformation of tobacco protoplast. All four constructs, YFP::CmI270; CmI270::YFP, YFP::CmT416 and CmT416::YFP exhibited a cytosolic localization pattern under the control of an Ubiquitin 10 promoter (Figure 6A). Transient transformation of *C. merolae* cells revealed the same cytosolic localization of both proteins (Figure 6B).

A

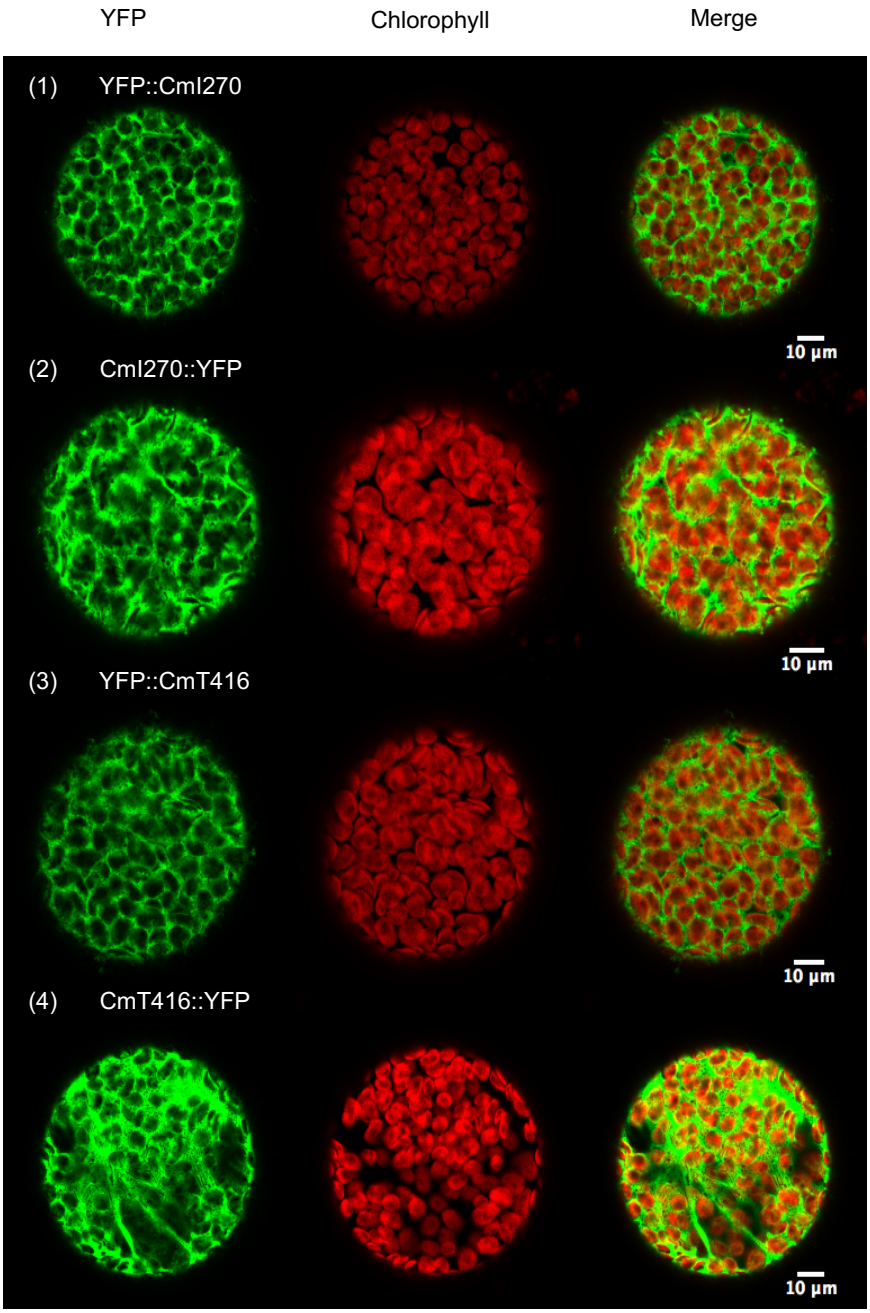
YFP
Chlorophyll
Merge
(1) YFP::CmI270
10 µm
(2) CmI270::YFP
10 µm
(3) YFP::CmT416
10 µm
(4) CmT416::YFP
10 µm

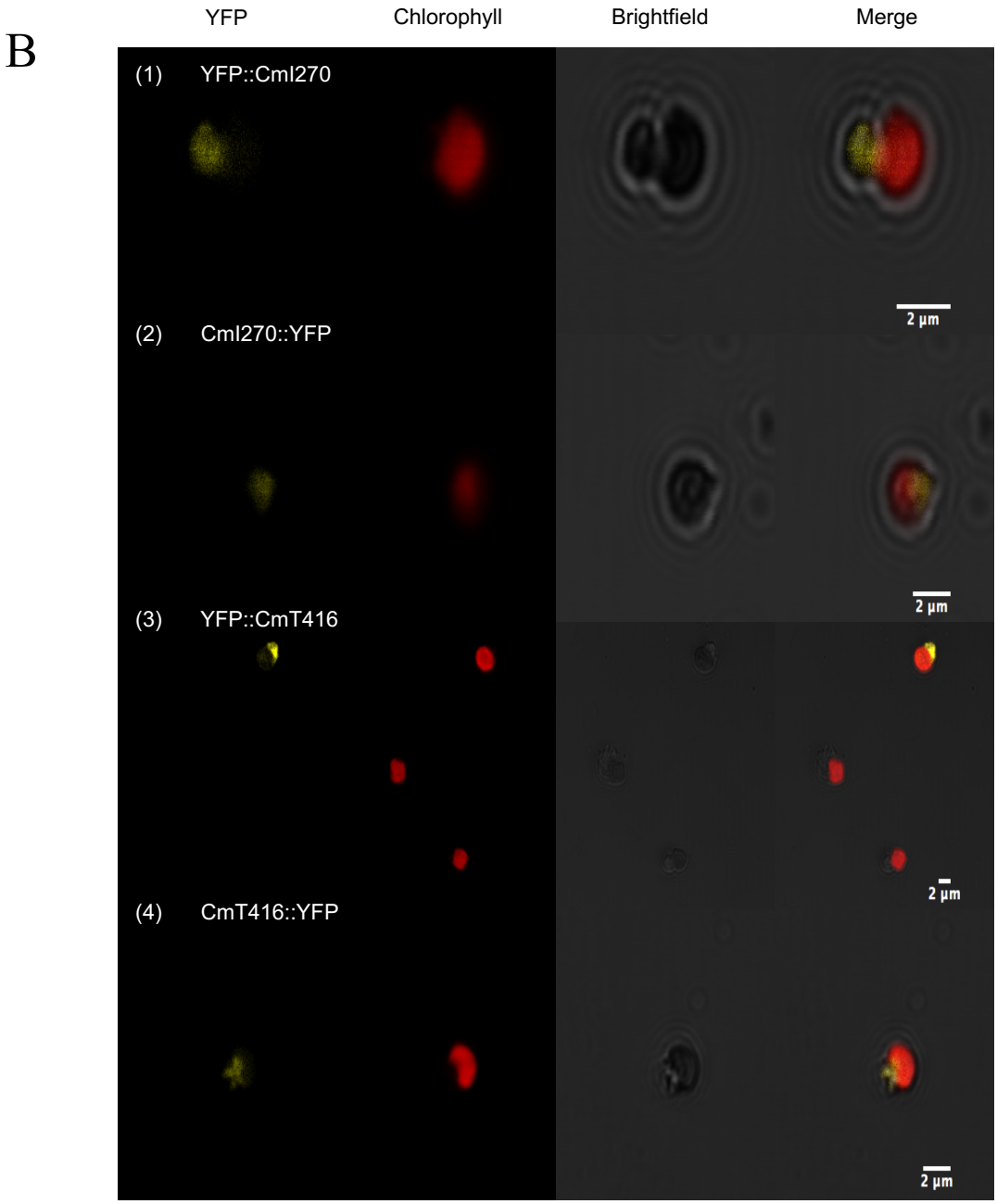

Figure 6: Subcellular localization studies of both α- carbonic anhydrases (α –CA1 (CmI270) and α-CA2 (CmT416)) with an N- ((1) and (3)) and a C-terminal ((2) and (3)) fluorescent protein (YFP). (A) Localization of α-carbonic anhydrases in tobacco protoplasts. From left to right: YFP signal of YFP::CmI270 (1), CmI270::YFP (2), YFP::CmT416 (3) and CmT416::YFP (4) constructs, Chlorophyll autofluorescence, bright-field picture and merge of all three pictures. Microscope analyses were performed with protoplasts isolated from transiently transformed *N. benthamiana* leaves. (B) Localization of both α-carbonic anhydrases in *C. merolae.* From left to right: Yellow: YFP signal from both α- carbonic anhydrases YFP constructs (1-4), Red: Chloroplast autofluorescence, bright-field picture and merge of all three pictures. *C. merolae* cells were transformed 24 h before microscope analysis.

Discussion

We could show in an earlier publication that *C. merolae* reacts with a strong decrease in growth rate after the shifting to LC and that the knock-out of the photorespiratory GOX leads to severe problems in growth and the photosynthetic efficiency (Rademacher *et al.,* 2016). Here we present the response to reduced CO_2 conditions on the transcriptional level with the benefit to identify possible components of a CCM in *C. merolae*.

Most significant changes in gene transcription in *C. merolae* occurred in the first 3 h after the shift from HC to LC conditions (Figure 2). The PCA of all four time points, 0 h, 3 h, 24 h after the shift and 24 h after the recovery in HC, revealed a common behavior in gene transcription for all three biological replicates directly after the shift to LC (LC 0 h) (Supplementary Figure 1). A grouped distribution could also be identified for the time point 3 h after the LC shift. The response in the transcriptional level 24 h after the shift to LC and after 24 h in recovery was more diverse. Noticeable is that 24 h recovery time in HC was not sufficient to reach the same transcriptional state as before the shift to LC conditions (Figure 2, Supplementary Figure 1). All genes involved in photorespiration, with exception of the Catalase 2 gene, reacted with a strong increase in their transcription level directly after the shift to LC and all genes are grouped together in Cluster 9 (Figure 1, Figure 3). In contrast to low CO_2 acclimation studies in *C. reinhardtii,* also the PGP transcript increased after a shift to LC (Fang *et al.*, 2012). A general comparison of gene expression dynamics in superior pathway categories supported these findings revealing a strong increase in the photorespiratory fraction combined with a reduction of gene transcript involved in photosynthetic processes (Figure 4). Unfortunately many genes of *C. merolae* are not assigned yet and/ or have an unknown function what complicates the analysis of general pathway changes due to limited CO_2 conditions.

It could be shown that *C. merolae* performs a plant-like energy metabolism, regarding pathways such as glycolysis, pyruvate metabolism, TCA cycle, oxidative and reductive pentose phosphate pathway (Moriyama *et al.*, 2014). The shift to LC conditions led in these pathways only to minor changes on the transcriptional level compared to the photorespiratory pathway, which could earlier been shown for genes involved in the CBB cycle in *C. reinhardtii*, where mainly the transcription regulator

CIA5 seems to be responsible for the gene transcript down regulation instead of the CO_2 concentration (Fang *et al.*, 2012). A protein homologous to CIA5 (Accession number: AAG37909.1) could not be identified in the *C. merolae* genome (data not shown). In general the transcriptional level of genes involved in the energy metabolism is slightly decreased after the shift to LC conditions after 24 h and is still decreased after the recovery phase in HC in comparison to the initial values. A common behavior for all genes as expected for genes involved in one pathway, like energy metabolism, could not be detected as a response to changing CO_2 conditions as it could be shown for the photorespiratory genes (reviewed in Bordych *et al.*, 2013). The minor changes in transcription of genes involved in energy metabolism might be explained by post-translational regulation processes or the loss of the regulation ability due to the natural high CO_2 environment of *C. merolae.*

Many aquatic algae perform a CCM in order to handle carbon limitation due to a 10,000 fold slower CO_2 diffusion rate in water than in air. CCM systems consist of the active transport of inorganic carbon as CO_2 or HCO_3^-, and the accumulation of inorganic carbon within the cell (Giordano *et al.*, 2005). The accumulation of inorganic carbon within the cell occurs as HCO_3^- due to its low permeability across the lipid membrane compared to CO_2 and the outside directed concentration gradient (Fang *et al.*, 2012). CAs perform the inter-conversion of CO_2 and HCO_3^- to support RubisCO with CO_2 and are therefore of great importance under CO_2 limiting conditions (Spalding *et al.*, 1983; Coleman and Grossman, 1984).

For the identification of possible CCM components in *C. merolae*, induced under CO_2 limiting conditions, we performed BlastP analysis of known α-, β-, and γ-CAs of *A. thaliana* (Fabre *et al.*, 2007) in the *C. merolae* genome and identified two possible α-CAs: α-CA1 (CMT416) and α-CA2 (CMI270) and one already published γ-CA (CMM052, Gawryluk and Gray, 2010) (Supplementary Figure 11). Localization studies of both α-CAs revealed a cytosolic localization. This finding is in disagreement with the assumption of a CA functioning in the chloroplast to enrich CO_2 next to RubisCO as part of a CCM (Zenvirth *et al.*, 1985) (Figure 6). Transcriptional analysis of both α-CAs demonstrated very low expression of the α-CA1 under HC conditions, while a shift to LC led to a strong increase in transcription indicating a function in low CO_2 acclimation (Figure 5). The transcript level of the second α-CA2 was already high under HC conditions and showed only a

small, but significant increase in transcript abundance after the shift to LC (Figure 5). A response to reduced CO_2 concentrations in transcript for the γ-CA could not be detected (Figure 5). The enhanced N' terminal tail of the α-CA2 protein suggest the function of a membrane bound protein used as an extracellular CA producing CO_2 out of HCO_3^-, which can easily pass the membrane under CO_2 limiting conditions as it was shown for the acid-tolerant green-algae *Chlamydomonas* (UTCC121) (Balkos and Colman, 2007).

It should be mentioned, that in the present experiment changes of the carbon concentration were followed by changes of the extracellular pH with a pH of 2 under 5 % CO_2 conditions and an increased pH of 3 to 4 after 24 h at 0.04% CO_2 due to the non-buffered 2x modified Allen's growth medium. This pH-shift led to an increase in the HCO_3^- concentration in the medium.

Additional experiments, including the measurement of external and internal CA activity under different CO_2 and pH conditions are necessary to test the assumption of an external CA. Analysis of HCO_3^- transport proteins known from *C. reinhardtii* revealed one possible candidate gene in *C. merolae* (CMN251) encoding for a homologous protein to the HLA3 HCO_3^- transporter (Tirumani *et al.,* 2014) induced under limiting CO_2 conditions. CMN251 is co-expressed with photorespiratory genes and cluster together with these genes in cluster number 9 (Figure 1). This finding supports its role as a HCO_3^- transporter in a hypothetical CCM according to the assumption that genes involved in photorespiration are co-regulated with genes involved in an induced CCM under CO_2 limiting conditions as shown for the green alga *Chlamydomonas* (Fang *et al.*, 2012). Further BlastP analysis of possible transport proteins grouped together with photorespiratory genes in Cluster 9 against HCO_3^- transporter known from *Chlamydomonas* did not reveal any further candidate gene for a possible CCM HCO_3^- transport protein (data not shown). The CMS091 gene encoding for a possible homolog protein to two known HCO_3^- transporter CCP1 and CCP2 localized to the chloroplast membrane in *Chlamydomonas* did not show a photorespiratory like transcription pattern. The CMS091 gene was down regulated after the shift to LC (cluster 6, Figure 1) and the protein is further annotated as a mitochondrial carrier protein, what makes a role as a HCO_3^- transport protein in CCM unlikely. It should be mentioned that CCP1 and CCP2 HCO_3^- transport proteins in *Chlamydomonas* are not necessary for an efficient CCM but

play an important role for long-term growth under low CO_2 conditions (Pollock *et al.*, 2004).

In summary *C. merolae* reacts with a strong decrease in growth rate and depends on the photorespiratory metabolism under reduced CO_2 conditions, but on the transcriptional level only minor changes with exception to photorespiratory genes could be detected. Evidence for an active, energy consuming CCM induced under CO_2 limitation as shown for other photosynthetic organisms could not be found. Moreover the function of both identified α-CAs and the hypothetical HCO_3^- transporter seems to be the maintenance of the required inner CO_2 concentration for survival of the organism and not the accumulation of CO_2 inside the cytosol or around RubisCO, which is supported by the absence of a CO_2 concentrating structure inside the cell, like carboxysomes in cyanobacteria or pyrenoids in *Chlamydomonas* (reviewed in Raven *et al.*, 2008).

Acknowledgement

We thank the Deutsche Forschungsgemeinschaft for funding (PROMICS Research Unit FG 1186, WE 2231/8-2).

Supplementary files

Supplementary Table S1: Oligonucleotides used in this study
Supplementary Table S2: List of *A. thaliana* carbonic anhydrases and identified homologous proteins in *C. merolae*
Supplementary Table S3: Fold change values of genes encoding for proteins involved in energy metabolisms, photorespiration and light reaction
Supplementary Table S4: BlastP analysis of known active HCO_3^- and CO_2 transport proteins of *C. reinhardtii* in *C. merolae*
Supplementary Table S5: Individual mapping statistics of each RNA-Seq Samples
Supplementary Table S6: Transcriptome mapping vs. genome mapping

Supplementary Figure 1: Principal component analysis (PCA)
Supplementary Figure 2: SS-Graph
Supplementary Figure 3: Heat map of gene transcript level clustered in 10 groups
Supplementary Figure 4: Detailed heat maps of each cluster (1-10)
Supplementary Figure 5: Fold change values in transcript of genes involved in glycolysis
Supplementary Figure 6: Fold change values in transcript of genes involved in pyruvate metabolism
Supplementary Figure 7: Fold change values in transcript of genes involved in oxidative and reductive pentose phosphate pathway metabolism
Supplementary Figure 8: Fold change values in transcript of genes involved in the citric acid cycle
Supplementary Figure 9: Fold change values in transcript of genes involved in the light reaction
Supplementary Figure 10: Fold change values in transcript of genes encoding for possible carbonic anhydrases.

Supplementary Figure 11: Maximum-Likelihood Phylogenetic tree of known carbonic anhydrases from *Arabidopsis thaliana* and three possible carbonic anhydrases of *C. merolae*

References

Anisimova M, Gascuel O. 2006. Approximate Likelihood-Ratio Test for Branches: A Fast, Accurate, and Powerful Alternative. Systematic Biology **55** , 539–552.

Badger MR, Price GD. 2003. CO_2 concentrating mechanisms in cyanobacteria : molecular components , their diversity and evolution. Journal of Experimental Botany **54**, 609–622.

Balkos KD, Colman B. 2007. Mechanism of CO_2 acquisition in an acid-tolerant Chlamydomonas. Plant, Cell and Environment **30**, 745–752.

Benjamini Y, Hochberg Y. 1995. Controlling the false discovery rate: a practical and powerful approach to multiple testing. J R Stat Soc Ser B Methodol **57**.

Bordych C, Eisenhut M, Pick TR, Kuelahoglu C, Weber APM. 2013. Co-expression analysis as tool for the discovery of transport proteins in photorespiration. Plant Biology **15**, 686–693.

Breuers FKH, Bräutigam A, Geimer S, Welzel U, Stefano G, Renna L, Brandizzi F, Weber APM. 2012. Dynamic remodeling of the plastid envelope membranes – a tool for chloroplast envelope in vivo localizations. Frontiers in Plant Science **3**, 1–10.

Burey SC, Poroyko V, Ergen ZN, Fathi-Nejad S, Schüller C, Ohnishi N, Fukuzawa H, Bohnert HJ, Löffelhardt W. 2007. Acclimation to low [CO_2] by an inorganic carbon-concentrating mechanism in *Cyanophora paradoxa*. Plant, Cell and Environment **30**, 1422–1435.

Castresana J. 2000. Selection of Conserved Blocks from Multiple Alignments for Their Use in Phylogenetic Analysis. Molecular Biology and Evolution **17** , 540–552.

Chevenet F, Brun C, Bañuls A-L, Jacq B, Christen R. 2006. TreeDyn: towards dynamic graphics and annotations for analyses of trees. BMC bioinformatics **7**, 439.

Coleman JR, Grossman AR. 1984. Biosynthesis of carbonic anhydrase in Chlamydomonas reinhardtii during adaptation to low CO_2. Proceedings of the National Academy of Sciences of the United States of America **81**, 6049–6053.

Dereeper A, Guignon V, Blanc G, *et al.* 2008. Phylogeny.fr: robust phylogenetic analysis for the non-specialist. Nucleic Acids Research **36** , W465–W469.

Edgar RC. 2004. MUSCLE: multiple sequence alignment with high accuracy and high throughput. Nucleic Acids Research **32** , 1792–1797.

Eisenhut M, Ruth W, Haimovich M, Bauwe H, Kaplan A, Hagemann M. 2008. The photorespiratory glycolate metabolism is essential for cyanobacteria and might have been conveyed endosymbiontically to plants. PNAS **105**, 17199–17204.

Eisenhut M, von Wobeser EA, Jonas L, Schubert H, Ibelings BW, Bauwe H, Matthijs HCP, Hagemann M. 2007. Long-Term Response toward Inorganic Carbon Limitation in Wild Type and Glycolate Turnover Mutants of the Cyanobacterium *Synechocystis sp*. Strain PCC 6803. Plant Physiology **144**, 1946–1959.

Emanuelsson O, Nielsen H, Brunak S. 2000. Predicting Subcellular Localization of Proteins Based on their N-terminal Amino Acid Sequence. Journal of molecular biology **4**, 1005-1016.

Emanuelsson O, Nielsen H, Heijne GVON. 1999. ChloroP , a neural network-based method for predicting chloroplast transit peptides and their cleavage sites. Protein Science **8**, 978–984.

Fabre N, Reiter IM, Becuwe-Linka N, Genty B, Rumeau D. 2007. Characterization and expression analysis of genes encoding alpha and beta carbonic anhydrases in Arabidopsis. Plant, cell & environment **30**, 617–629.

Fang W, Si Y, Douglass S, Casero D, Merchant SS, Pellegrini M, Ladunga I, Liu P, Spalding MH. 2012. Transcriptome-wide changes in *Chlamydomonas reinhardtii* gene expression regulated by carbon dioxide and the CO_2-concentrating mechanism regulator CIA5/CCM1. The Plant Cell **24**, 1876–1893.

Fathinejad S, Steiner JM, Reipert S, Marchetti M, Allmaier G, Burey SC, Ohnishi N, Fukuzawa H, Löffelhardt W, Bohnert HJ. 2008. A carboxysomal carbon-concentrating mechanism in the cyanelles of the ‘coelacanth’ of the algal world, *Cyanophora paradoxa.* Physiologia Plantarum **133**, 27–32.

Gawryluk R, Gray MW. 2010. Evidence for an early evolutionary emergence of γ -type carbonic anhydrases as components of mitochondrial respiratory complex I. BMC Evolutionary Biology **10**, 1–11.

Geman S, Geman D. 1984. Stochastic relaxation, Gibbs distributions, and the bayesian restoration of images. IEEE **6**, 721–741.

Giordano M, Beardall J, Raven JA. 2005. CO_2 concentrating mechanism in algae: mechanisms, environmental modulation, and evolution. Annual Review of Plant Biology **56**, 99–131.

Grefen C, Donald N, Hashimoto K, Kudla J, Schumacher K, Blatt MR. 2010. A ubiquitin-10 promoter-based vector set for fluorescent protein tagging facilitates temporal stability and native protein distribution in transient and stable expression studies. Plant Journal **64**, 355–365.

Guindon S, Dufayard J-F, Lefort V, Anisimova M, Hordijk W, Gascuel O. 2010. New Algorithms and Methods to Estimate Maximum-Likelihood Phylogenies: Assessing the Performance of PhyML 3.0. Systematic Biology **59** , 307–321.

Hagemann M, Kern R, Maurino VG, Hanson DT, Weber APM, Sage RF, Bauwe H. 2016. Evolution of photorespiration from cyanobacteria to land plants, considering protein phylogenies and acquisition of carbon concentrating mechanisms. Journal of Experimental Botany in press.

Hirokawa T, Boonćchieng S, Mitaku S. 1998. SOSUI : classification and secondary structure prediction system for membrane proteins. Bioinformatics applications note **14**, 378–379.

Hohmann-Marriott MF, Blankenship RE. 2011. Evolution of photosynthesis. Annu Rev Plant Biol **62**, 515–548.

Imamura S, Terashita M, Ohnuma M, et al. 2010. Nitrate assimilatory genes and their transcriptional regulation in a unicellular red alga *Cyanidioschyzon merolae*: Genetic evidence for nitrite reduction by a sulfite reductase-like enzyme. Plant and Cell Physiology **51**, 707–717.

Kern R, Bauwe H, Hagemann M. 2011. Evolution of enzymes involved in the photorespiratory 2-phosphoglycolate cycle from cyanobacteria via algae toward

plants. Photosynthesis Research **109**, 103–114.

Kim D, Pertea G, Trapnell C, Pimentel H, Kelley R, Salzberg SL. 2013. TopHat2: accurate alignment of transcriptomes in the presence of insertions, deletions and gene fusions. Genome Biology **14**, 1–13.

Langmead B, Salzberg SL. 2012. Fast gapped-read alignment with Bowtie 2e. Nat Meth **9**, 357–359.

Langmead B, Trapnell C, Pop M, Salzberg S. 2009. Ultrafast and memory efficient alignment of short DNA sequences to the human genome. Genome biology **9**, 357–359.

Li B, Dewey CN. 2011. RSEM: accurate transcript quantification from RNA-Seq data with or without a reference genome. BMC Bioinformatics **12**, 1–16.

Love MI, Huber W, Anders S. 2014. Moderated estimation of fold change and dispersion for RNA-seq data with DESeq2. Genome Biology **15**, 1–21.

Matsuzaki M, Misumi O, Shin-I T, *et al.* 2004. Genome sequence of the ultrasmall unicellular red alga *Cyanidioschyzon merolae* 10D. Nature **428**, 653–657.

Minoda A, Sakagami R, Yagisawa F, Kuroiwa T, Tanaka K. 2004. Improvement of culture conditions and evidence for nuclear transformation by homologous recombination in a red alga, *Cyanidioschyzon merolae* 10D. Plant and Cell Physiology **45**, 667–671.

Moriyama T, Sakurai K, Sekine K, Sato N. 2014. Subcellular distribution of central carbohydrate metabolism pathways in the red alga *Cyanidioschyzon merolae*. Planta **240**, 585–598.

Nozaki H, Takano H, Misumi O, *et al.* 2007. A 100%-complete sequence reveals unusually simple genomic features in the hot-spring red alga *Cyanidioschyzon merolae*. BMC Biology **5**, 28.

Ohnuma M, Yokoyama T, Inouye T, Sekine Y, Tanaka K. 2008. Polyethylene glycol (PEG)-mediated transient gene expression in a red alga, *Cyanidioschyzon merolae* 10D. Plant and Cell Physiology **49**, 117–120.

Pollock S V., Prout DL, Godfrey AC, Lemaire SD, Moroney J V. 2004. The *Chlamydomonas reinhardtii* proteins Ccp1 and Ccp2 are required for long-term

growth, but are not necessary for efficient photosynthesis, in a low-CO_2 environment. Plant Molecular Biology **56**, 125–132.

Price DC, Chan CX, Yoon HS, *et al.* 2012. *Cyanophora paradoxa* genome elucidates origin of photosynthesis in algae and plants. Science **335**, 843–847.

Raven JA, Cockell CS, Rocha CLD La. 2008. The evolution of inorganic carbon concentrating mechanisms in photosynthesis. Philosophical transactions of the Royal Society of London. Series B, Biological sciences **363**, 2641–2650.

Raven JA, Giordano M, Beardall J, Maberly SC. 2012. Algal evolution in relation to atmospheric CO_2: carboxylases, carbon-concentrating mechanisms and carbon oxidation cycles. Philosophical transactions of the Royal Society of London. Series B, Biological sciences **367**, 493–507.

Savir Y, Noor E, Milo R, Tlusty T. 2010. Cross-species analysis traces adaptation of Rubisco toward optimality in a low-dimensional landscape. Proceedings of the National Academy of Sciences of the United States of America **107**, 3475–3480.

Seckbach J. 1995. The First Eukaryotic Cells - Acid Hot-Spring Algae. Journal of Biological Physics **20**, 335–345.

Spalding MH, Spreitzer RJ, Ogren WL. 1983. Carbonic Anhydrase-deficient mutant of *Chlamydomonas reinhardii* requires elevated carbon dioxide concentration for photoautotrophic growth. Plant Physiology **73**, 268–272.

Thimm O, Bläsing O, Gibon Y, Nagel A, Meyer S, Krüger P, Selbig J, Müller LA, Rhee SY, Stitt M. 2004. MAPMAN: A user-driven tool to display genomics data sets onto diagrams of metabolic pathways and other biological processes. Plant Journal **37**, 914–939.

Tirumani S, Kokkanti M, Chaudhari V, Shukla M, Rao BJ. 2014. Regulation of CCM genes in *Chlamydomonas reinhardtii* during conditions of light-dark cycles in synchronous cultures. Plant Molecular Biology **85**, 277–286.

Uemura K, Anwaruzzaman, Miyachi S, Yokota a. 1997. Ribulose-1,5-bisphosphate carboxylase/oxygenase from thermophilic red algae with a strong specificity for CO_2 fixation. Biochemical and biophysical research communications **233**, 568–571.

Watanabe S, Ohnuma M, Sato J, Yoshikawa H, Tanaka K. 2011. Utility of a GFP reporter system in the red alga *Cyanidioschyzon merolae*. The Journal of general and applied microbiology **57**, 69–72.

Yates A, Akanni W, Amode MR, *et al.* 2015. Ensembl 2016. Nucleic Acids Research, 1-7.

Zenvirth D, Volokita M, Kaplan A. 1985. Photosynthesis and inorganic carbon accumulation in the acidophilic alga *Cyanidioschyzon merolae*. Plant Physiology **77**, 237–239.

SUPPLEMENTARY DATA

Transcriptional response of the extremophile red algae *Cyanidioschyzon merolae* to changes in CO_2 concentrations

Nadine Rademacher[1], Thomas Wrobel[1], Marion Eisenhut[1], Samantha Kurz[1], Andrea Bräutigam, Andreas P.M. Weber[1*]

[1]Institute of Plant Biochemistry, Cluster of Excellence on Plant Sciences (CEPLAS), Heinrich Heine University, Universitätsstraße 1, 40225 Düsseldorf, Germany
[2]Leibniz-Institut für Pflanzengenetik und Kulturpflanzenforschung (IPK), Corrensstraße 3, 06466 Stadt Seeland, OT Gatersleben, Germany

E-mail addresses:
Nadine.Rademacher@hhu.de
Thomas.Jan.Wrobel@hhu.de
M. Eisenhut@hhu.de
Samantha.Kurz@hhu.de
brauetigam@IPK-gatersleben.de
Andreas.Weber@hhu.de

*corresponding author:
Andreas P. M. Weber
andreas.weber@hhu.de
Phone: +49 211 81-12347
Fax: not available

Supplementary Table S1: Oligonucleotides used in this study. Gateway adaption sites are underlined.

Name		Sequence
P1	CMI270C-pUBC-YFP-fv	GGGGACAAGTTTGTACAAAAAAGCAGGCT ACCATATGCAAACGTACACGCAAGC
P2	CMI270C-pUBC-YFP-rev	GGGGACCACTTTGTACAAGAAAGCTGGGTA CCCACTGCCCAGAGATTGCGTTG
P3	CMI270C-pUBN-YFP-rev	GGGGACCACTTTGTACAAGAAAGCTGGGTA CCCTCAACTGCCCAGAGATTGCG
P4	CMI270C-pUBC-YFP-fv	GGGGACAAGTTTGTACAAAAAAGCAGGCT ACCATATGGGGTTCTTGTTGTGTAGAGC
P5	CMI270C-pUBC-YFP-rev	GGGGACCACTTTGTACAAGAAAGCTGGGT ACCCACTGCCCAGAGGTTGCGTT
P6	CMI270C-pUBC-YFP-rev	GGGGACCACTTTGTACAAGAAAGCTGGGTA CCCTCAACTGCCCAGAGGTTGC

Supplementary Table S2: List of *A. thaliana* carbonic anhydrases and identified homologous proteins in *C. merolae*.

Clade	Arabidopsis thaliana ID	Cyanidioschyzon merolae ID	Identity (%)	Similarity
γ-CA	At5g63510	CmM052	36	56
γ-CA	At3g48680	CmM052	41	63
γ-CA	At1g47260	CmM052	44	64
γ-CA	At1g19580	CmM052	44	63
γ-CA	At5g66510	CmM052	43	62
β-CA	At1g23730	no		
β-CA	At1g70410	no		
β-CA	At3g01500	no		
β-CA	At5g14740	no		
β-CA	At4g33580	no		
β-CA	At1g58180	no		
α-CA	At5g04180	CmI270	42	64
		CmT416	36	59
α-CA	At4g20990	CmT416	34	58
		CmI270	32	53
α-CA	At4g21000	CmT416	33	56
α-CA	At2g28210	no		
α-CA	At1g08080	no		
α-CA	At5g56330	no		
α-CA	At1g08065	CmI270	46	57
		CmT416	46	56
α-CA	At3g52720	CmI270	38	58
		CmT416	38	55

Supplementary Table S3: Fold change values of genes encoding for proteins involved in energy metabolisms, photorespiration and light reaction.

Gene number	Protein name	Function	Fold change 0 hours to 3 hours LC ± SD	Fold change 3 hours to 24 hours LC ± SD	Fold change 0 hours LC to 24 hours recovery HC ± SD
Glycolysis					
CMO276C	GLK^{+}	Glucokinase	-	-	-
CMJ272C	PGM-1	Phosphoglucomutase	-0.42 ± 0.04^{c}	-0.09 ± 0.02	-0.39 ± 0.06^{c}
CMT285C	PGM-2^{+}		-0.49 ± 0.04	-0.10 ±0.2	-0.51 ±0.32
CMO124C	PGI-1	Phosphoglucose isomerase	-1.64 ± 0.30^{c}	0.76 ± 0.54	-0.69 ± 0.30^{b}
CMT497C	PGI-2^{+}		-0.66 ± 0.29	0.22 ± 0.37	-0.41 ± 0.48
CMI162C	PFK-1^{+}	Phosphofructokinase, ATP-dependent	0.60 ± 0.13	-0.48 ± 0.47	0.08 ± 0.40
CMM196C	PFK-2		-0.67 ± 0.19^{b}	0.57 ± 0.17^{a}	-0.31 ± 0.19
CMH052C	PFP*	Phosphofructokinase, PPi-dependent	-2.51± 0.45	1.25 ± 1.40	-1.28 ± 1.10
CMD041C	FBP-1^{+}	Fructose-1,6-bisphosphatase	1.80 ± 0.45	0.85 ± 1-06	0.64 ± 0.71
CMO245C	FBP-2		-0.15 ± 0.04	-0.15 ± 0.06	-0.15 ± 0.04
CMP129C	FBP-3^{+}		-0.36 ± 0.15^{a}	0.14 ± 0.17	0.04 ± 0.11
CME145C	FBA-1^{+}	Fructose-1,6-bisphosphate aldolase	-0.78 ± 0.19	0.47 ± 0.54	0.00 ± 0.41
CMI049C	FBA-2		1.11 ± 0.15^{b}	-0.85 ± 0.40^{a}	0.37 ± 0.34
CMQ172C	TPI^{+-}	Triosephosphate isomerase	-0.18 ± 0.08	-0.38 ± 0.26	-0.17 ± 0.16
CMJ250C	GAPC-1^{+}	GAP dehydrogenase, NAD+-dependent, phosphorylating	-0.40 ± 0.14^{a}	-0.16 ± 0.26	-0.70 ± 0.12^{b}
CMM167C	GAPC-2^{+}		-1.91 ± 0.38	1.62 ± -0.01	-1.68 ± 1.08
CMJ042C	GAPA	GAP dehydrogenase, NADP+-dependent, phosphorylating	0.61 ± 0.07	-0.90 ± 0.13^{a}	0.18 ± 0.12
CMT034C	GAPN^{+}	GAP dehydrogenase, NADP+-dependent, non- phosphorylating	1.97 ± 0.12^{b}	-1.03 ± 0.68^{b}	0.60 ± 0.61
CMJ305C	PGK^{+-}	Phosphoglycerate kinase	0.59 ± 0.04^{a}	-1.10 ± 0.18^{c}	-0.27 ± 0.21
CMK188C	PGAM^{+}	Phosphoglycerate mutase	-1.40 ± 0.15^{a}	-0.69 ± 1.33	-1.72 ± 1.13^{b}
CMK131C	ENO^{+}	Enolase	-0.91 ± 0.11	-0.13 ± 0.65	-0.80 ± 0.49
CMA030C	PK-1	Pyruvate kinase	-0.66 ± 0.10^{b}	-0.24 ± 0.42	-0.82 ± 0.27^{b}
CMC021C	PK-2^{+}		-1.09 ± 0.20^{a}	0.18 ± 0.67	-1.04 ± 045^{a}
CMK041C	PK-3		-0.65 ± 0.03^{b}	0.03 ± 0.26	-0.54 ± 0.23^{b}
CMP260C	PK-4^{+}		-036 ± 0.05^{b}	-0.25 ± 0.22	-0.78 ± 0.12^{c}
CME095C	PEPC^{+}	Phosphoenolpyruvate carboxylase	1.08 ± 020^{a}	-0.85 ± 0.58^{a}	-0.02 ± 0.54
CMN285C	PEPCK^{+}	Phosphoenolpyruvate carboxykinase	0.96 ± 0.09^{c}	-0.45 ± 0.19^{b}	0.39 ± 0.20^{a}

***** *Cyanidioschyzon merolae* gene ID taken from Moriyama *et al.,* 2014.
****** Significance test on single reads (RPKM) measured in triplicates: OneWay Anova and Newman-Keuls; a: p<0.05; b: p<0.01; c: p<0.005

Gene number *	Protein name	Function	Fold change 0 hours to 3 hours LC ± SD**	Fold change 3 hours to 24 hours LC ± SD**	Fold change 0 hours LC to 24 hours recovery HC ± SD**
Pyruvate Metabolism					
CMS327C	PDH-E1 beta	Pyruvate dehydrogenase E1	0.27 ± 0.06[b]	-0.69 ± 0.11[c]	-0.62 ± 0.05[c]
CMT256C	PDH-E1 alpha		-0.57 ± 0.18	0.21 ± 0.43	-0.43 ± 0.17
CMV153C	ptPDH-E1 alpha		-0.07 ± 0.49	0.26 ± 0.59	0.44 ± 0.38
CMV154C	ptPDH-E2 beta		-	-	-
CMI273C	PDH-E2-1	Malic enzyme, $NADP^+$-dependent	-0.67 ± 0.07[a]	0.10 ± 0.10	-0.54 ± 0.33
CMN017C	PDH-E2-2		-1.06 ± 0.11[b]	0.24 ±0.44	-0.25 ± 0.13[b]
CMN233C	PDH-E2-3		-0.31 ± 0.14	-0.14 ± 0.08	-0.25 ± 0.13
CMM299C	LPD (E3)-1	Pyruvate dehydrogenase E3/ Dihydrolipoamide dehydrogenase	2.24 ± 0.26[c]	-1.96 ± 0.57[c]	-0.03 ± 0.63
CMQ234C	LPD (E3)-2		-0.78 ± 0.05[a]	0.17 ± 0.22	-0.34 ± 0.34
CMJ051C	ME	Malic enzyme, $NADP^+$-dependent	-0.38 ± 0.08[b]	-0.08 ± 0.19	-0.47 ± 0.12[b]

***** *Cyanidioschyzon merolae* gene ID taken from Moriyama *et al.,* 2014.
****** Significance test on single reads (RPKM) measured in triplicates: OneWay Anova and Newman-Keuls; a: $p<0.05$; b: $p<0.01$; c: $p<0.005$
$^+$Cytosolic localization, $^{+-}$ Cytosolic and plastidic localization

Gene number*	Protein name	Function	Fold change 0 hours to 3 hours LC ± SD**	Fold change 3 hours to 24 hours LC ± SD**	Fold change 0 hours LC to 24 hours recovery HC ± SD**
Oxidative and reductive Pentose Phosphate pathway					
CMI224C	G6PDH-1	Glucose-6-phosphate dehydrogenase	-0.07 ± 0.19	0.41 ± 0.18	0.13 ± 0.18
CMR014C	G6PSH-2		-1.53 ± 0.37[a]	0.81 ± 0.86	-0.84 ± 0.45
CMC120C	PGL	6-phosphogluconolactonase	-0.19 ± 0.10	0.06 ± 0.13	-0.13 ± 0.10
CML037C	6PGDH-1	6-phosphogluconate dehydrogenase	-0.31 ± 0.17[a]	0.38 ± 0.18[a]	0.15 ± 0.04
CML036C	6PGDH-1b		-0.22 ± 0.29	0.21 ± 0.07	-0.05 ± 0.32
CML059C	6PGDH-2		-0.61 ± 0.25[a]	0.10 ± 0.24	-0.49 ± 0.21[a]
CMM231C	6PGDH-3		-0.50 ± 0.19[a]	0.12 ± 0.10	-0.41 ± 0.18[a]
CMS195C	6PGDH-4		-0.97 ± 0.20[a]	0.68 ± 0.44	-0.23 ± 0.24
CMO291C	RPI	Ribose-5-phosphate isomerase	0.09 ± 0.08	-1.15 ± 0.44	-0.28 ± 0.52
CMI084C	RPE-1	Ribulose-5-phosphate-3-epimerase	-0.12 ± 0.10	-0.10 ± 0.08	-0.01 ± 0.24
CMO229C	RPE-2		-0.16 ± 0.34	0.32 ± 0.47	0.21 ± 0.25
CMT633	RPE-3		-0.10 ± 0.05	0.17 ± 0.04	0.21 ± 0.11
CMO121C	TKT-1	Transketolase	2.30 ± 0.16[b]	-1.49 ±1.07[b]	0.33 ± 1.03
CMO128C	TKT-2		0.21 ± 0.20	-0.42 ± 0.23	-0.13 ± 0.14
CMI196C	SBP-1	Sedoheptulose-1,7-bisphosphatase	0.52 ± 0.02	-0.23 ± 0.30	0.50 ± 0.26
CMT362C	SBP-2		-0.51 ±0.17[b]	0.20 ± 0.06	-0.38 ± 0.11[b]
CMF117C	PRK	Phosphoribulokinase	0.28 ± 0.01[b]	-0.40 ± 0.04	0.25 ± 0.04[b]
CMV013C	RBCL	Ribulose bisphosphate carboxylase	1.11 ± 0.18[b]	-1.64 ±0.67[b]	-0.97 ± 0.58
CMV014C	RBCS		-	-	-

***** *Cyanidioschyzon merolae* gene ID taken from Moriyama *et al.,* 2014.
****** Significance test on single reads (RPKM) measured in triplicates: OneWay Anova and Newman-Keuls; a: $p<0.05$; b: $p<0.01$; c: $p<0.005$

Gene number*	Protein name	Function	Fold change 0 hours to 3 hours LC ± SD**	Fold change 3 hours to 24 hours LC ± SD**	Fold change 0 hours LC to 24 hours recovery HC ± SD**
TCA cycle					
CMA040C	CS-1	Citrate synthase	1.02 ± 0.07	-0.21 ± 0.51	0.54 ± 0.61
CMJ193C	CS-2		-	-	-
CMM068C	CS-3		0.16 ± 0.19	-0.18 ± 0.27	0.03 ± 0.10
CMQ191C	CS-4		-0.64 ± 0.04	-0.95 ± 0.74	-0.93 ± 0.76
CMT561C	ACO	Aconitase	-0.67 ± 0.02[a]	-0.02 ± 0.20	-0.37 ± 0.24
CMS242C	IDH2	Isocitrate dehydrogenase, NAD^+-dependent	-	-	-
CMT412	IDH1		-0.63 ± 0.16[a]	-0.47 ± 0.60	-1.06 ± 0.41[a]
CMT216C	ICDH	Isocitrate dehydrogenase, $NADP^+$-dependent	-0.26 ± 0.19	0.50 ± 0.17[b]	0.32 ± 0.19[a]
CMF068C	2OGH-E1	2-oxoglutarate dehydrogenase E1	-0.03 ± 0.23	0.23 ± 0.34	0.14 ± 0.12
CMJ055C	2OGH-E2	2-oxoglutarate dehydrogenase E2	-0.74 ± 0.21[a]	-0.19 ± 0.64	-0.73 ± 0.41[a]
CMH132C	SCS-alpha	Succinyl-CoA synthetase	-0.43 ± 0.06[a]	0.19 ± 0.17	0.03 ± 0.15
CMT209C	SCS-beta		-0.37 ± 0.11[b]	0.25 ± 0.18[a]	-0.12 ± 0.04
CMT582C	SDH1	Succinate dehydrogenase (complex II) flavoproteinsubunit	0.04 ± 0.05	0.16 ± 0.14	0.06 ± 0.17
CMW001C	SDH3	Succinate dehydrogenase cytochrome B560 subunit	-	-	-
CMW002C	SDH2	Succinate iron-sulfur protein	-	-	-
CMW055C	SDH4	Succinate dehydrogenase hydrophobic subunit	-	-	-
CMD058C	FUM	Fumarase	-0.90 ± 0.14[a]	0.58 ± 0.10[a]	-0.08 ± 0.23
CMP193C	MDH-1	Malat dehydrogenase	-0.75 ± 0.17[b]	-0.29 ± 0.52[a]	-0.94 ± 0.31[b]
CMT611C	MDH-2		-1.17 ± 0.24	-0.09 ± 0.94	-1.20 ± 0.80

* *Cyanidioschyzon merolae* gene ID taken from Moriyama *et al.,* 2014.
** Significance test on single reads (RPKM) measured in triplicates: OneWay Anova and Newman-Keuls; a: $p<0.05$; b: $p<0.01$; c: $p<0.005$

Gene number*	Protein name	Function	Fold change 0 hours to 3 hours LC ± SD**	Fold change 3 hours to 24 hours LC ± SD**	Fold change 0 hours LC to 24 hours recovery HC ± SD**
Photorespiration					
CMR421C	PGP	Phosphoglycolate phosphatase	3.79 ± 0.17[c]	-2.23 ± 1.31[c]	0.94 ± 1.25
CMQ436C	GOX	Glycolate oxidase	4.07 ± 0.05[b]	-2.20 ± 1.78[b]	1.06 ± 1.75
CMI050C	CAT2	Catalase	3.40 ± 0.06	-0.97 ± 1.53	1.78 ± 1.44
CMS429C	SGT	Serine: glyoxylate aminotransferase	5.71 ± 0.08[c]	-2.73 ± 2.19[b]	1.83 ± 2.09
CMM066C	GGT	Glutamate: glyoxylate aminotransferase	1.90 ± 0.16[a]	-0.86 ± 0.95	0.94 ± 0.82
CMG086C	GDC T-protein	Glycine decarboxylase	3.61 ± 0.14[c]	-2.56 ± 1-26[c]	0.66 ± 1.57
CMR282C	GDC P-protein		3.66 ± 0.20[c]	2.29 ± 1.33[c]	0.80 ± 1.11
CMF098C	GDC H-protein		1.41 ± 0.13[c]	-1.61 ± 0.15[c]	-0.05 ± 0.23
CMM299C	GDC L-protein		2.24 ± 0.26[c]	-1.96 ± 0.57[c]	-0.03 ± 0.63
CMO142C	SHMT	Serine hydroxymethlytransferase	4.06 ± 0.18[b]	-2.16 ± 1.40[b]	1.13 ± 1.38
CMS425C	HPR1	Peroxisomal hydroxypyruvat reductase	3.30 ± 0.03[a]	-1.46 ± 1.31[a]	1.30 ± 1.37
CMQ289C	HPR2	Cytosolic hydroxypyruvat reductase	1.34 ± 0.17[c]	-1.03 ± 0.23[c]	0.08 ± 0.17
CMK141C	GLYK	Glycerate kinase	3.04 ± 0.28[b]	-1.74 ± 1.12[b]	0.72 ± 1.06

* *Cyanidioschyzon merolae* gene ID taken from Rademacher *et al.,* 2016.
** Significance test on single reads (RPKM) measured in triplicates: OneWay Anova and Newman-Keuls; a: $p<0.05$; b: $p<0.01$; c: $p<0.005$

Gene number*	Protein name	Function	Fold change 0 hours to 3 hours LC ± SD**	Fold change 3 hours to 24 hours LC ± SD**	Fold change 0 hours LC to 24 hours recovery HC ± SD**
Light reaction					
CMV082C	PsbC	Photosystem II	1.70 ± 0.55	-1.31 ± 0.62	0.43 ± 0.23
CMV124C	psbB		1.50 ± 0.39	-0.14 ± 0.35	1.14 ± 0.37
CMT182C	PsbM		-1.05 ± 0.27	0.83 ± 0.34	0.52 ± 0.38
CMI290C	PsbO/P		-0.91 ± 0.18	0.99 ± 0.15	0.63 ± 0.18
CMC133C	PsbQ		-0.61 ± 0.20[a]	0.43 ± 0.42[a]	0.51 ± 0.28[a]
CMI248C	PsbU		-0.46 ± 0.20	0.71 ± 0.11[a]	0.65± 0.08[b]
CMV206C	PsbX		-0.25 ± 0.27	1.35 ± 0.57	0.93 ± 0.49
CMK176C	Psb27		-0.11 ± 0.18	-0.02 ± 0.32	0.25 ± 0.11
CMV136C	PsaB	Photosystem I	1.73 ± 0.64	-0.95 ± 0.07	0.68 ± 0.83
CMV144C	PsaD		-0.08 ± 0.26	0.40 ± 0.41	0.38 ± 0.48
CMV128C	PsaE		1.18 ± 0.36	0.03 ± 0.39	1.32 ± 1.01
CMV201C	PsaF		1.03 ± 0.97	-0.56 ± 0.16	0.36 ± 0.50
CMV227	PsaI		0.75 ± 0.65	-1.47 ± 0.21[a]	0.99 ± 0.97
CMV055C	PsaK		0.23 ± 0.18	0.84 ± 0.41 [a]	0.82 ± 0.43
CMP086C	PsaO		-0.42 ± 0.23	0.32 ± 0.22	0.56 ± 0.27
CMQ142C	LHP	PSI associated antenna	-0.92 ± 021	1.53 ± 0.18[a]	1.30 ± 0.22[b]
CMN234C	CP24a		-1.06 ± 0.26	1.71 ± 0.43	1.19 ± 0.50[a]
CMN235C	CP24b		-0.99 ± 028	1.07 ± 0.26	0.71 ± 0.24
CMV051C	RCL-1		0.43 ± 0.19	0.97 ± 0.59	1.11 ± 0.61
CMV157C	LP		0.12 ± 0.15	0.11 ± 0.40	0.39 ± 0.27
CMP166C	RCL-2		-1.08 ± 0.10	2.08 ± 0.10[b]	1.58 ± 0.28[c]
CMV063C	PC-alpha		1.28 ± 0.63	-1.25 ± 0.86	0.74 ± 0.72
CMV064C	PC-beta		1.16 ± 0.69	-0.51 ± 1.01	1.32 ± 0.79
CMV158C	ApcA	Allophycocyanin	-0.47 ± 0.26	0.86 ± 0.53[a]	0.69 ± 0.26
CMV159C	ApcB		-0.43 ± 0.26	0.74 ± 0.48	0.72 ± 0.31[a]
CMO250C	ApcC		-0.77 ± 0.16[a]	1.00 ± 0.18[b]	0.68 ± 0.16[b]
CMV204C	ApcD		1.50 ± 1.26	0.10 ± 0.20	1.33 ± 0.51
CMV063C	CpcA	Phycocyanin/ Phycoerythrocyanin	1.28 ± 0.63	-1.25 ± 0.86	0.74 ± 0.72
CMP166C	CpcC		-1.08 ± 0.10	2.08 ± 0.10[b]	1.58 ± 0.28[c]
CMJ043C	CpcE		0.15 ± 0.09	0.16 ± 0.36	0.32 ± 0.33
CMJ049C	CpcF		-0.05 ± 0.07	0.45 ± 0.19	0.21 ± 0.30
CMV051C	CpcG		0.43 ± 0.19	0.67 ± 0.59	1.11 ± 0.61
CMV064C	PBC		1.16 ± 0.69	-0.51 ± 1.01	1.32 ± 0.79

* *Cyanidioschyzon merolae* gene ID taken from KEGG database (Kanehisa Laboratories), gene ID for photosystem I associated antenna proteins taken from Busch *et al.,* 2010.
** Significance test on single reads (RPKM) measured in triplicates: OneWay Anova and Newman-Keuls; a: $p<0.05$; b: $p<0.01$; c: $p<0.005$

Supplementary Table S4: List of known active HCO_3^- and CO_2 transport proteins in *Chlamydomonas reinhardtii*. Shown are the best hits identified by BlastP analysis in *C.merolae* including gene name, annotation, identity and similarity.

CCM Genes in *Chlamydomonas reinhardtii (1)*			Best Blast hits *Cyanidioschyzon merolae*			
Protein name	Gene ID	Annotation	Gene ID	Annotation	Identity (%)	Similarity (%)
LCI1	XM_001703335.1	Low-CO_2-inducible membrane protein	No hits			
LCIA	AY612639.1	Low CO_2 inducible protein – HCO_3 transport	No hits			
LCIB	XM_001698292.1	Low CO_2 inducible protein –CO_2 transport	No hits			
HLA3	XM_001699988.1	Low CO_2 inducible protein – HCO_3^- transport, ABC transport protein	CMN251C	ATP binding cassette	30	46
CCP1	U75345.1	HCO_3^- transport chloroplast membrane	CMS091C	Probable mitochondrial carrier protein	22	38
CCP2	U75346.1	HCO_3^- transport chloroplast membrane	CMS091C	Probable mitochondrial carrier protein	22	39

(1) Tirumani S, Kokkanti M, Chaudhari V, Shukla M, Rao BJ. 2014. Regulation of CCM genes in Chlamydomonas reinhardtii during conditions of light--dark cycles in synchronous cultures. Plant Molecular Biology **85**, 277–286.

Supplementary Table S5: Individual mapping statistics of each RNA-Seq sample

Sample ID	Total Reads of Sample	aligned 0 times	aligned 0 times (%)	unique alignment	unique alignment (%)	multiple alignment	multiple alignment (%)	overall alignment rate
1-WT-LC0-1	18050693	7131492	39,51	9793982	54,26	1125219	6,23	60,49
2-WT-LC0-2	21198111	8429122	39,76	11416399	53,86	1352590	6,38	60,24
3-WT-LC0-3	20983072	8248105	39,31	11454571	54,59	1280396	6,10	60,69
7-WT-LC3-1	19361712	7838728	40,49	10205257	52,71	1317727	6,81	59,51
8-WT-LC3-2	21535828	8147369	37,83	11978617	55,62	1409842	6,55	62,17
9-WT-LC3-3	17373578	6717941	38,67	9340717	53,76	1314920	7,57	61,33
13-WT-LC24-1	42219029	16264555	38,52	23229260	55,02	2725214	6,45	61,48
14-WT-LC24-2	46424543	18915024	40,74	24617004	53,03	2892515	6,23	59,26
15-WT-LC24-3	34080492	13424624	39,39	18750763	55,02	1905105	5,59	60,61
19-WT-HC24-1	24695649	9604129	38,89	13675287	55,38	1416233	5,73	61,11
20-WT-HC24-2	46432290	18397995	39,62	25249652	54,38	2784643	6,00	60,38
21-WT-HC24-3	53206149	21486917	40,38	28554268	53,67	3164964	5,95	59,62
Average	30463428.83	12050500.08	39.43	16522148.08	54.27	1890780.667	6.30	60.57
Sum	365561146	144606001		198265777		22689368		

Supplementary Table S6: Resullts of transcriptome mapping vs. genome mapping

Algorithm	Mapping	Total reads	aligned 0 times	aligned 0 times (%)	aligned 1 time	aligned 1 time (%)	multiple alignment	multiple alignment (%)	overall alignment rate
Bowtie2 (very-sensitive)	Transcriptome only	53206149	21486917	40.38	28554268	53.67	3164964	5.95	59.62
Tophat2 (very-sensitive)	Transcriptome + Genome	53206149	4215236	7.92	46078112	86.60	2912801	5.47	92.08
Tophat2 (very-fast)	Transcriptome + Genome	53206149	4202510	7.90	46033579	86.52	2970059.5	5.58	92.10

Supplementary Table S7: List of identified transport proteins co-expressed with photorespiratory genes in cluster 9. Shown are related *A. thaliana* gene IDs identified by BlastP, long description and Mapman Categories. * indicates possible HCO_3^- (HLA3) transporter

C. merolae	*A. thaliana*	BlastP e-value	Long description	Mapman Category
CMP064C	AT4G39460	9.00E-041	S-adenosylmethionine transmembrane transporter1	Metabolite transporters at the mitochondrial membrane
CMQ427C	AT5G61810	3.00E-005	mitochondrial substrate carrier family protein	Metabolite transporters at the mitochondrial membrane
CMR382C	AT1G79610	1.00E-018	sodium proton exchanger, putative (NHX6)	Transport unspecified cations
CMS453C	AT1G34065	1.00E-035	S-adenosylmethionine carrier 2	Metabolite transporters at the mitochondrial membrane
CMN295C	AT1G31770	5.00E-071	ABC transporter family protein	ABC transporters and multidrug resistance systems
CMN115C	AT2G38330	6.00E-028	MATE efflux family protein	Transport misc.
CMT284C	AT5G43340	1.00E-025	PHT6 carbohydrate/ inorganic phosphate transmembrane transporter	Transport phosphate
CMC075C	AT1G79520	7.00E-046	cation efflux family protein	Transport metal
CMG103C	AT2G42005	1.00E-027	amino acid transporter family protein	Transport amino acids
CMI004C	AT1G15460	2.00E-031	BOR4 anion exchanger	Transport unspecified anions
CMT006C	AT1G15460	2.00E-031	BOR4 anion exchanger	Transport unspecified anions
CMJ216C	AT5G64840	1.00E-064	general control non-repressible 5 transporter	ABC transporters and multidrug resistance systems
CMN105C	AT5G58270	2.00E-158	ATPase, coupled to transmembrane movement of substances	ABC transporters and multidrug resistance systems
CMJ195C	AT5G55630	6.00E-010	ATKCO1 calcium-activated potassium channel/ ion channel/ outward rectifier potassium channel	Transport potassium
CMF138C	AT2G17500	3.00E-012	auxin efflux carrier family protein	Transport misc
CMQ364C	AT1G10830	1.00E-061	sodium symporter-related	Transport unspecified cations
CMN251C*	AT2G34660	0	multidrug resistance-associated protein 2, ATPase, coupled to transmembrane movement of substances	ABC transporters and multidrug resistance systems
CMN092C	AT4G22200	2.00E-005	potassium transport 2/3 cyclic nucleotide binding/ inward rectifier potassium channel	Transport potassium
CMM153C	AT3G58970	1.00E-031	magnesium transporter CorA-like family protein	Transport unspecified cations
CMN328C	AT3G01550	7.00E-075	Phosphoenolpyruvate/ Phosphate translocator antiporter/ triose-phosphate transmembrane transporter	Metabolite transporters at the envelope membrane
CMN021C	AT4G31600	3.00E-023	UDP-glucuronic acid/UDP-N-acetylgalactosamine transporter-related	Transport
CMD148C	AT4G18050	2.00E-128	Symbols: P-glycoprotein 9 ATPase, coupled to transmembrane movement of substances	ABC transporters and multidrug resistance systems
CMR009C	AT5G25430	3.00E-042	anion exchanger	Transport unspecified anions
CMK126C	AT1G64780	2.00E-054	ammonium transmembrane transporter 12	Transport ammonium
CMR388C	AT3G47760	6.00E-041	ATATH4 ATPase, coupled to transmembrane movement of substances / transporter	ABC transporters and multidrug resistance systems
CMW029C	AT1G63270	7.00E-017	ATNAP10 transporter	ABC transporters and multidrug resistance systems

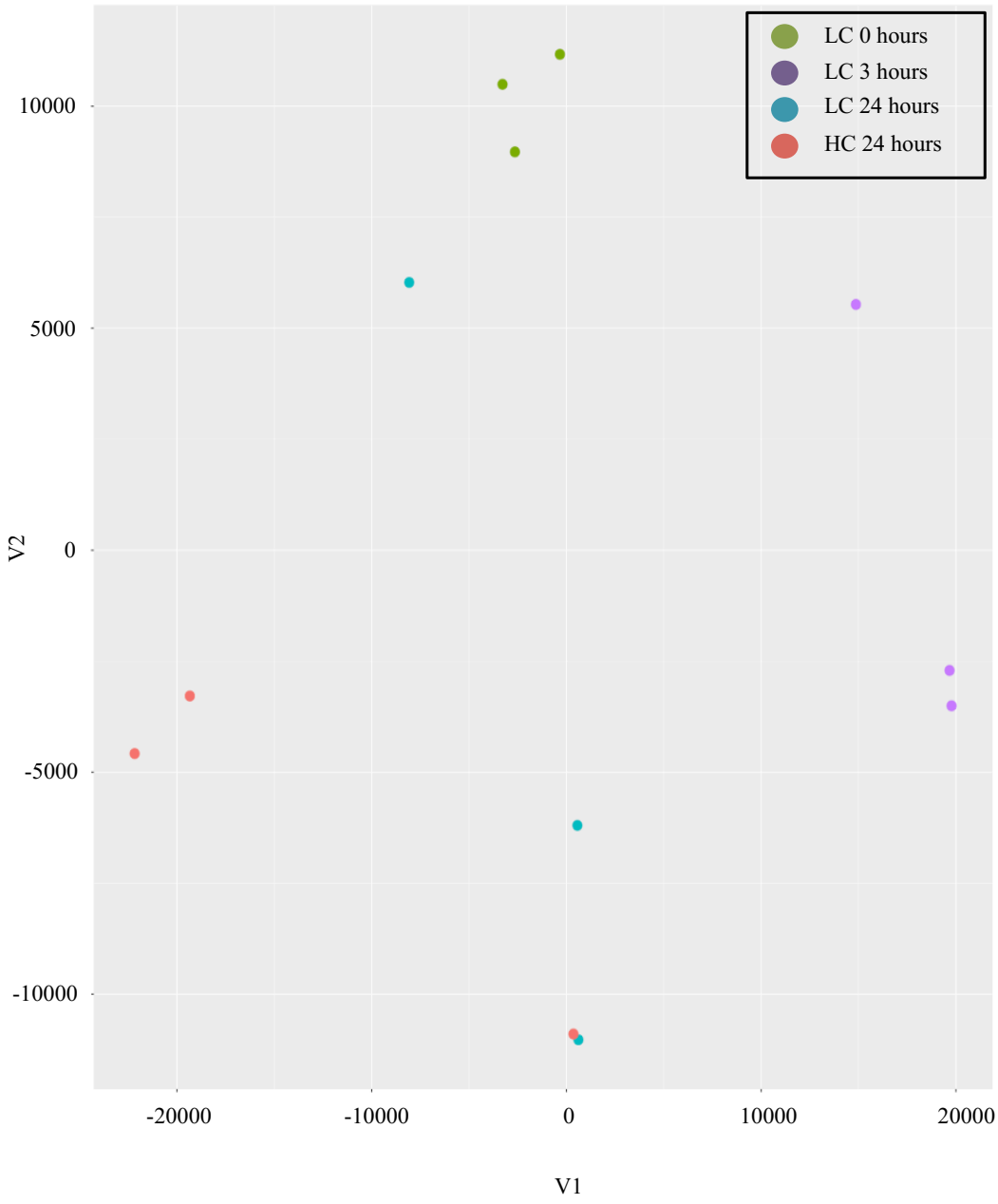

Supplementary Figure 1: Principal component analysis (PCA) of different sampling time points: 0 h (LC 0 h), 3 h (LC 3 h) and 24 h (LC 24 h) after the shift from high carbon to low carbon conditions and after the recovery time 24 h in high carbon (HC 24 h). Analysis includes transcriptome datasets of three biological replicates.

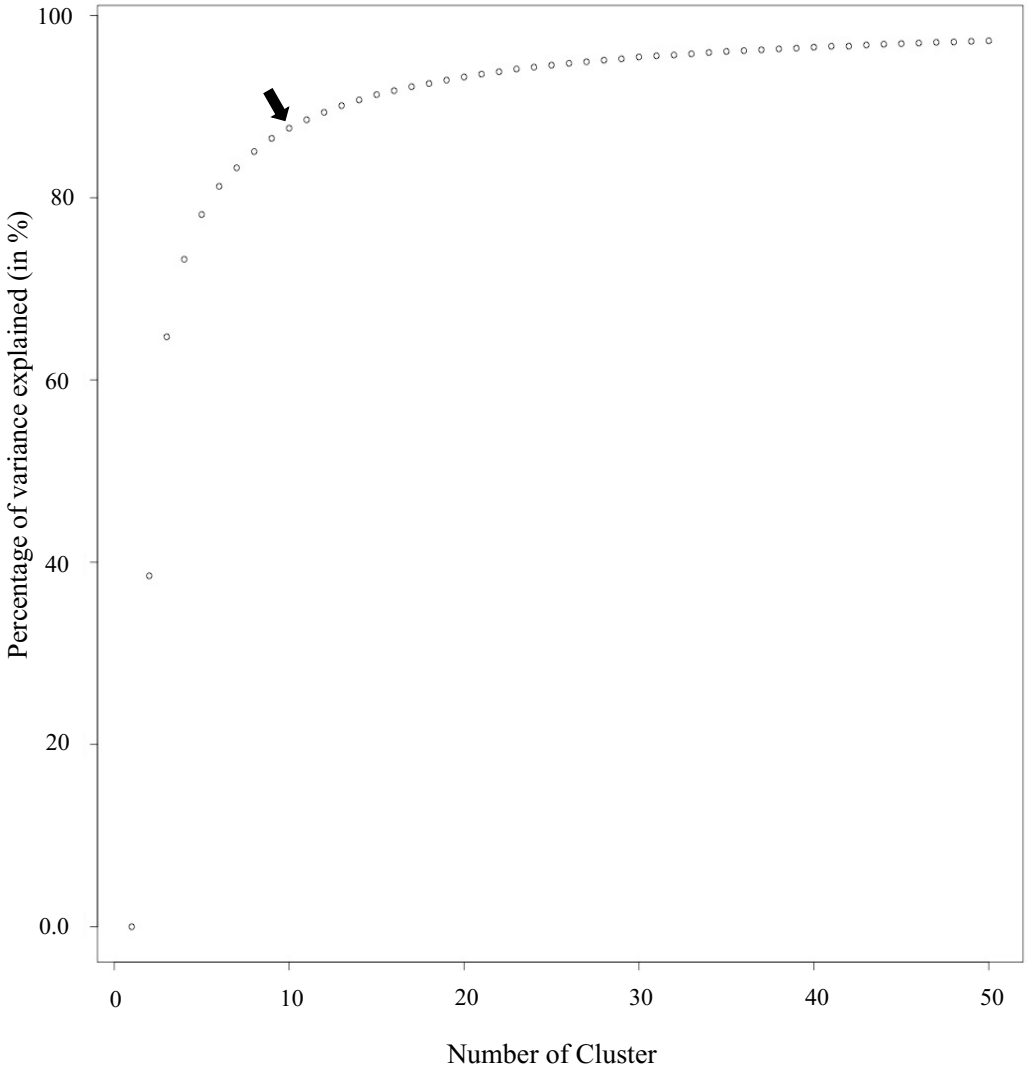

Supplementary Figure 2: Graph used for determination of necessary number of clusters. Shown are sum of squares divided by total sum of squares in dependency of number of clusters.

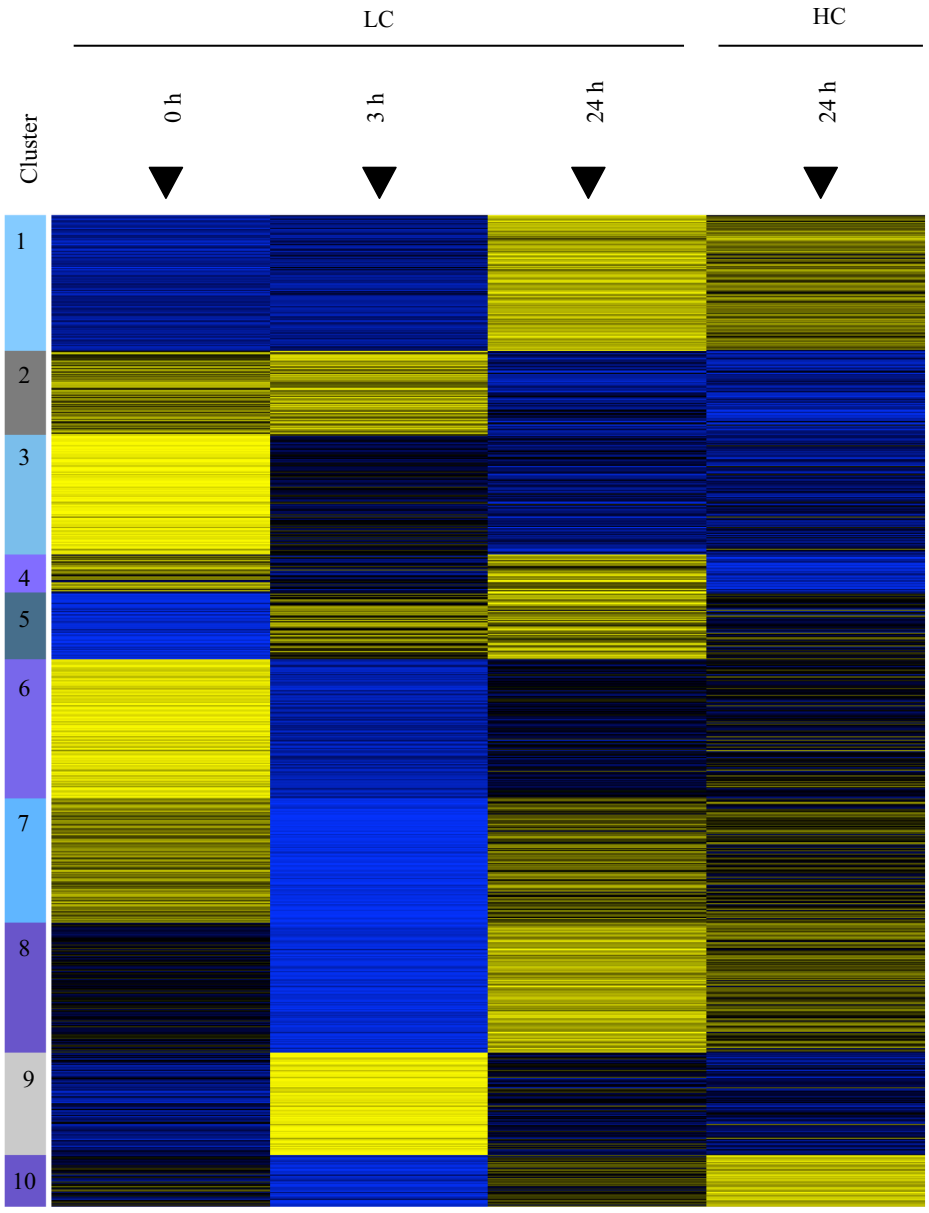

Supplementary Figure 3: Heat map of gene transcript level clustered in 10 groups. Shown are transcript level of all genes at four different conditions: 0 h (LC 0 h), 3 h (3 h LC) and 24 h (24 h LC) after the HC-LC shift and 24 h after the recovery phase in HC (24 h HC). Color code indicates transcript level: Blue: low transcript level; yellow: high transcript level.

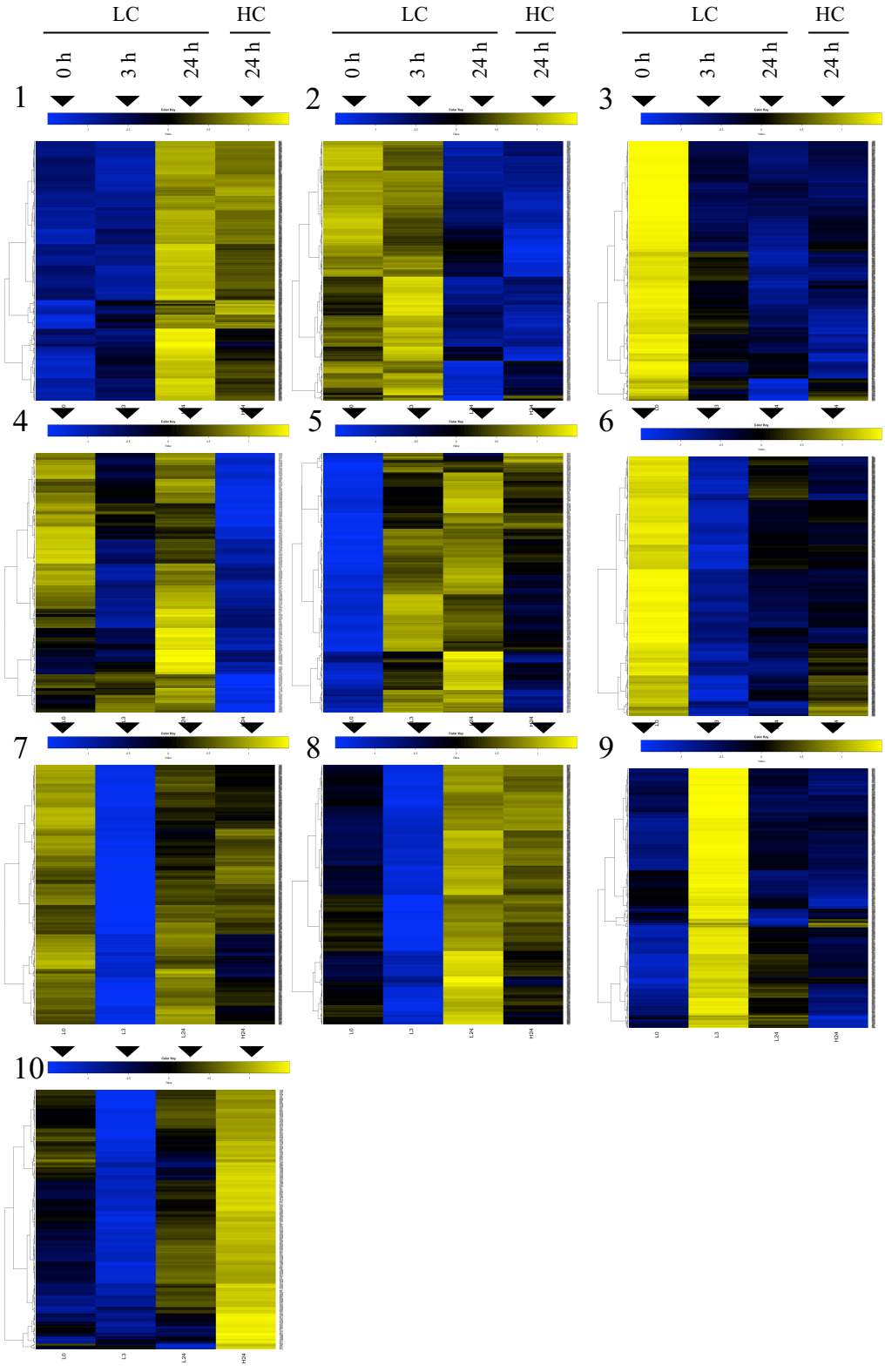

Supplementary Figure 4: Detailed heat maps of each cluster (1-10). Shown are transcript levels of all genes at four different conditions: 0 h (LC 0 h), 3 h (3 h LC) and 24 h (24 h LC) after the HC-LC shift and 24 h after the recovery phase in HC (24 h HC). Color code indicates transcript level: Blue: low transcript level; yellow: high transcript level.

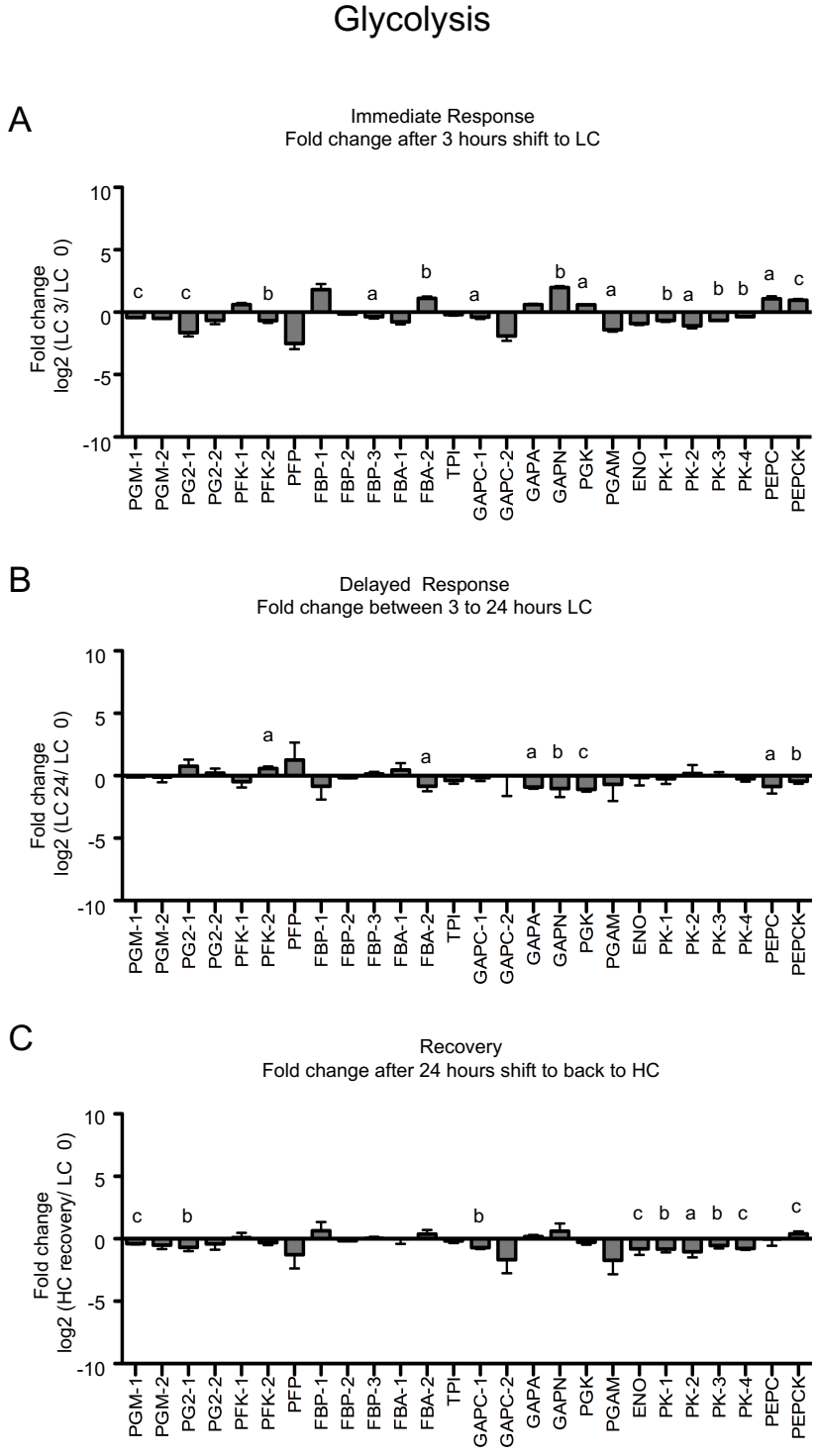

Supplementary Figure 5: Fold change values in transcript of genes involved in glycolysis. Shown are the immediate response in transcript level in the time between 0 h and 3 h after the shift to LC (A), the delayed response in transcript between 3 h and 24 h after the shift to LC (B) and the recovery rate 24 h after the shift back to HC compared to initial value 0 h after shift to LC (C). Significant changes between to time points in transcript level are indicated as a ($p<0.05$), b ($p<0.01$) and c ($p<0.01$). Enzyme abbreviations are explained in supplementary table S3.

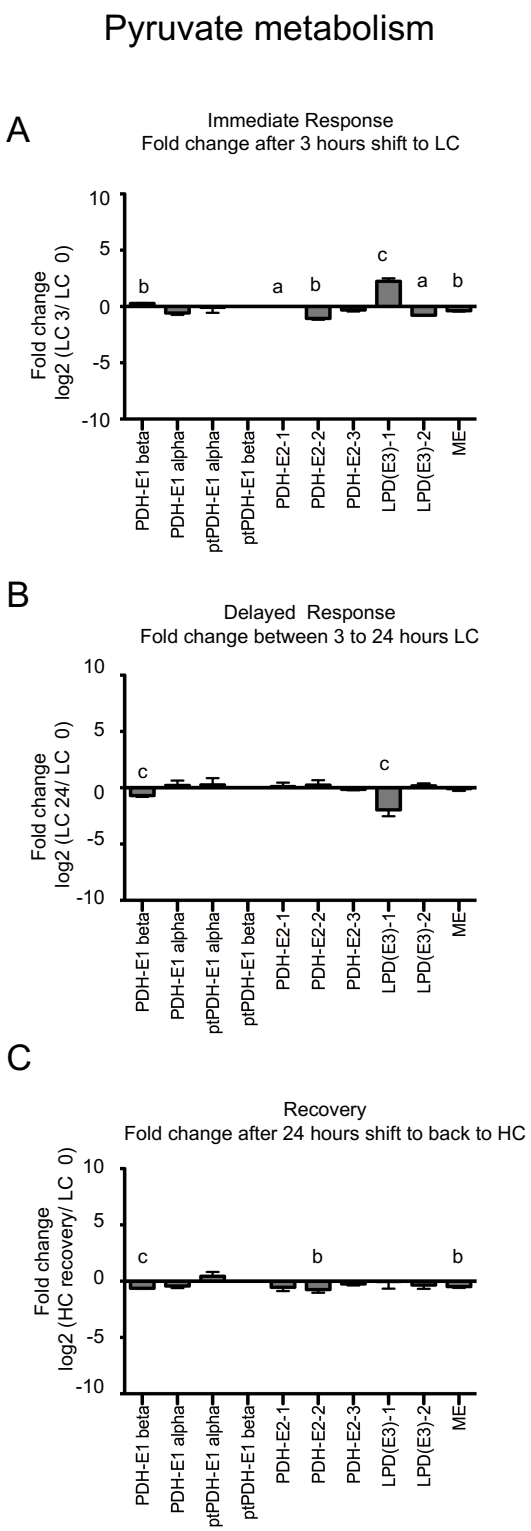

Supplementary Figure 6: Fold change values in transcript of genes involved in pyruvate metabolism. Shown are the immediate response in transcript level in the time between 0 h and 3 h after the shift to LC (A), the delayed response in transcript between 3 h and 24 h after the shift to LC (B) and the recovery rate 24 h after the shift back to HC compared to initial value 0 h after shift to LC (C). Significant changes between to time points in transcript level are indicated as a ($p<0.05$), b ($p<0.01$) and c ($p<0.01$). Enzyme abbreviations are explained in supplementary table S3.

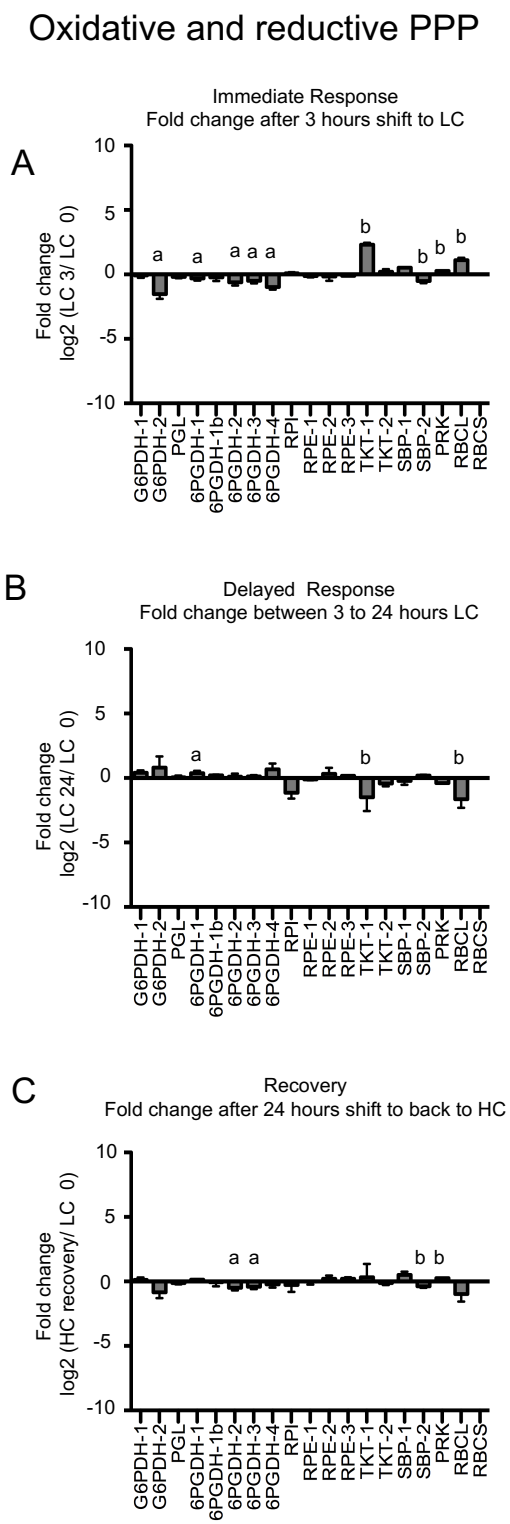

Supplementary Figure 7: Fold change values in transcript of genes involved in oxidative and reductive pentose phosphate pathway metabolism. Shown are the immediate response in transcript level in the time between 0 h and 3 h after the shift to LC (A), the delayed response in transcript between 3 h and 24 h after the shift to LC (B) and the recovery rate 24 h after the shift back to HC compared to initial value 0 h after shift to LC (C). Significant changes between to time points in transcript level are indicated as a ($p<0.05$), b ($p<0.01$) and c ($p<0.01$). Enzyme abbreviations are explained in supplementary table S3.

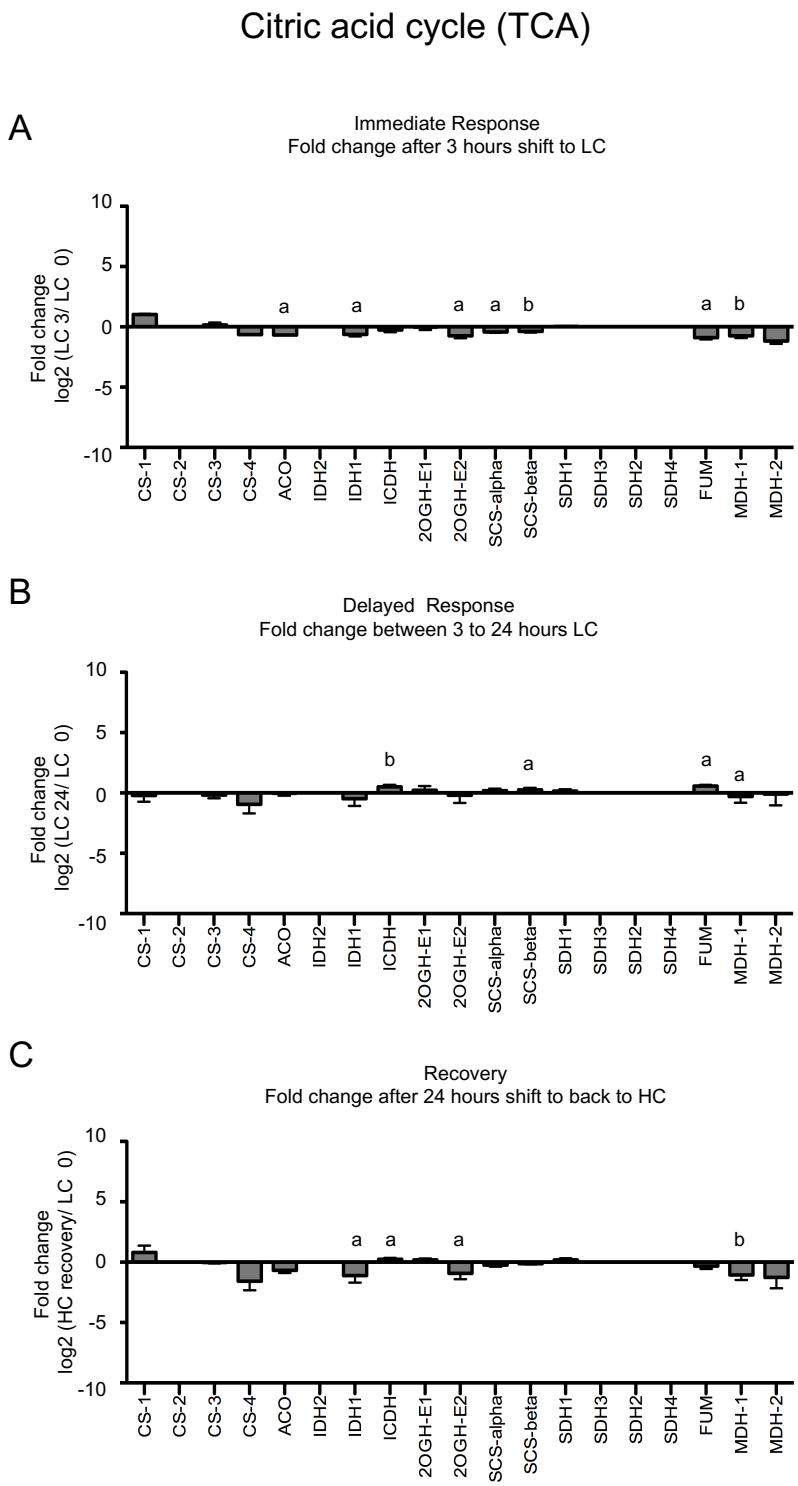

Supplementary Figure 8: Fold change values in transcript of genes involved in the citric acid cycle (TCA). Shown are the immediate response in transcript level in the time between 0 h and 3 h after the shift to LC (A), the delayed response in transcript between 3 h and 24 h after the shift to LC (B) and the recovery rate 24 h after the shift back to HC compared to initial value 0 h after shift to LC (C). Significant changes between to time points in transcript level are indicated as a ($p<0.05$), b ($p<0.01$) and c ($p<0.01$). Enzyme abbreviations are explained in supplementary table S3.

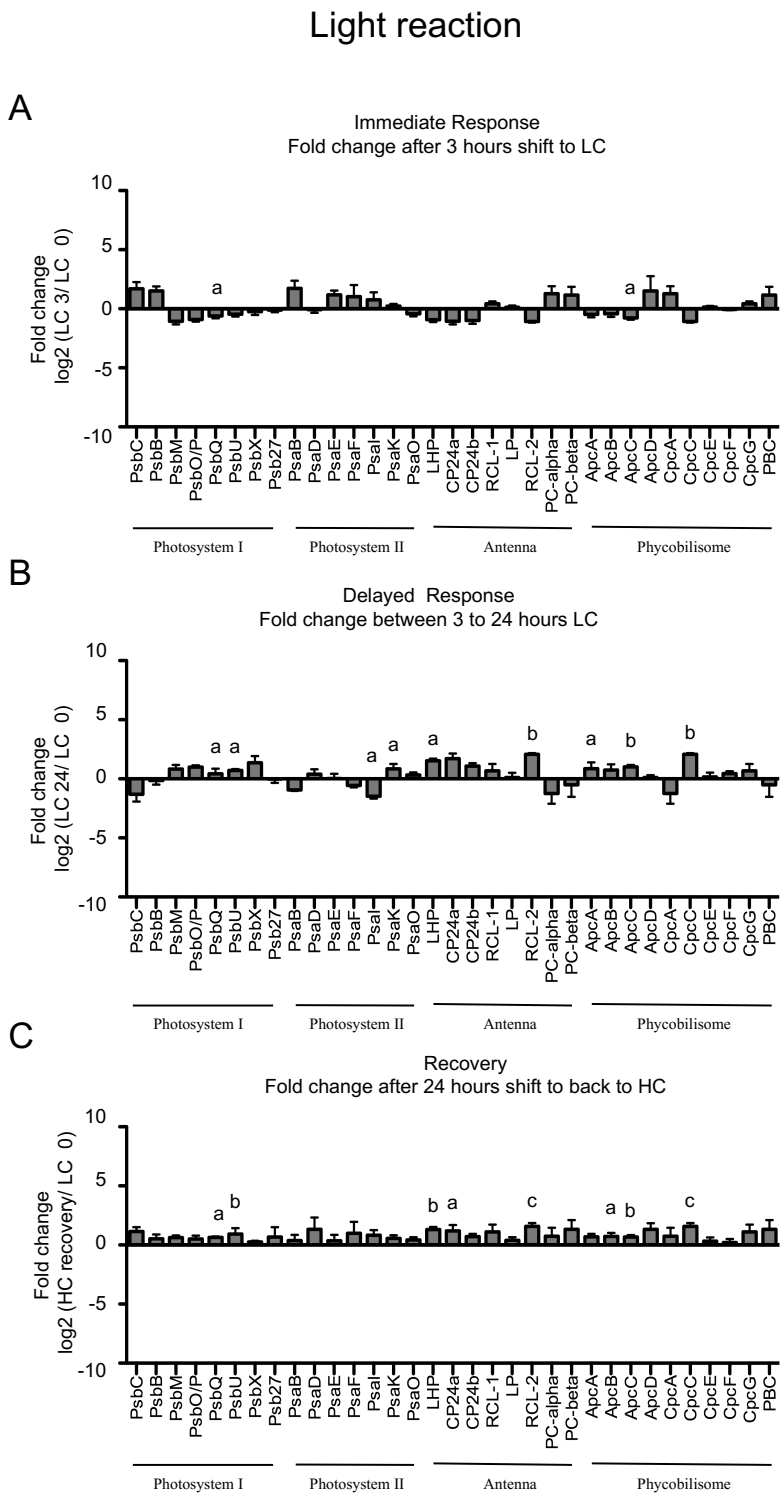

Supplementary Figure 9: Fold change values in transcript of genes involved in the light reaction. Shown are the immediate response in transcript level in the time between 0 h and 3 h after the shift to LC (A), the delayed response in transcript between 3 h and 24 h after the shift to LC (B) and the recovery rate 24 h after the shift back to HC compared to initial value 0 h after shift to LC (C). Significant changes between to time points in transcript level are indicated as a ($p<0.05$), b ($p<0.01$) and c ($p<0.01$). Enzyme abbreviations are explained in supplementary table S3.

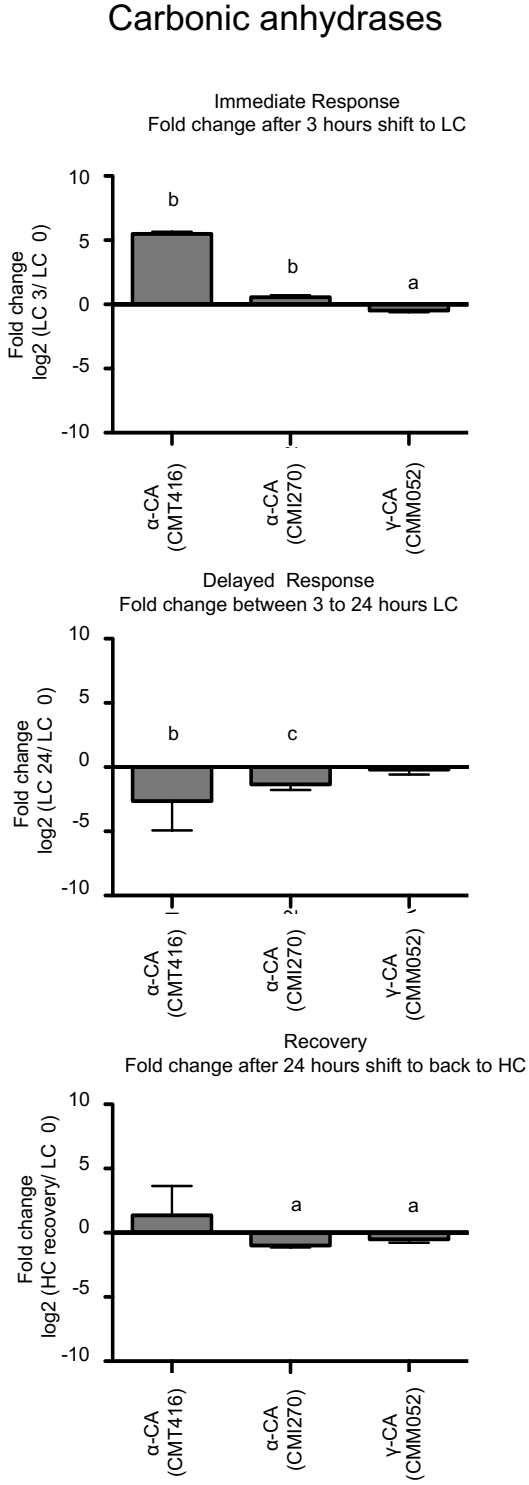

Supplementary Figure 10: Fold change values in transcript of genes encoding for possible carbonic anhydrases. Shown are the immediate response in transcript level in the time between 0 h and 3 h after the shift to LC (A), the delayed response in transcript between 3 h and 24 h after the shift to LC (B) and the recovery rate 24 h after the shift back to HC compared to initial value 0 h after shift to LC (C). Significant changes between to time points in transcript level are indicated as a ($p<0.05$), b ($p<0.01$) and c ($p<0.01$).

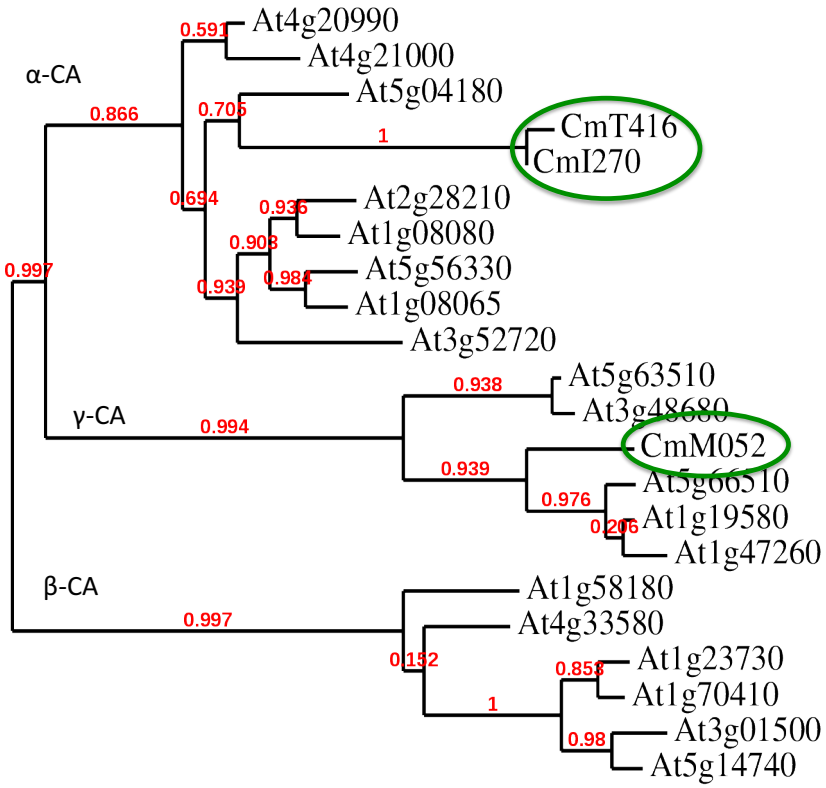

Supplementary Figure 11: Maximum-Likelihood Phylogenetic tree of known carbonic anhydrases from *Arabidopsis thaliana* and three possible carbonic anhydrases of *C. merolae* (green circles). Different branches indicate α-, β- and γ- carbonic anhydrases. Branch support values are shown in red. Phylogenetic tree analysis was performed using Phylogeny.fr (Dereeper *et al.*, 2008).

Author's contribution to manuscript III:

Nadine Rademacher: Wrote manuscript. Performed *Cyanidioschyzon merolae* cultivation, carbon shift experiment, RNA extraction, fold-change analysis of specific pathways, BlastP analysis for carbonic anhydrase and bicarbonate transporter identification and localization studies.

Thomas Wrobel: Performed Bioinformatic analysis: PCA, Kmeans clustering and corresponding heat maps, general fold change analysis, comparison of gene transcript amount in superior pathway categories.

Alessandro W. Rossoni: Performed read mapping and gene/ transcript expression profiling.

Marion Eisenhut: Supervision of experimental design.

Samantha Kurz: Performed TruSeq RNA library preparation.

Andrea Bräutigam: Performed initial read mapping using the CLC server.

Andreas P.M. Weber: Helped with experimental design.

CONCLUDING REMARKS

This PhD thesis started with a review on the actually state of knowledge of the photorespiratory cycle. It could be shown that photorespiration fulfills many important processes next to the function of a 2-PG detoxification process with a special focus on the interconnection with the nitrogen and the sulfur process (Eisenhut and Hocken *et al*., 2015). Although a lot is known about the main enzymes involved in photorespiration and their evolution, especially due to the work of the PROMICS research unit in the last years (Photorespiration: Origin and Metabolic Integration in Interacting Compartments, germane research foundation), some transport processes are still unidentified (see for review: Bauwe *et al*., 2010; Hagemann *et al*., 2013; Hagemann *et al.,* 2016). A future challenge will be to identify missing translocators in the peroxisome and the mitochondrion for the complete understanding of the photorespiratory cycle.

Task of the second part of the thesis was to test the assumption, if photorespiration is essential in red algae using the ancient, extremophile red algae *C. merolae.* Additionally analyzing of GOX knock-out mutant strains enabled to show, that already ancient red algae uses the plant-like photorespiratory cycle, indicating a high photorespiratory flux before the colonization of land mass (Rademacher *et al.,* 2016). In future the exchange of the GOX enzyme in *C. merolae* by a GlcD used in the photorespiratory cycle of Chlamydomonas, including detailed photorespiratory flux measurements, would help to get a better understanding of the GOX evolution in most photosynthetic eukaryotes.

The general severe growth problems of *C. merolae* under ambient CO_2 conditions led to the question for transcriptional changes due to CO_2 limitation. A strong CO_2 dependent up and down regulation of genes involved in photorespirations could be shown. However only minor changes occur in most other pathways, including the energy metabolism, which might be explained by the loss of regulatory processes due to CO_2 depletion in a natural high CO_2 habitat. Approaches to identify possible candidates of a CCM due to their co-regulation with photorespiratory enzymes revealed only one possible HCO_3^- transporter candidate, which has to be confirmed in future studies (Fang et al, 2012, reviewed in Hagemann *et al.,* 2016, Rademacher

manuscript III). Moreover functional studies on both identified cytosolic CAs will help to understand their physiological role in *C. merolae* in response to a changing carbon availability.

REFERENCES:

Bauwe H, Hagemann M, Fernie AR. 2010. Photorespiration: players, partners and origin. Trends in Plant Science **15**, 330–336.

Eisenhut M, Hocken N, Weber APM. 2015. Plastidial metabolite transporters integrate photorespiration with carbon, nitrogen, and sulfur metabolism. Cell Calcium **58**, 98–104.

Fang W, Si Y, Douglass S, Casero D, Merchant SS, Pellegrini M, Ladunga I, Liu P, Spalding MH. 2012. Transcriptome-wide changes in *Chlamydomonas reinhardtii* gene expression regulated by carbon dioxide and the CO_2-concentrating mechanism regulator CIA5/CCM1. The Plant Cell **24**, 1876–1893.

Hagemann M, Fernie AR, Espie GS, Kern R, Eisenhut M, Reumann S, Bauwe H, Weber APM. 2013. Evolution of the biochemistry of the photorespiratory C2 cycle. Plant Biology **15**, 639–647.

Hagemann M, Kern R, Maurino VG, Hanson DT, Weber APM, Sage RF, Bauwe H. 2016. Evolution of photorespiration from cyanobacteria to land plants, considering protein phylogenies and acquisition of carbon concentrating mechanisms. Journal of Experimental Botany, in press.

Rademacher N, Kern R, Fujiwara T, Mettler-Altmann T, Miyagishima SY, Hagemann M, Eisenhut M, Weber APM (2016) Photorespiratory glycolate oxidase is essential for survival of the red alga *Cyanidioschyzon merolae* under ambient CO_2 conditions. Journal of Experimental Botany, in press.

.

PUBLICATIONS

The following manuscripts were published while working for the thesis are presented here:

Eisenhut M, **Hocken N,** Weber APM. 2015. Plastidial metabolite transporters integrate photorespiration with carbon, nitrogen, and sulfur metabolism. Cell Calcium 58, 98–104

Rademacher N, Kern R, Fujiwara T, Mettler-Altmann T, Miyagishima SY, Hagemann M, Eisenhut M, Weber APM (2016) Photorespiratory glycolate oxidase is essential for survival of the red alga *Cyanidioschyzon merolae* under ambient CO_2 conditions. Journal of Experimental Botany, in press.

ACKNOWLEDGMENT

Prof. Dr. Andreas Weber: Für die Möglichkeit meine Doktorarbeit in seinem Labor anzufertigen, sowie die Diskussions- und Hilfsbereitschaft .

PD. Dr. Veronica Maurino: Für die schnelle Übernahme der Rolle als Zweitgutachterin meiner Arbeit.

Dr. Marion Eisenhut: Für die Betreuung meiner Arbeit und Schokoladen-Sofortmaßnahmen bei aufkommender Frustration.

Dr. Tabea Mettler-Altmann und dem gesamten MS-Team für Ihre Einsatzbereitschaft die Metabolitextraktion aus *C. merolae zu* verbessern.

Allen Doktoranten, Master und Bachelorstudenten: Für unzählige, inspirierende Mittagspausen und helfende Hände im Labor.

Samantha Kurz: Für experimentelle Unterstützung und Motivation in gemütlichen Kaffeepausen.

Anja Nöcker: Für Ihre Hilfe bei allen bürokratischen Problemen.

Allen Autoren und Co-Autoren, die an der Anfertigung der Publikationen beteiligt waren.

Meinen Eltern: Für ihre Unterstützung während des gesamten Studiums, vieler aufbauender Worte und ihrem Interesse an meiner Arbeit.

Meinem Ehemann Peter: Für die tägliche Motivation, die Liebe, den Rückhalt und seine Wissbegier.